U.PORTO

FEUP FACULDADE DE ENGENHARIA
UNIVERSIDADE DO PORTO

PROBABILISTIC UNDRAINED STRENGTH EVALUATION OF SOFT SOIL FOR SLOPE STABILITY DESIGN

LOURENÇO LOPES CRISTO GOMES DE SOUSA

Dissertação submetida para satisfação parcial dos requisitos do grau de

MESTRE EM ENGENHARIA CIVIL – ESPECIALIZAÇÃO EM GEOTECNIA

Orientador: Professora Doutora Sara Rios da Rocha e Silva

Coorientador: Professor Doutor Ole Hededal

MARÇO DE 2021

MESTRADO INTEGRADO EM ENGENHARIA CIVIL 2020/2021

DEPARTAMENTO DE ENGENHARIA CIVIL

Tel. +351-22-508 1901

Fax +351-22-508 1446

✉ miec@fe.up.pt

Editado por

FACULDADE DE ENGENHARIA DA UNIVERSIDADE DO PORTO

Rua Dr. Roberto Frias

4200-465 PORTO

Portugal

Tel. +351-22-508 1400

Fax +351-22-508 1440

✉ feup@fe.up.pt

http://www.fe.up.pt

Reproduções parciais deste documento serão autorizadas na condição que seja mencionado o Autor e feita referência a *Mestrado Integrado em Engenharia Civil - 2020/2021 - Departamento de Engenharia Civil, Faculdade de Engenharia da Universidade do Porto, Porto, Portugal, 2021.*

As opiniões e informações incluídas neste documento representam unicamente o ponto de vista do respetivo Autor, não podendo o Editor aceitar qualquer responsabilidade legal ou outra em relação a erros ou omissões que possam existir.

Este documento foi produzido a partir de versão eletrónica fornecida pelo respetivo Autor.

Aos meus pais e irmã

While doctors bury their failures, Geotechnical Engineers bury their successes

Jørgen S. Steenfelt

ACKNOWLEDGEMENTS

I want to express my special and deepest gratitude to my supervisor Professor Sara Rios for the dedication, suggestions, patience and constant guidance during all this period. For the interest, availability and valuable knowledge demonstrated throughout the course of this dissertation.

To Ole Hededal for welcoming me in COWI/AS, for giving the proposal of such an interesting theme and for sharing his knowledge and experience.

To Laurentiu Floroiu for the interest demonstrated in the project and for all the availability, support and friendship.

To Dimitris Fotiadis for all the knowledge and discussions we had during our meetings and for all the feedback provided.

To José Calejo for the support during the time spent in Denmark, the valuable companionship, suggestions and supervision.

I wish to express acknowledge for all the staff in COWI/AS, specially to the 1703 Friday Bar crew for making the effort in providing amusement to the staff during this difficult pandemic situation.

To Tia Lucia for the motivation and kindness demonstrated by reviewing the dissertation.

To my mother, who is always present when I needed the most, and for motivated and comforted me all the time.

To my father, who always show concern for my well-being and for all the encouragement given.

To my sister for all the everyday care demonstrated and for always being present.

ABSTRACT

This work addresses a specific issue of a land reclamation project in Copenhagen. The new peninsula to be built will be confined in it perimeter by several dykes and sheet pile walls. The dykes in particular, cannot be founded on the local soft soil, gyttja, which needs to be dredged before building the dykes. In this work, the stability of the surrounding gyttja during that dredging operation is analysed in detail using probabilistic and limit equilibrium analysis.

Since this is a very soft soil the most important strength parameter for the stability analysis is the undrained shear strength, c_u.

The geotechnical tests that were analysed to evaluate the c_u evolution with depth were anisotropically consolidated undrained triaxial compression tests, CAUC, and cone penetration tests with water pressure measurements, CPTU. The first were used to calibrate the cone factor, N_{kt}, so that the CPTU data (performed in a much higher number) could be used. The presence of strength anisotropy in this particular soil was also analysed.

A huge amount of CPTU results was analysed in order to evaluate c_u from a statistical point of view. The work will have a focus on three statistical approaches in order to produce the best analysis that reflects a considerable level of statistical variability.

Following the selected approach, a probabilistic slope stability analysis using SLOPE/W was performed. This problem is related to structural optimization along the perimeter, considering the depth variation of gyttja and sea water depth. The probabilistic procedure used herein was the Monte Carlo method, integrated in SLOPE/W. Within the probabilistic procedure the impact of detailing the probabilistic analysis (i.e the effect of the number of Monte Carlo samples), was also analysed relating the final results with the computational effort. A comparison between the produced probabilistic approach and a conventional deterministic procedure, was performed concerning the obtained results.

KEYWORDS: land reclamation, gyttja, soft soil dredging, undrained shear strength, triaxial tests, CPTU, N_{kt}, probabilistic slope stability analysis, Monte Carlo method, SLOPE/W.

RESUMO

Este trabalho aborda uma questão específica de um projeto de aterro de conquista de terras em Copenhaga. A nova península a ser construída será delimitada por vários diques e cortinas estacas-prancha. Os diques, em particular, não podem ser fundados no solo mole local, *gyttja*, que necessita de ser dragado antes da construção dos diques. Neste trabalho, a estabilidade da *gyttja* circundante durante a operação de dragagem é analisada em detalhe usando análises probabilísticas e de equilíbrio limite.

Como este é um solo muito mole, o parâmetro de resistência mais importante para a análise de estabilidade é a resistência não drenada, c_u.

Os testes geotécnicos que foram analisados para avaliar a evolução com a profundidade de c_u foram testes de compressão triaxial não drenados consolidados anisotropicamente, CAUC e ensaios de piezocone, CPTU. Os primeiros foram usados para calibrar o fator de cone, N_{kt}, para que os dados dos ensaios CPTU (realizados em um número muito maior) pudessem ser usados. A presença de anisotropia induzida neste solo em particular foi também analisada.

Foi analisada e tratada uma grande quantidade de resultados CPTU, de forma a caracterizá-la do ponto de vista estatistico. O trabalho terá como foco três abordagens estatísticas a fim de produzir a melhor análise que reflita um nível considerável de variabilidade estatística.

Seguindo a abordagem selecionada, foi realizada uma análise probabilística de estabilidade de taludes utilizando o software SLOPE/W. Este problema está relacionado com a otimização estrutural ao longo do perímetro, considerando a variação da profundidade de *gyttja* e a profundidade da água do mar. O procedimento probabilístico aqui utilizado foi o método de Monte Carlo, integrado no SLOPE/W. Dentro do procedimento probabilístico, o impacto do detalhe da análise probabilística (ou seja, o efeito do número de amostras Monte Carlo), também foi analisado, relacionando os resultados finais com o esforço computacional. Uma comparação entre a abordagem probabilística produzida e um procedimento determinístico convencional, foi realizada em relação aos resultados obtidos.

PALAVRAS CHAVE: aterros de conquista, *gyttja*, dragagem de solo mole, resistência não drenada, ensaios triaxiais, CPTU, N_{kt}, análise probabilistica de estabilidade de taludes, método Monte Carlo, SLOPE/W.

ABSTRAKT

Denne rapporte omhandler et landgenvindingsprojekt i København. Den nye halvø som skal bygges vil være begrænset i det omkreds af flere diger og spunsvægge. Især digerne, kan ikke funderes på den lokale bløde jord, gytje, som skal udmudres inden opbygningen af digerne. I dette projekt analyseres stabiliteten af gytje under udgravning ved hjælp af en probabilistisk og brudgrænsetilstand analyse.

Da dette er en meget blød jord, er den vigtigste styrkeparameter for stabilitetsanalysen det udrænet forskydningsstyrke, c_u.

De geotekniske undersøgelser der blev analyseret for at evaluere cu-udvikling med dybde var anisotropisk konsolideret udrænet triaksial kompressionstest (CAUC) og tryksondering med vand trykmålinger, CPTU. De første blev brugt til at kalibrere keglefaktoren, N_{kt}, således at CPTU data (udført i et meget højere antal) kunne bruges. Styrkeanisotropi i dette type jord blev også analyseret.

En enorm mængde CPTU-resultater blev analyseret for at evaluere c_u fra et statistisk perspektiv. Denne opgave fokuserer på tre statistiske tilgange for at producere den bedste analyse, der afspejler en betydelig grad af statistisk variation.

Efter den valgte tilgang blev der udført en probabilistisk skråningsstabilitetsanalyse ved hjælp af SLOPE/W. Dette problem er relateret til strukturel optimering langs omkredsen i betragtning af dybdevariationen af gytje og havvanddybde. Den anvendte probabilistiske procedure var Monte Carlo-metoden, integreret i SLOPE/W. Inden for den sandsynlige procedure er indvirkning af detaljering af den sandsynlige analyse (dvs. effekten af antallet af Monte Carlo-prøver) blev også analyseret vedrørende den endelige resultater med beregningstid. En sammenligning mellem den producerede probabilistiske tilgang og en konventionel deterministisk procedure blev udført vedrørende de opnåede resultater.

NØGLEORD: landgenvinding, gytje, blød jordmudring, udrænet forskydningsstyrke, triaksialtest, CPTU, N_{kt}, probabilistisk hældningsstabilitetsanalyse, Monte Carlo-metode, SLOPE/W.

TABLE OF CONTENTS

ACKNOWLEDGEMENTS i
ABSTRACT iii
RESUMO v
ABSTRAKT vii

1. INTRODUCTION 1
1.1. SCOPE 1
1.2. OBJECTIVES 1
1.3. THESIS STRUCTURE 2

2. LAND RECLAMATION 5
2.1. LAND RECLAMATION 5
2.1.1. DIRECT SOIL DUMPING 5
2.1.2. HYDRAULIC FILLING 6
2.1.3. ROTTERDAM PORT 7
2.2. SOFT SOIL DREDGING 8
2.2.1. MECHANICAL DREDGING EQUIPMENT 8

3. CASE STUDY 11
3.1. PROJECT INTRODUCTION 11
3.1.1. URBAN DEVELOPMENT 12
3.1.1.1. Østlig Ringvej 12
3.1.1.2. Metro 12
3.1.2. DESIGN PROPOSALS 13
3.2. LOCAL GEOLOGICAL PAST 14
3.3. SOIL CONDITIONS IN LYNETTEHOLM 15
3.3.1. IN-SITU CAMPAIGN OVERVIEW 15
3.3.2. SOIL MODEL 15
3.3.2.1. Layers Description 16
3.3.3. POST-GLACIAL DEPOSITS THICKNESS 17
3.3.4. GYTTJA 18
3.3.4.1. Organic Content 18
3.3.4.2. Soil Plasticity 20
3.3.4.3. Sensitivity 20
3.4. PROBLEM DESCRIPTION 22

4. GEOTECHNICAL DATA 27
4.1. CPTU DATA 27
4.1.1. TEST DESCRIPTION 27

4.1.2. Derived Geotechnical Parameters 28
4.1.3. Data Presentation 29
4.1.3.1. CPTU Readings Errors 29
4.1.4. CPTU Parameters 30
4.1.5. Gyttja Thickness Evaluation 33
4.1.6. CPTU Soil Classification Charts 34
4.1.6.1. Non-Normalized Charts (SBT) 35
4.1.6.2. Normalized Charts (SBT_n) 37
4.1.6.3. Eslami-Fellenius Chart 40
4.2. Undrained Shear Strength 42
4.2.1. CAUC Laboratory Data 42
4.2.2. Similar soils experience 48
4.2.3. Effect of Anisotropy 50
4.2.4. Estimation of the N_{kt} 53
4.3. Chapter Summary 56
5. PROBABILISTIC APPROACHES 57
5.1. Introduction 57
5.2. Linear regression theoretical explanation 57
5.2.1. Undrained Shear Strength estimation with depth 58
5.3. Undrained Strength Approaches 59
5.3.1. Approach 1 - Every CPTU in The Same Evaluation 59
5.3.2. Approach 2 - Separated CPTU Analysis 61
5.3.3. Approach 3 - Impact of Nkt variation 66
5.4. Chapter Summary 72
6. SLOPE STABILITY 73
6.1. Introduction 73
6.2. Factor of Safety Method 73
6.3. Probabilistic Methods applied to Slope Stability 73
6.3.1. Monte Carlo Method 73
6.3.2. Number of Monte Carlo Samples 74
6.3.3. Reliability Assessment 74
6.3.4. Probability of failure 75
6.3.5. Reliability Index 75
6.3.5.1. Reliability Classes 76
6.4. Types of Stability Analysis 77
6.4.1. Short Term Analysis 78
6.4.2. Medium Term Analysis 78
6.4.3. Long Term Analysis 80
6.5. Stability Analysis Results 80
6.5.1. Factor of Safety Interpretation 81

6.5.2. MONTE CARLO CONVERGENCE 83
6.5.2.1. Probability of Failure 83
6.5.2.2. Mean Factor of Safety 83
6.5.2.3. Standard Deviation of the Mean Factor of Safety 84
6.5.3. COMPARISON OF FACTORS OF SAFETY 84
6.6. EUROCODE 7 - SAFETY FACTORS 87
6.6.1. OVER DESIGN FACTOR 87
6.6.2. MONTE CARLO CONVERGENCE 88
6.6.2.1. Probability of Over Design Failure 88
6.6.2.2. Mean Over Design Factor 89
6.6.2.3. Standard Deviation of the Mean Over Design Factor 89
6.6.3. RUN ANALYSIS DURATION 91
6.7. CHAPTER SUMMARY 92

7. CONCLUSION 93
7.1. CONCLUSIONS 93
7.2. FUTURE DEVELOPMENTS 95

BIBLIOGRAPHY 97

LIST OF FIGURES

Figure 2.1 – Direct soil dumping method with bottom dump barge (Babak Hamidi, 2015) 6
Figure 2.2 – Pipeline discharge method (Babak Hamidi, 2015) 6
Figure 2.3 – Rainbow discharge method (Babak Hamidi, 2015) 7
Figure 2.4 – Satellite image of Rotterdam Port in 2010 (NASA Earth Observatory, n.d.) 7
Figure 2.5 – Example of a non-self-propelled chain bucket dredger (Jiangsu ShunYou Shipping Engineering Co., Ltd, n.d.) 9
Figure 2.6 – Example of a backhoe dredger (Seatools, n.d.) 9
Figure 2.7 – Gosho, considered to be the biggest grab dredger in the world by (Kojimagumi, n.d.) 10

Figure 3.1 – Location of Lynetteholm with the representation of the two perimeter proposals (By og Havn, 2020) 11
Figure 3.2 – Connection with Øresundsmotorvejen solution (KK, 2020) 12
Figure 3.3 – Blue line solution (M4) (KK, 2020) 13
Figure 3.4 – Design Proposals for Lynetteholm (a) first Proposal, (b) second proposal (COWI, 2020) 13
Figure 3.5 – Scandinavian Ice Sheild 14
Figure 3.6 – Overall site test campaign (COWI, 2020) 15
Figure 3.7 – Gyttja thickness map 17
Figure 3.8 – Different samples of gyttja (Wikipedia, n.d.) 18
Figure 3.9 – Organic content in gyttja samples 19
Figure 3.10 – Soil categories based on organic content (Larsson, 1990) 19
Figure 3.11 – Gyttja samples distribution in the Casagrande chart (COWI/AS, 2020) 20
Figure 3.12 – Measured gyttja sensitivity based on VST and CAUC (COWI/AS, 2020) 21
Figure 3.13 – Example of a perimeter structure from a land reclamation project (Structurae, n.d.) 22
Figure 3.14 – Phase 0 of perimeter cross section 23
Figure 3.15 – Gyttja thickness map indicating the slope scenarios perimeter location considered 23
Figure 3.16 – Bathymetry map from the project area 24
Figure 3.17 – Phase 1 of perimeter cross section 24
Figure 3.18 – Phase 2 of perimeter cross section 25
Figure 3.19 – Phase 3 of perimeter cross section 25
Figure 3.20 – Phase 4 of perimeter cross section 25

Figure 4.1 – CPTU equipment representation 27
Figure 4.2 – Determination of the cone area ration in a calibration vessel (Lunne, Robertson, & Powell, 1997) 28
Figure 4.3 – Cone resistance readings in the first 16cm depth of specimen CPT_A_111 29
Figure 4.4 – Cone resistance, q_c, evolution with depth for the entire CPTU data 30
Figure 4.5 – Pore pressure, u_2, evolution with depth for the entire CPTU data 31
Figure 4.6 – Normalized cone resistance, q_t, evolution with depth for the entire CPTU data 32
Figure 4.7 – Sleeve friction, f_s, evolution with depth for the entire CPTU data 33

Figure 4.8 – CPTU single specimen tip resistance (q_c) and friction sleeve stress (f_s) 34
Figure 4.9 – CPT soil behaviour type classification chart (Robertson, Campanella, Gillespie, & Greig, 1986) . 35
Figure 4.10 – CPTU Soil behaviour chart with CPTU data 36
Figure 4.11 – Soil behaviour type variation with depth classification from (Robertson, 2010) 37
Figure 4.12 – CPTU soil behaviour type by (Robertson, 1990) 38
Figure 4.13 – CPTU Soil behaviour chart with CPTU data 39
Figure 4.14 – Normalized soil behaviour type variation with depth classification from (Robertson, 1990) 40
Figure 4.15 – Eslami and Fellenius soil profiling chart with soil type classification (Eslami & Fellenius, 1997)... 41
Figure 4.16 – Eslami and Fellenius soil scatter..... 41
Figure 4.17 – Total stress Mohr envelope for clays (Matos Fernandes, 2016) 42
Figure 4.18 – Undrained shear strength as a function of rate of deformation in organic clays from: (a) Valen , (b) Lilla Mellosa (Larsson, 1990) 43
Figure 4.19 – Peak deviator stress variation with axial strain during shear phase for specimen 3_2 from BH_P_25 (COWI/AS, 2020) 44
Figure 4.20 – Evaluation of the undrained shear strength, cu_{TC} of the triaxial tests, with the representation of the linear regression 46
Figure 4.21 – Boreholes location in site where CAUC specimens where taken 47
Figure 4.22 – Effective peak stresses..... 48
Figure 4.23 – Undrained shear strength evaluation from Swedish soils: (a) Lilla Mellosa , (b) Gideabacka (Larsson, 1990) 49
Figure 4.24 – Simplified total and effective stress path obtained from triaxial compression and extension tests over similar samples (Matos Fernandes, 2016) 50
Figure 4.25 – Evolution of excess pore pressure and strength ratio with axial strain, during shear phase (specimen 3_2 from BH_P_25) (COWI/AS, 2020)..... 51
Figure 4.26 – Evolution of k_s depending on A_f and ϕ' (Matos Fernandes, 2016) 53
Figure 4.27 – N_{kt} historical range recommendations (Rémai, 2013) 54
Figure 4.28 – Cross section showing an example location where both CPTU and Boreholes were executed ... 55
Figure 4.29 – Flowchart indicating the N_{kt} procedure..... 55

Figure 5.1 – Resume of the approaches for c_u evaluation from CPTU 57
Figure 5.2 – Undrained shear strength linear evaluation with depth (Veritas, 2012) 58
Figure 5.3 – Undrained shear strength, c_u, evaluation using the average value for the cone factor, $Nkt, avg = 19.2$. The line in black represents the linear regression of the scatter 60
Figure 5.4 – Histogram and Normal distribution Probability Density Function, considering the distribution of c_u without depth dependency..... 61
Figure 5.5 – Linear regression for c_u evaluation in every CPTU log..... 62
Figure 5.6 – Histogram for the rate of change of every linear regression 63
Figure 5.7 – Histogram for the undrained strength at the top of the gyttja layer considering every linear regression 63
Figure 5.8 – Linear regression for c_u evaluation in every CPTU result filtered ($0.15 < c_u/\sigma'_{vo} < 0.85$)..... 64
Figure 5.9 – Histogram for the rate of change considering the range: $0.15 \leq c_u/\sigma'_{vo} \leq 0.85$..... 65

Figure 5.10 – Histogram for the undrained strength at the top of the gyttja layer considering the range: $1 \leq c_u(0m) \leq 13$ 66
Figure 5.9 – Undrained shear strength evaluation from using different values for N_{kt}: (a) N_{kt}=16.6, (b) N_{kt}=16.7, (c) N_{kt}=17.2, (d) N_{kt}=21.2, (e) N_{kt}=24.5. For each scatter, the line in black represents the linear regression of data 68
Figure 5.10 – Truncated probability density function for c_u/σ'_{vo} 69
Figure 5.11 – Cumulative density function for c_u/σ'_{vo} 69
Figure 5.12 – Truncated probability density function for the undrained shear strength at the top of layer 70
Figure 5.13 – Cumulative density function for the undrained strength at the top of the layer 70
Figure 5.14 – Relation between N_{kt} and c_u/σ'_{vo}, indicating the linear regression (dotted line) 71
Figure 5.15 – Relation between N_{kt} and $c_{u,0m}$, indicating the linear regression (dotted line) 71
Figure 5.16 – Relation between $c_{u,0m}$ and c_u/σ'_{vo}, indicating the linear regression (dotted line) 71

Figure 6.1 – Reliability classes from the Eurocode approach (EN 1990, 2002) 77
Figure 6.2 – Probability of failure criteria for slope stability purposes (Santamarina, Altschaeffl, & Chameau, 1992) 77
Figure 6.3 – Shear strength as a function of depth below the seabed surface (short term analysis) 78
Figure 6.4 – Variation of pore water pressure and safety factor with time (Bishop & Bjerrum, 1960) 79
Figure 6.5 – Shear strength as a function of depth (medium term analysis) 80
Figure 6.6 – Slope geometry of the represented results case 81
Figure 6.7 – Factor of Safety histogram distribution and the fitted normal distribution to the values obtained .. 81
Figure 6.8 – Factor of safety for the critical slice in the considered scenario (deterministic analysis) 82
Figure 6.9 – Cumulative density function for the factor of safety 82
Figure 6.10 – Probability of failure - MC convergence graph 83
Figure 6.11 – Mean factor of safety - MC convergence graph 84
Figure 6.12 – Standard deviation of the mean factor of safety - MC convergence graph 84
Figure 6.13 – Over Design Factor histogram distribution and the fitted normal distribution to the values obtained 88
Figure 6.14 – Cumulative density function for the over design factor 88
Figure 6.15 – Probability of over design failure - MC convergence graph 89
Figure 6.16 – Mean over design factor - MC convergence graph 89
Figure 6.17 – Standard deviation of the mean over design factor - MC convergence graph 90

LIST OF TABLES

Table 3.1 – Soil model layers 16
Table 3.2 – Sensitivity classification of clay, according to the Swedish classification system (Karlsson & Hansbo, 1989) 21
Table 3.3 – Construction phase description 22
Table 3.4 – Correspondent gyttja and sea water level depth considered 24

Table 4.1 – Area factors for all the CPTU 28
Table 4.2 – Soil behaviour type description from (Robertson et al., 1986) 35
Table 4.3 – Soil behaviour type description from 1990 38
Table 4.4 – Laboratory CAUC results 45
Table 4.5 – Effective cohesion and friction angle obtained 47
Table 4.6 – Laboratory determination of anisotropy 52
Table 4.7 – Average values for A_f and k_s 52
Table 4.8 – Typical values for A_f from triaxial tests. Adapted from Matos Fernandes (2016) 52
Table 4.9 – Representation of the values of $c_{u,TC,avg}$, $q_{net,avg}$ and N_{kt} for each specimen, corresponding to the indicated adjacent CPTU 56

Table 5.1 – Linear regression results depending on the N_{kt} variation 68
Table 5.2 – Indication of the linear regressions of 72

Table 6.1 – Relation between p_f and β (adapted from (EN 1990, 2002)) 76
Table 6.2 – Medium term stability results from SLOPE/W (characteristic values) 85
Table 6.3 – Short term stability results from SLOPE/W (characteristic values) 86
Table 6.4 – Gyttja design slope solutions for both long and short term 86
Table 6.5 – Factor of safety obtained from drained strength parameters (Long term analysis) 87
Table 6.6 – Medium term stability results from SLOPE/W (EC7 partial factor values) 90
Table 6.7 – Short term stability results from SLOPE/W (EC7 partial factor values) 91
Table 6.8 – Run analysis duration for each one of the 92

SYMBOLS, ACRONYMS AND ABBREVIATIONS

CPT - cone penetration test

CPTU - cone penetration testing with water pressure measurements

BH - borehole

VST - vane shear test

c_u - undrained shear strength

c_{ur} - remoulded undrained shear strength

$c_{u,TC}$ - undrained shear strength determined from triaxial compression

$cu(v)$ - undrained shear strength under compression

$cu(h)$ - undrained shear strength under extension

$c_{u,avg}$ - average undrained shear strength

$c_{u,st.dev.}$ - undrained shear strength standard deviation

k_s - anisotropy parameter

$\bar{k_s}$ - average anisotropy parameter

N_{kt} - cone factor

$N_{kt,avg}$ - average cone factor

σ'_{vo} - initial vertical effective stress

$\sigma'_{vo,est}$ - estimated initial vertical effective stress

σ'_1 - major effective stress

$\sigma'_{1,peak}$ - peak major stress

$\sigma'_{1,cons}$ - major stress at the end of the consolidation stage

σ'_3 - minor effective stress

τ_{max} - maximum shear stress

R^2 - coefficient of determination

q_{peak} - peak deviator stress

q_c - cone resistance

q_t - normalized cone resistance

q_{net} - net cone resistance

q_E - effective cone resistance

f_s - sleeve friction

u_2 - pore pressure

A_n - cross sectional area of the load cell

A_c - projected area of the cone

R_f - friction ratio

Q_t - normalized cone resistance

F_r - normalized friction ratio

OCR - overconsolidation Ratio

CAUC - anisotropically consolidated undrained triaxial compression

SBT - soil behaviour type

SBT_n - normalized soil behaviour type

I(SBT) - soil behaviour type index

GPS - global positioning system

a - area factor

S_t - soil sensitivity

TSP - total stress path

TSP_{ext} - total stress path under extension

ϕ - friction angle

ϕ' - effective friction angle

c' - effective cohesion

Δu - excess pore pressure

Δu_f - excess pore pressure at failure

K_o - earth pressure coefficient at rest

A_f - pore pressure parameter at failure

A - pore pressure parameter

$\bar{A_f}$ - average pore pressure parameter at failure

$\Delta\sigma_{1f}$ - major total stress variation at failure

$\Delta\sigma_3$ - minor total stress variation

σ'_{1o} - initial major effective axial stress

σ'_A - effective total axial stress

σ'_R - effective total radial stress

$\Delta\varepsilon_{sA}$ - variation of the axial strain during shear phase

$q_{net,avg}$ - average net cone resistance for each location.

$c_{u,TC,avg}$ - average undrained shear strength of each specimen for the average depth of the specimen

Y - soil variable

z - depth below the soil surface

ε - natural variability of Y about the mean

a_0 - surface intercept

a_1 - depth gradient

σ - standard deviation

$\sigma_{FS,avg}$ - standard deviation of the mean factor of safety

n - number of observations

$\bar{y}$ - average value for the strength parameter Y

$\bar{z}$ - average value for the depth parameter z

$\hat{a}_0$ - surface intercept estimator

$\hat{a}_1$ - depth gradient estimator

$se(\hat{a}_0)$ - standard error of the surface intercept estimator

$se(\hat{a}_1)$ - standard error of the depth gradient estimator

c_u/σ'_{vo} - undrained strength rate of change

$c_{u,0m}$ - undrained strength at the top of the layer

PDF - probability density function

CDF - cumulative density function

MC - Monte Carlo

MCM - Monte Carlo method

LEM - limit equilibrium method

p_f - probability of failure

FS - factor of safety

FS_{avg} - average factor of safety

FS_{det} - deterministic factor of safety

ODF - overdesign factor

ODF_{avg} - mean overdesign factor

σ_{ODFavg} - standard deviation of the mean overdesign factor

β_{OD} - overdesign reliability index

$p_{f,OD}$ - probability of over design failure

β - reliability index

Φ - cumulative distribution function a standardised normal distribution

p_d - admissible failure probability

β_d - acceptable reliability index

RC - reliability class

T_d - design working life

γ_{c_u} - partial factor for the undrained shear strength

EC7 - Eurocode 7

1 INTRODUCTION

1.1. SCOPE

The increase of global population is leading to a rising consumption of natural resources such as clean air, land and water. Demand for land has increased significantly over the past 40 years (Stauber, Chariton, & Apte, 2016), both inland and at the coast. In coastal regions, reclamation of land from the sea has often been the preferred solution towards meeting the need for more land for urban development.

On one hand there are the advantages in land reclamation projects such as the creation of a new area that is able to accommodate new citizens, reduce the city center traffic, create tourist attractions and boost the economic development. There is also the value in serving as an useful dumping site from other excavation works. However it is also important to access the impact of this type of construction and how it affects the natural environment. In 1996 the Hong Kong government stated that land reclamation would result in “large displacement of the marine sediments and the development of mud-waves beneath the reclamation fill". This would lead to soil liquefaction, disrupt the ocean’s ecosystem and pollute the marine water (Duong, 2017).

With that said it can be stated that is essential to evaluate the advantages in creating this new areas. It is necessary to carry out a feasibility study to determine whether reclamation of land from the sea is a reasonable option for a specific location. It is demanded to take into account the most relevant environmental, technical, legal and economic factors. In other words, it is extremely important the need for intensive site investigations and pre-feasibility studies in order to establish an informed basis for a decision on whether or not to proceed with a certain land reclamation project (Environment & Authority, 2008).

1.2. OBJECTIVES

The main purpose of this work is to access the importance in producing a probabilistic analysis in a large amount of cone penetration testings with water pressure measurements, CPTU. This work is focused in the estimation of the undrained shear strength, c_u, with depth. The impact in having such a huge amount of data from a geotechnical and statistical point of view is evaluated. This research is focused in carrying that analysis in a typical soft soil in Denmark called gyttja. The first step concerned filtering the soil data in order to evaluate only this critical layer. Then, a probabilistic analysis was performed to obtain the undrained strength evolution with depth.

This included a detailed analysis for the determination of the cone factor, N_{kt} which has an important influence on the evaluation of the undrained strength. This cone factor relates data from anisotropically consolidated undrained triaxial compression, CAUC tests with CPTU results.

From the treated parameters, a slope stability problem was studied aiming at finding the most optimized geometry for this structure. A comparison was made between this approach and a simpler conventional deterministic analysis. In more simplified terms the answers to the following questions were pursued:

- How much quality does the filtered CPTU data have?
- What is the spacial variability of the CPTU data?
- Is is worth to produce a CPTU probabilistic analysis for slope stability design?
- What is the most appropriate probabilistic method to use for CPTU data in order to evaluate c_u?
- What is the impact of the determination of the N_{kt} in the c_u evaluation?

The safety factor assessment will be carried out in limit equilibrium slope stability software where probabilistic data was used as input, in order to achieve an optimized solution for the slope geometry. The aim of this analysis is to reveal an interval for the failure probability of the considered slope for each geometry scenario.

1.3. THESIS STRUCTURE

This document is divided in seven chapters. In this first chapter a brief introduction to the thesis topic is made indicating the main objectives.

Chapter 2 is a brief introduction to the topic of reclamation projects, describing land reclamation methods and mechanical equipment that can be potentially used in this project.

Chapter 3 describes the case study project and explains the urban impact related to the construction of this land reclamation area. A brief historical background about the geological past of this region is also addressed in this chapter. Also, it describes the in-situ tests campaign that were conducted during the preliminary part of the project. The soil model and different soil layers are also described in this part. A specific kind of soil, gyttja, will be also described with more detail. Finally the construction procedure of the problem in hands is also synthesized.

The geotechnical data is dealt with in Chapter 4 where the relevant data is selected and filtered. This includes mainly data from the cone penetration testing with water pressure measurements, CPTU. The anisotropically consolidated undrained triaxial compression tests, CAUC, will also be discussed in order to correlate the cone factor, N_{kt}, of the CPTU. Chapter 4 presents also an insight about the method used in order to evaluate the soft soil thickness for each CPTU result.

Chapter 5 is oriented for the production of different approaches to evaluate the undrained shear strength, c_u from CPTU. Here different statistical methods are produced, considering different strategies and perspectives. The objective here is to decide the best method to be used later for the probabilistic geotechnical design.

Chapter 6 covers a practical problem of slope stability in which the chosen probabilistic analysis was used in order to achieve the required design solutions. A brief explanation about the probabilistic methodology regarding slope stability is also addressed.

The final chapter provides the conclusion of the dissertation, including the critical analysis of the obtained results and proposed future developments.

2
LAND RECLAMATION

2.1. LAND RECLAMATION

Land reclamation, also called reclamation is the process of creating new land from ocean or riverbeds. It is aimed at increasing the amount of land that is available and suitable for being used. It requires heavy construction work and a great sort of machinery like bulldozers, scrapers, excavators and digging machines. The most common type of land reclamation are lands with unfavourable water conditions. In swampy areas or wet land, reclamation is aimed at increasing dry land. This is done by removing excess water from the soil by means of trenches or pipes that runs into the watercourses (Stauber et al., 2016).

Land reclamation can be achieved with a different number of methods. The type of method used depends on different aspects like the type of foundation soil, fill material, topography of the seabed and the availability of the different types of equipment.

2.1.1. DIRECT SOIL DUMPING

This type of method is used when the seabed is too deep or the underlying seabed soil is soft. A bottom-opening barge usually carries fill material from the borrow source and either sails with a self-propeller or is pushed by a powerful tugboat to the designated location. At the location, fill material is dumped by opening the bottom of the barge (Figure 2.1). Direct soil dumping is used not only for granular material but also for stiff and soft clay. However, dumping of soft clay is not appropriate for deeper seabed conditions since soft clay can be detached, and the environment can be affected (Bo & Choa, 2004). The dumping location is normally controlled by a global positioning system (GPS). However, bottom dumping alone cannot complete the reclamation because it can only operate up to 2 – 3 meters depth below sea level. The next level of fill has to be raised by hydraulic filling or other means.

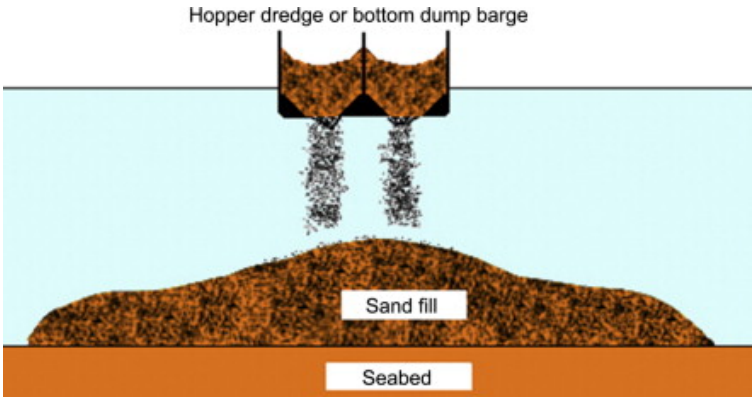


Figure 2.1 – Direct soil dumping method with bottom dump barge (Babak Hamidi, 2015)

2.1.2. Hydraulic Filling

When filling is carried out from an offshore foundation, either from a rehandling pit or from a trailer suction hopper dredger the hydraulic filling method can be used. This technique is normally appropriate for granular fill and not desirable when the seabed is too shallow or its soil is too soft. The percentage of fill material to water is adjusted corresponding to the grain size of the fill material. A large ratio of material to water would lead to wearing of the inner walls of the sand transportation pipe. In Figure 2.2 there is an example of hydraulic filling using direct pumping.

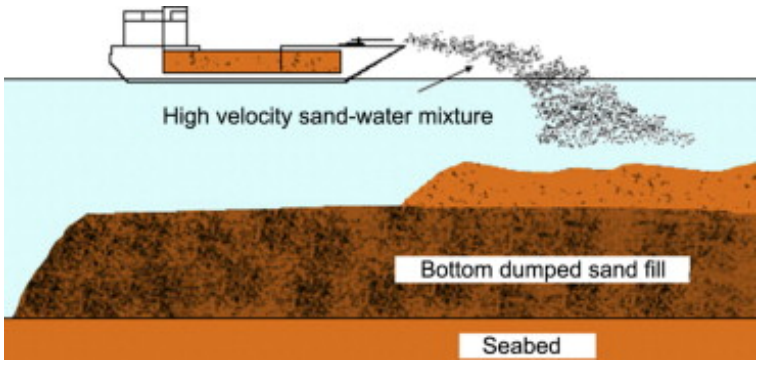


Figure 2.2 – Pipeline discharge method (Babak Hamidi, 2015)

Conversely, a lesser ratio of material to water will decrease the production rate. After a certain amount of land has formed, the pipes are extended accordingly. Pipes that have to run above water can be floated with floaters attached to the pipes. When the reclamation location is away from the dredger location, the rainbow pumping method (Figure 2.3) can be implemented (Bo & Choa, 2004).

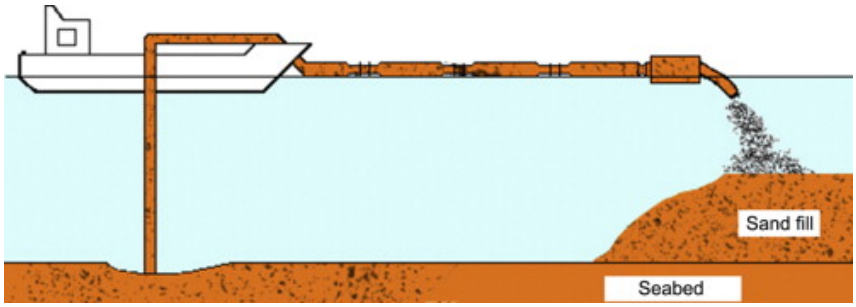


Figure 2.3 – Rainbow discharge method (Babak Hamidi, 2015)

2.1.3. Rotterdam Port

In the 1970s, one of the first major land reclamations was carried out, when the Port of Rotterdam in the Netherlands was extended. This was the start of the modern era of reclamation, which rapidly spread around the world (Duong, 2017). Netherlands is situated between Germany and France, where a great part of the land surface lies near or even below the sea level.

The Port of Rotterdam, also known as Maasvlakte 2 is a project for 240 million cubic metres of sand to create land, raise industrial sites and construct 7.5 kilometres of beach and dunes. It includes 7 million tonnes of riprap, 20000 concrete blocks, each weighing more than 40 tonnes and 150,000 tonnes of clay were processed in the 3.5 kilometres of hard seawall. Around 300,000 cubic metres of concrete was used in the construction of the quay walls (Port of Rotterdam, n.d.). By 2009, 400 million tons of cargo traveled through the port, but Rotterdam was nearing its capacity. To keep the port competitive, authorities undertook an ambitious project aimed at tripling the port's capacity (NASA Earth Observatory, n.d.). In Figure 2.4 it is possible to see the 2010 image of the Rotterdam Port with this second extension.



Figure 2.4 – Satellite image of Rotterdam Port in 2010 (NASA Earth Observatory, n.d.)

2.2. Soft Soil Dredging

Excavation in organic deposits will inevitably give rise to sediment spreading to the surrounding marine environment. The significance of sediment dispersal for the marine environment depends partly on the amounts of suspended sediment and partly on how much the sediment is dispersed. The consequences of sediment dispersal will form the basis for the limit values for sediment spreading that the contractor must comply with during the execution. The study carried out shows that the most important parameters that influence spillage during dredging are (COWI/AS, 2020):

- Gyttja properties (grain size distribution, strength, sensitivity, etc.)
- Dredging equipment
- Productivity (cubic meters of dredging per hour)
- Water depth
- Waves and currents

2.2.1. Mechanical Dredging Equipment

In order to conduct the excavation in the post glacial soft soil, a possible solution can be a backhoe dredger or a bucket dredger. The reason choosing one of this solutions is due to the expectancy that both of them to give rise to the least agitation of the gyttja and thus the least sediment spillage (i.e. less environmental impact).

A bucket dredger is a stationary dredger that is equipped with a continuous chain of buckets (Figure 2.5). The buckets are filled on the underside and emptied on the upper side into a chute along which the dredged material can slide into the barges moored alongside. Normally, bucket dredgers are used in dredging projects when the initial depth of the area to be dredged is too shallow for other dredgers and the distances involved are too long for hydraulic transport. For projects with environmental concerns, which require the dredging of in situ soil, the bucket dredger is a suitable equipment. When dredging construction materials such as sand, gravel, or minerals such as gold and tin ores, bucket dredgers are still frequently used (Vlasblom, 2004).



Figure 2.5 – Example of a non-self-propelled chain bucket dredger (Jiangsu ShunYou Shipping Engineering Co., Ltd, n.d.)

A backhoe dredger (Figure 2.6) is a type of mechanical dredging equipment. It consists of a hydraulic excavator mounted on a pontoon. The dredger bucket excavates the soil in a combined backward and upward movement of the boom, stick and bucket. When the bucket is full, an upward movement of the boom and stick lifts the bucket above the water to start swinging. The filled bucket is positioned above the barge by rotating the excavator on the turntable. The dredged material is then discharged into a transport barge. Finally, the full barge transports the dredged material to a designated location (Boskalis, n.d.). They can dredge a wide range of materials very precisely and mainly operate in shallow and enclosed waters.



Figure 2.6 – Example of a backhoe dredger (Seatools, n.d.)

There are some locations where the existence of contained gyttja requires a different dredging method, so that the risk of pollution spread can be minimised. By using a closed grab to excavate the material, sediment spills are expected to be limited. In fact, since the closed grabs confine the sediments, there is almost no spread of sediments when raising the grab through the sea water column. The disadvantage of using a closed grab is that production is expected to be lower than using an open grab or a bucket chain machine. An example of a closed environmental barrier is shown in Figure 2.7.



Figure 2.7 – Gosho, considered to be the biggest grab dredger in the world by (Kojimagumi, n.d.)

3
CASE STUDY

3.1. Project Introduction

Lynetteholm will be a future artificial peninsula, built outside the Copenhagen harbour. This artificial peninsula will span over 282 hectares over the North of Refshaleøen and will be delimited to the north with Nordhavn and to the west with the Trekroner (Figure 3.1). The main purpose for its construction is to prevent the city of Copenhagen from the occurrence of floods and storm surges. In fact, it is predicted that by the end of 2100, the sea level will rise between 54 cm (under the "Paris agreement") and 74 cm ("business as usual" scenario), according to the Geological Survey of Denmark and Greenland (GEUS). Lynetteholm is expected to be completed in 2070. The hope is that the first homes can begin building in 2035. It will cost around 20 billion Danish crowns (€2.7 billion) and will be self-financed, according to Miner (2018). There is the prediction that the payment received for disposing the waste earth and selling new land for construction will finance the construction of the peninsula.

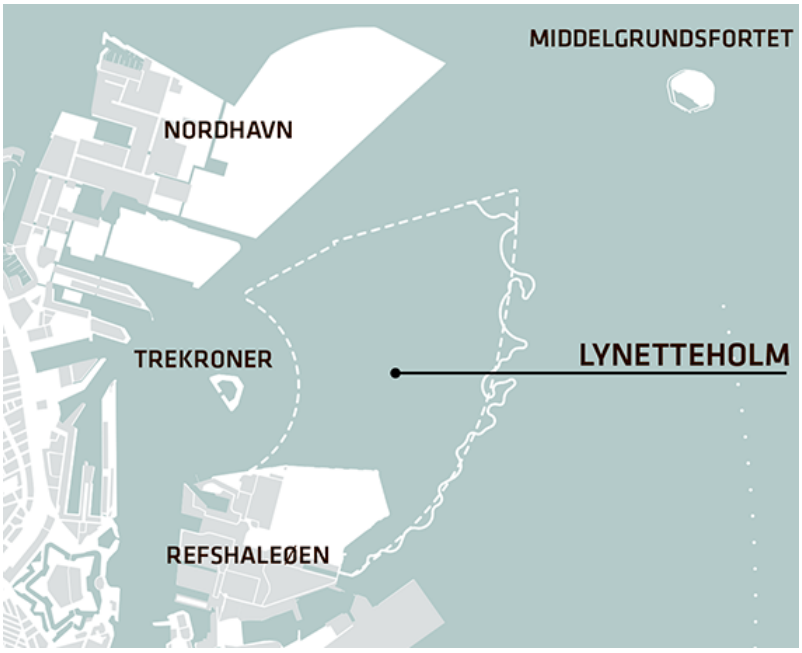


Figure 3.1 – Location of Lynetteholm with the representation of the two perimeter proposals (By og Havn, 2020)

3.1.1. URBAN DEVELOPMENT

Since the 1960s, Copenhagen has had a considerable suburban growth. The suburbanisation rate has slowed down in the 1980s due to population decrease and economical recession. However, since the 1990s, the region has experienced a significant economic and population growth, which led the migration of many households to the peri-urban and rural countryside areas (Fertner, 2012). With the construction of this new district, and since there will be approximately 35 000 new residents in this area, it is expected that the reduction of the traffic pressure from the city center will occur.

3.1.1.1. Østlig Ringvej

Additionally, further urban infrastructures such as the Østlig Ringvej are also predicted. This infrastructure will consist in a immersed road tunnel which connects the eastern part of the Metropolitan area. In practice it could be seen as an extension of the Northhavnsvej (which opened in 2017) and Nordhavnstunnel (expected to open in 2027) and thus could connect the Helsingør motorway in the north with either Amagermotorvejen or Øresundsmotorvejen (Figure 3.2) in the south.

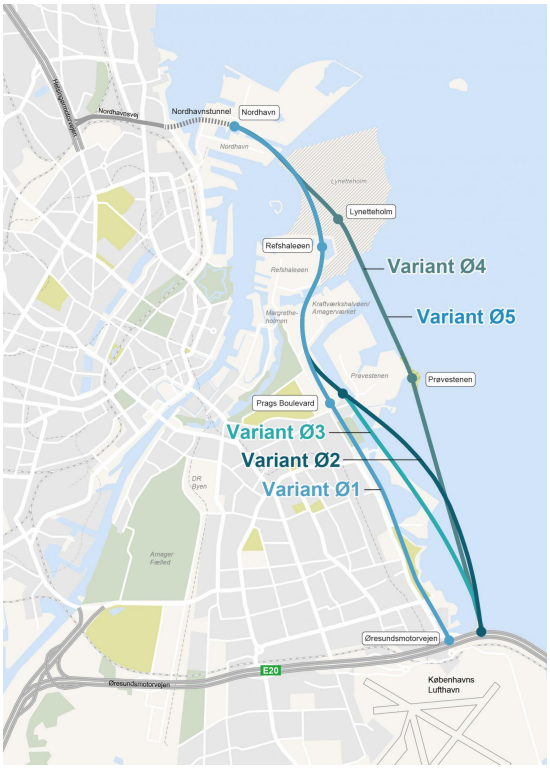


Figure 3.2 – Connection with Øresundsmotorvejen solution (KK, 2020)

3.1.1.2. Metro

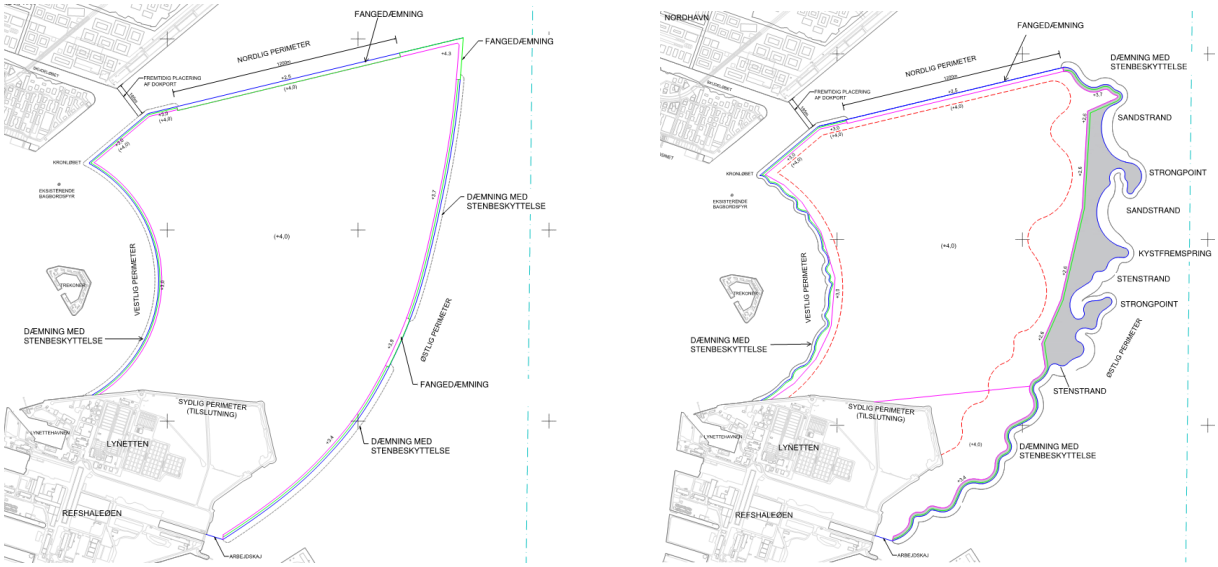
There is also the motivation to link the Lynetteholm with the city center with a metro line. The feasibility study of the metro maps three different line proposals that can intersect the area. The proposals have been assessed on the basis of, among other things, finances, passenger potential, capacity and travel time gains. Figure 3.3 shows the solution M4 for the blue line that goes from Orientkaj to Kløverparken



Figure 3.3 – Blue line solution (M4) (KK, 2020)

3.1.2. Design Proposals

Regarding the perimeter design layout, two final proposals were elaborated Figure 3.4. The first proposal didn't include any coastal landscape in the eastern part of the perimeter. Here the perimeter structures consisted in dams with stone protection. In the second one, the eastern perimeter was established with a coastal landscape where perimeter structures consisted of a combination of dams with rock protection and dams with the front with sand and rock for the beaches.



(a) (b)

Figure 3.4 – Design Proposals for Lynetteholm (a) first Proposal, (b) second proposal (COWI, 2020)

3.2. Local Geological Past

For long periods of the late Weichsel, the entire project area has been covered by an up to 2 km thick ice cap, the Scandinavian Ice Sheet (Figure 3.5). It reached its largest extent during three major ice thrusts from southern Norway through the Kattegat, from Sweden and finally east Jutland ice thrusts, which reached the East Jutland islands line and were followed by two re-propellers: the Belt and Øresund Glacier from the south-east through the Baltic Sea (Houmark-Nielsen, Krüger, & Kjær, 2005). The material of the ice has been deposited in the form of well-graded moraine deposits, silt, sand, gravel and stones, while in connection with the melting of the ice, meltwater formations of clay, silt, sand, gravel, stones and blocks below and in front of the ice rim have been set aside. The active ice was away from the Danish territory during the transition period between the last ice age, Weichsel, and the current ice age, the Holocene.

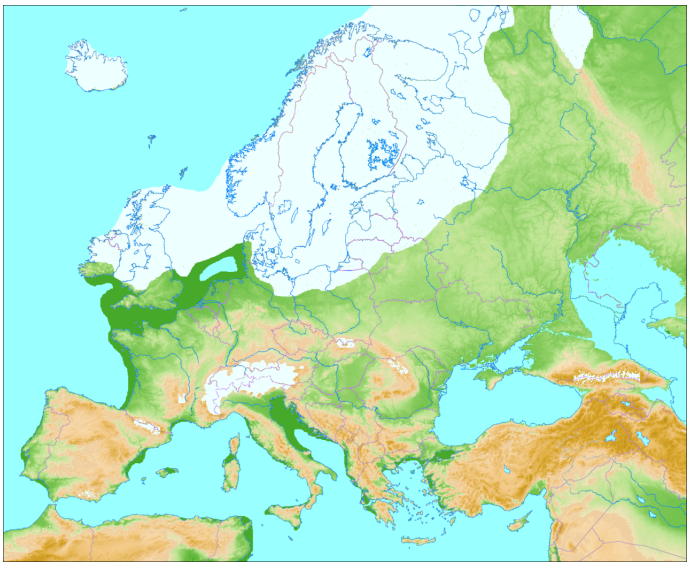


Figure 3.5 – Scandinavian Ice Sheild

After the melting of the ice, Denmark became settled with people from southern Sweden and southern England during the so-called *Senglacialtid*. During a period of about 6000-7000 years ago, large parts of the seabed were deposited in the Lynetteholm area as a land area. In the valleys, the glacial moraine and meltwater deposits are completely or partially eroded by river currents. A similar threshold of high limestone with flint layers prevented the river from digging deeper than to about 10-12 m below current sea level between Dragør and Limhamn, south of the project area (Richardt, Belhage, & Funder, 1999). Another threshold of high limestone crossing the project area from Trekroner to the east, prevented the river from digging deeper than to about -16 m below the sea water level. In the northern part of the project area, the river has eroded down from the level -23 until -25 m, while further north, in the northern parts of the Sound, reached down to about 40m below current sea mirror. In the last 2000 years of *Senglacialtid*, the Øresund (Richardt et al., 1999) dried up, after which the drainage of the freshwater lake took place through the middle of Swedish alleys.

3.3. Soil Conditions in Lynetteholm

3.3.1. In-situ campaign overview

COWI carried out extensive geotechnical studies in order to obtain factual geological, geotechnical and hydrogeological data for the area. The geotechnical studies included 301 CPTU tests and 191 boreholes (Figure 3.6).

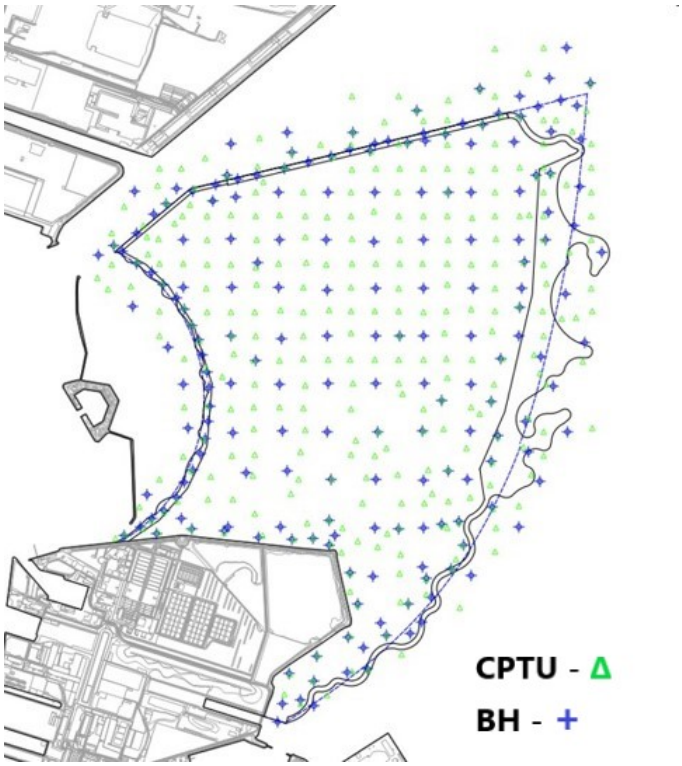


Figure 3.6 – Overall site test campaign (COWI, 2020)

3.3.2. Soil Model

Based on boreholes, CPTU and geophysics, COWI has developed a geological 3D model in the GeoScene3D program. The model is based on the general layer sequence in the geological model of Copenhagen area which divides the layer sequence into eight quaternary layers and two pre-quaternary layers as specified in Table 3.1.

Table 3.1 – Soil model layers

Era	Layers
Holocene	L1A: Fill
	L1B: Post glacial deposits
	Marine and freshwater organic deposits and clay
	Marine sand and gravel
Pleistocene	L2: Upper meltwater sand/gravel
	L3: Upper moraines and upper meltwaters/silt
	L4: Between meltwater sand/gravel
	L5: Lower moraines and medium/lower meltwaters/-silt
	L6A: Lower meltwater sand /gravel
	L6B: Lower moraines and lower meltwater/silt
Selandia	L7: Green Sands/Silt/Sand/Limestone
Danien	Copenhagen Limestone

3.3.2.1. Layers Description

Each layer has the following description:

- L1a: The top layer consists in filling material which is typically highly alternating and can include all grain fractions. Close to the harbour (to the west), the filling often consists in material from the dredging of harbour basins, mainly sand, which is locally mixed with gyttja. Ashes and slag from power plants, rubble, concrete rubble and other man-made components can be included in fill layers.
- L1b: Mixed with the fill, or in the harbour basin (directly from the seabed), post-glacial marine deposits are taken. The upper post-glacial layers typically consist in gyttja, which is locally overlaid by a relatively thin layer of marine sand. Gyttja is predominantly fat to very fat and contains touches of strong sandy gyttja and marine sand. In the lower parts of gyttja there are local freshwater/brackish deposits of peat. For several boreholes, layers of marine gyttja have been found under freshwater turf.
- L2, L4, L6a: The pleistocene layer sequence is divided into sand/gravel units, which primarily include deposits of meltwater sand and gravel containing moraine sand and gravel. In most of the Copenhagen area, as mentioned below, there are lower seabed and medium/lower meltwater/silt. Like the upper moraines, the moraine is very firm and locally rich in stones and blocks. Layers of meltwater and silt can also be included, as well as flakes of sand and moraine sand in the layer. Under the lower moraines, local lower meltwater sand/gravel, which can be sublayered locally by lower moraines and lower meltwater and silt.

- L3, L5, L6B: Intermediate clay units include predominantly moraines with touches of meltwater, silt and locally highly-clayed moraine sand and gravel. Moraine is usually sublayered between meltwater sand/gravel, which is typically taken between the upper and lower moraines. Locally, the sand has either not been deposited or has since been eroded.
- L7: The pre-quaternary surface consists either of green sand deposits from Zealand or Copenhagen limestone from danien. The green sand deposits include green sands, silt, sand and limestone and are mainly taken in the westernmost parts of the project area. During the green sand deposits, or directly below the quarterly deposits where green sand deposits have been eroded, danien limestone is taken. Copenhagen limestone is divided into three units: upper, medium and lower Copenhagen limestone based on litology and geophysical log stratigraphy.

3.3.3. Post-Glacial Deposits Thickness

Based on boreholes and CPTU, a thickness map was developed indicating the thickness of soft post-glacial deposits, including gyttja, peat and clay. The thickness of the organic post-glacial deposits are greatest in the former meltwater valleys, where up to 6-9 m thick layers of gyttja and peat have been taken. On top of the gyttja layers, slag that was thrown overboard from steamships is frequently found. The map in Figure 3.7 indicates the gyttja thickness throughout the entire study area. It is possible to identify three areas that possess a high level of thickness in the perimeter of Lynetteholm in which it is included the mid-east, north-east and mid-western part where the soft soil thickness are higher than 6m.

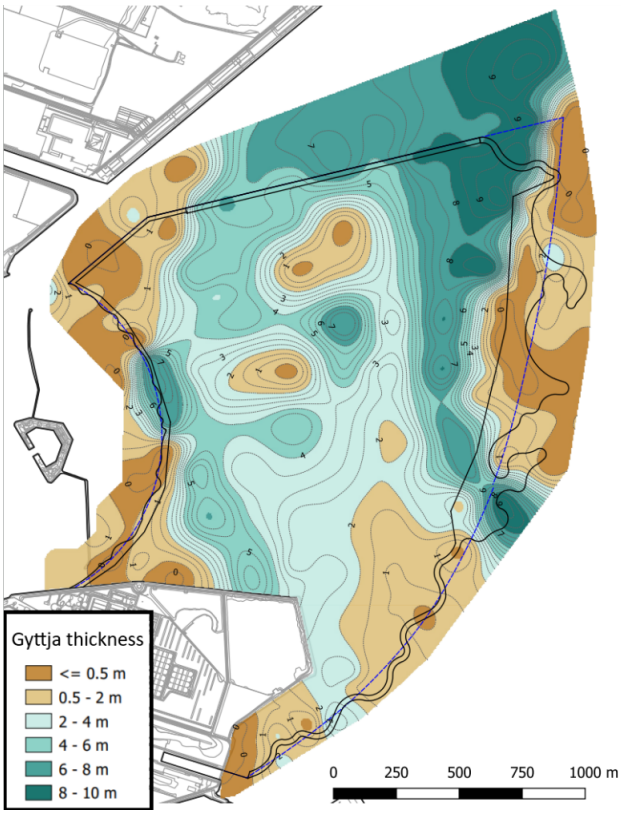


Figure 3.7 – Gyttja thickness map

3.3.4. GYTTJA

Gyttja is a very soft and odorous soil that originates from remains of plants and animals rich in fats and proteins. The material consists of both organic matter and inorganic (clay, silt, fine sand, shells or limescale). During its formation, varying quantities of inorganic material are mixed with the organic and when examined, a lower loss of filament and water content is found which is common for peat. This soil often has a grey-green colour, and it is a mixture of fine-grained, organic material with inorganic particles (Larsen et al., 1995).



(a) Shelly gyttja sample



(b) Organic gyttja sample

Figure 3.8 – Different samples of gyttja (Wikipedia, n.d.)

3.3.4.1. Organic Content

Based on 235 samples it was determined the organic content of gyttja based on the loss on ignition method. This method determines the organic matter content of soil by oxidizing organic matter to CO2 at an elevated temperature in a muffle furnace and measuring the weight loss (Zhang, Wang, Sikora, & Moore, 2014). In Figure 3.9 the organic content in the gyttja samples is represented.

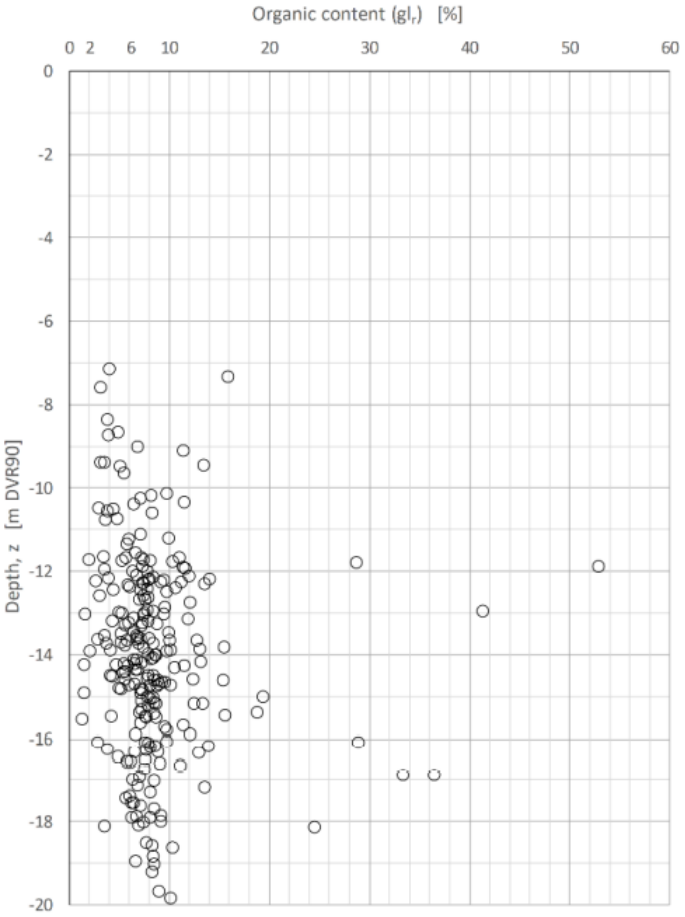


Figure 3.9 – Organic content in gyttja samples

The average value obtained for this property is 7.83%. With the information included in the Figure 3.10 it is possible to say that the project area material is a medium organic soil, corresponding to a clayey gyttja designation.

Soil group	Organic content in weight % of dry material (<2 mm)	Examples of designations
Low-organic soils	2-6	Gyttja-bearing clay Dy-bearing silt Humus-bearing sand
Medium-organic soils	6-20	Clayey gyttja Silty dy Humus-rich sand
High-organic soils	>20	Gyttja Dy Peat Humus-rich topsoil

Figure 3.10 – Soil categories based on organic content (Larsson, 1990)

3.3.4.2. Soil Plasticity

One of the methods widely used in engineering practice to classify plastic soils is the Casagrande chart that relates the plasticity index with the liquid limit. Figure 3.11 reveals the sampling distribution for the plasticity chart. This soil categories were modified to suit the Danish deposits. It can be observed that most of the samples are included in the category of clay of high plasticity (CH) and gyttja of high plasticity (OH).

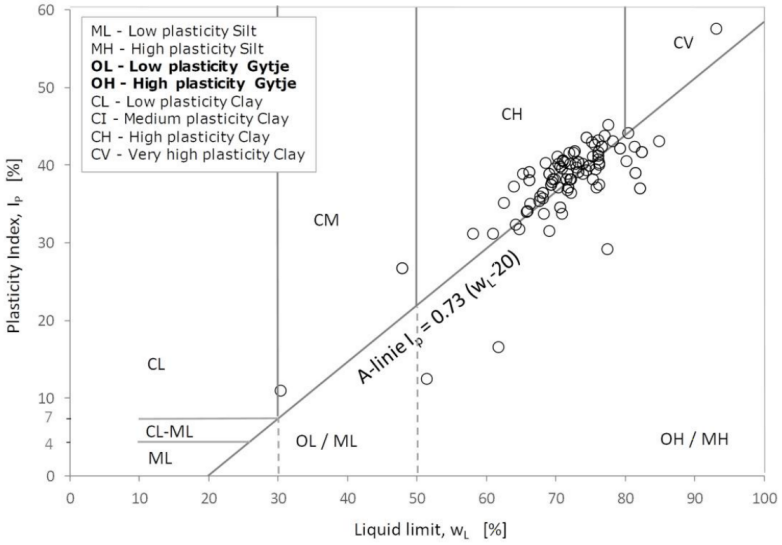


Figure 3.11 – Gyttja samples distribution in the Casagrande chart (COWI/AS, 2020)

3.3.4.3. Sensitivity

One interesting property to evaluate in a very soft soil like gyttja is the sensitivity, S_t, which can be used to determine the ability of a certain soil to loose resistance when remoulded. It can be obtained dividing the undrained shear strength, c_u, of the intact soil by the remoulded one, c_{ur} (Matos Fernandes, 2016).

$$S_t = \frac{c_u}{c_{ur}} \tag{3.1}$$

The sensitivity analysis was determined for using different geotechnical tests. It was evaluated using vane shear tests, VST, directly from triaxial tests, CAUC, and from a linear regression obtained from the triaxial tests. In Figure 3.12 it is possible to observe signs of low sensitivity for the VST. A great dispersion of results is observed for both the triaxial test approaches.

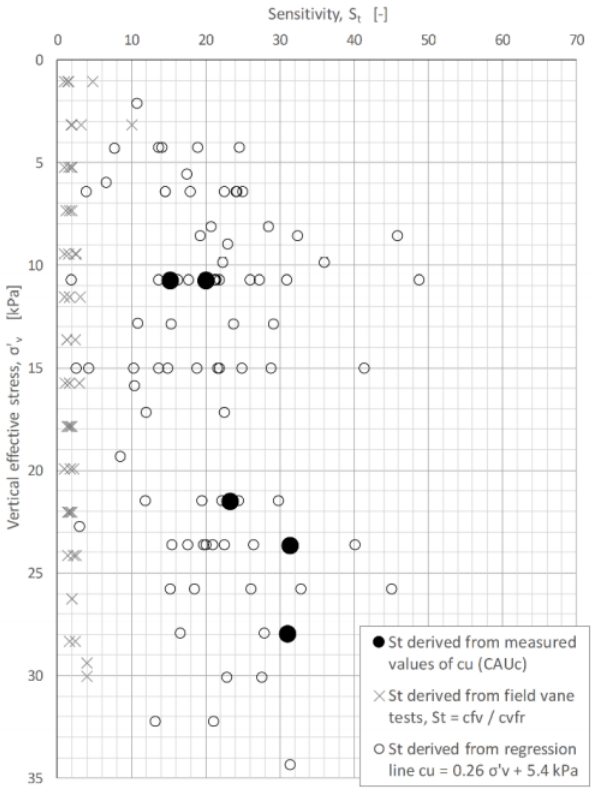


Figure 3.12 – Measured gyttja sensitivity based on VST and CAUC (COWI/AS, 2020)

Previous experience with similar soils observed by Larsson (1990), concluded that the sensitivity of organic clay and gyttja is relatively low in comparison to normal values for inorganic soft clays in Sweden. The range varied mainly from $5 < S_t < 14$, performed by fall cone tests. Karlsson and Hansbo (1989) proposed a sensitivity classification, according to the Swedish classification system (Table 3.2). However the design experience from COWI with this soil reveals that there is no signs of sensitivity in practice.

Table 3.2 – Sensitivity classification of clay, according to the Swedish classification system (Karlsson & Hansbo, 1989)

Designation	Sensitivity, S_t
Low-sensitive	<8
Medium-sensitive	8-30
High-sensitive	>30

3.4. PROBLEM DESCRIPTION

The first step for the construction of this land reclamation project is to build perimeter elements that can sustain the soil placed inside. In order to do so it is necessary to create perimeter structures like sheet pile walls and embankments to create a protection for the filling works inside the peninsula. An example of perimeter structures for land reclamation projects in shown in Figure 3.13 for the Airbus facilities in a area reclaimed to the Elba river in Germany.



Figure 3.13 – Example of a perimeter structure from a land reclamation project (Structurae, n.d.)

In the study case analyzed in this work, the perimeter structures comprise sections with sheet pile walls, but also sections with embankments. This chapter is dedicated to analyze the stability of one of those embankments. On Table 3.3 the construction steps for this particular section are described, which is important to understand the performed stability analysis. In the following, each one of these steps will be described in detail.

Table 3.3 – Construction phase description

Phase	Description
0	Initial soil conditions
1	Excavation of gyttja from perimeter cross section
2	Filling of the foundation gap with sand
3	Construction of the perimeter embankment
4	Filling the peninsula with borrowed fill material

As it was previously referred, the soil conditions that were considered for stability purposes, consisted simply in a single layer of gyttja above the limestone. Figure 3.14 shows a schematic profile of the soil profile. It should be noted that the main geometrical variables that change throughout the perimeter are the gyttja layer thickness and the sea water depth.

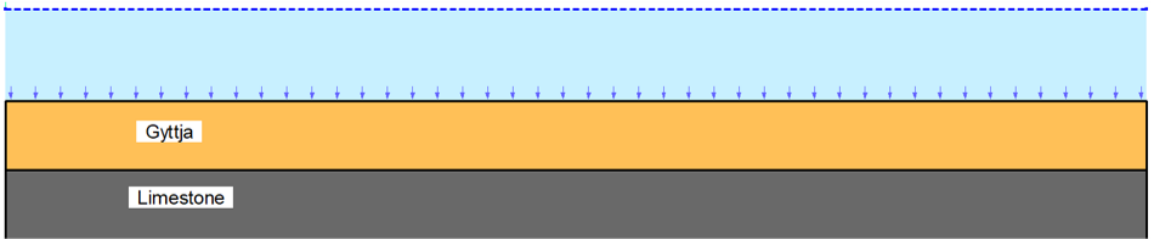


Figure 3.14 – Phase 0 of perimeter cross section

Based on the information from the gyttja thickness map, plotted in Figure 3.15 it was decided to create 3 slope scenarios that would represent the entire perimeter based on the depth of this post glacial deposit (3m, 6m and 9m depth). Figure 3.15 also shows the three selected scenarios indicating (from a simplistic point of view) the extension and location of each scenario around the perimeter.

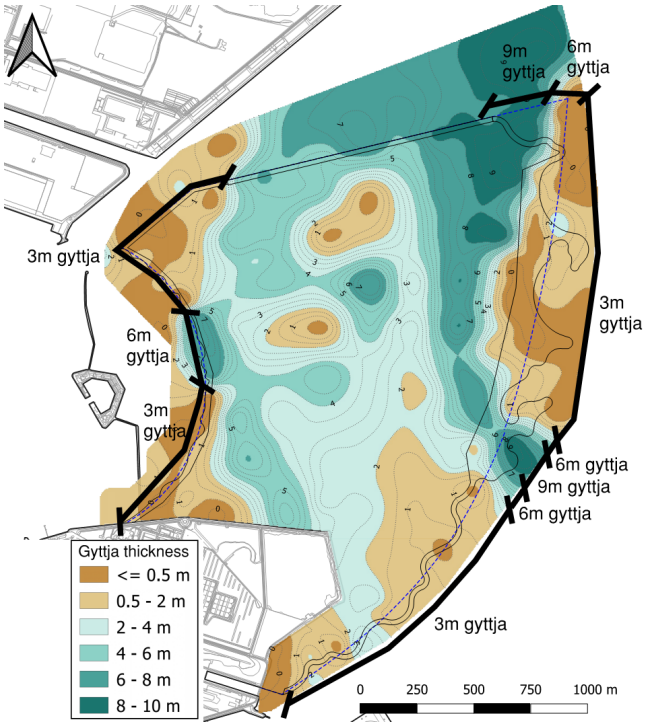


Figure 3.15 – Gyttja thickness map indicating the slope scenarios perimeter location considered

For the determination of the sea water level for each scenario, it was admitted a single water depth for each soil thickness according to Figure 3.15. The selection of the water depth for each scenario was performed by a visual average value within each one of gyttja thickness scenario. The reference water depths for each scenario is mentioned in Figure 3.16.

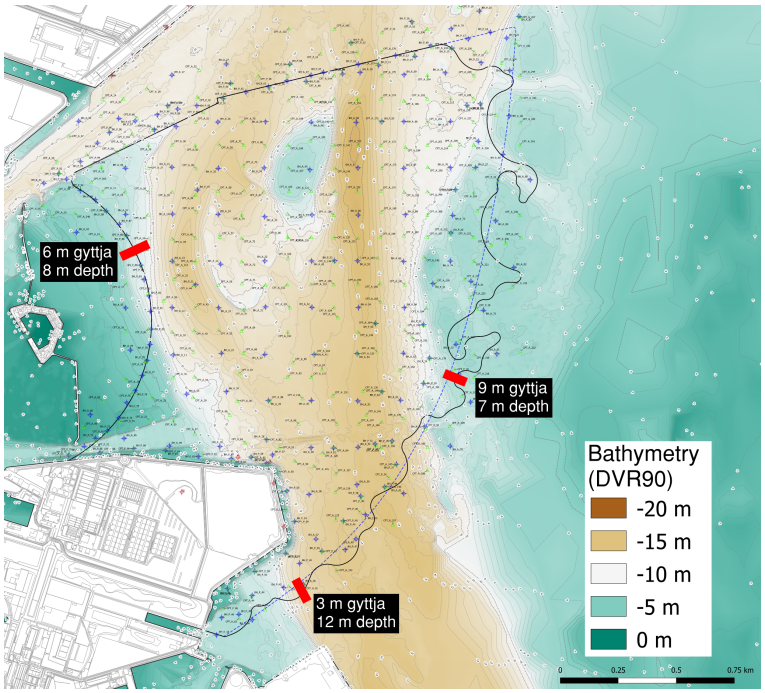


Figure 3.16 – Bathymetry map from the project area

In Table 3.4 it is indicated the matching information for both water and soil depth.

Table 3.4 – Correspondent gyttja and sea water level depth considered

Gyttja depth (m)	Bathymetry (m)
3	12
6	8
9	7

The first phase, as described in Figure 3.17 will be the excavation of gyttja for the foundation of the future perimeter embankment. Based on studies carried out by COWI, the waste percentage of excavation in gyttja is expected to be a maximum of 15%. The focus of this stability analysis will be the determination of the optimal slope of gyttja for both sides of the cross section that guaranties safety. For each slope scenario considered it was created four different slope geometries (1:3, 1:2, 2:3, 1:1) that are current slopes for engineering practice. From local experience in similar soils it is not recommended to consider slopes steeper than 1:1.

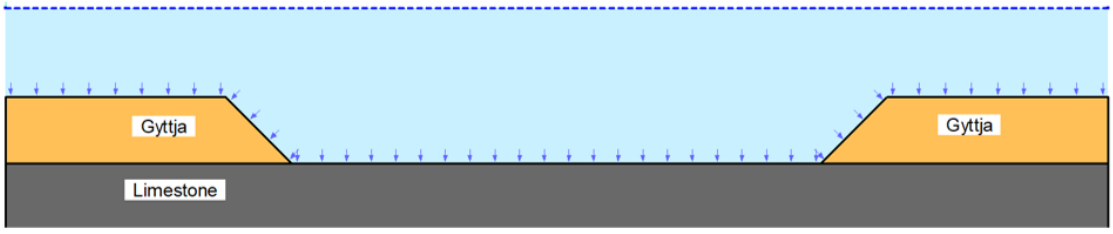


Figure 3.17 – Phase 1 of perimeter cross section

Since gyttja is a very soft and collapsible soil, it was decided, for safety purposes to dredge all this material that is contained between the perimeter embankment and replace it with sand fill Figure 3.18. This procedure will result in an improvement of the foundation bearing capacity for the construction of the future embankment.

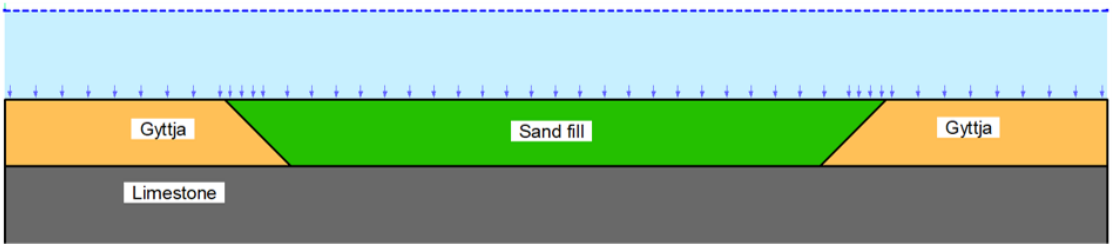


Figure 3.18 – Phase 2 of perimeter cross section

The next step will be the construction of the perimeter embankment above the sand fill layer (Figure 3.19). The soil that will be used for the construction of this structure will be mainly sand and gravel. There will be also the inclusion of an erosion protection capping layer on the external part of the embankment. Finally, will be conducted the filling inside the peninsula with borrow material from excavations (Figure 3.20).

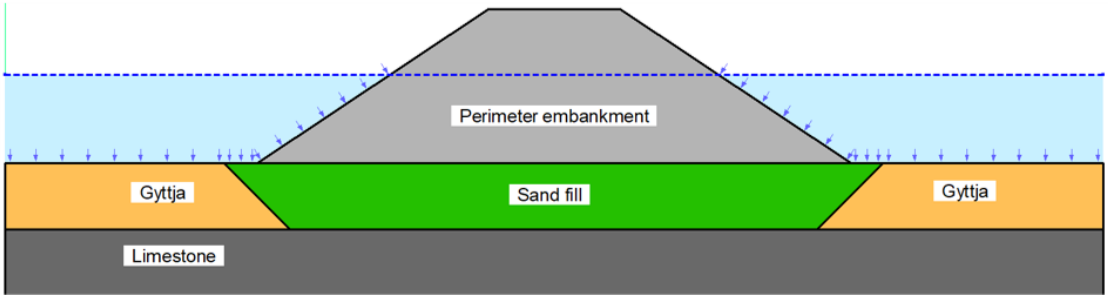


Figure 3.19 – Phase 3 of perimeter cross section

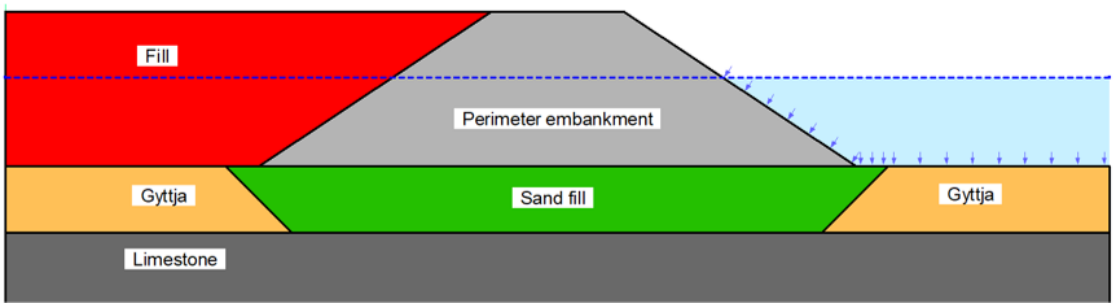


Figure 3.20 – Phase 4 of perimeter cross section

4
GEOTECHNICAL DATA

4.1. CPTU DATA

The CPTU campaign consisted in 302 tests done around the entire area of the project. Those tests will be used herein to characterize the soil, using the parameters directly obtained from the CPTU (i.e cone resistance, pore pressure and sleeve friction). The method to evaluate the gyttja thickness from those tests and the behaviour type of this soil (proposed from different authors) is also evaluated.

4.1.1. TEST DESCRIPTION

The Cone penetration test, CPT is a geotechnical in-situ test widely used in the world. It was developed in 1932 and the first tests were carried out by Pieter Barentsen, who was an engineer in Rijkwaterstaat, Holland. The test is conducted by pushing the cone penetrometer vertically through the soil with a rig that usually consists of a hydraulic jack and a reaction system. The cone penetrometer is mounted on a string of rods that are used to push down the cone, while measuring cone tip resistance, q_c, sleeve friction, f_s, and pore pressure, u_2 (Lunne et al., 1997). Further, the depth and time are also registered, while the testing is conducted. The description of the cone penetrometer is shown in Figure 4.1.

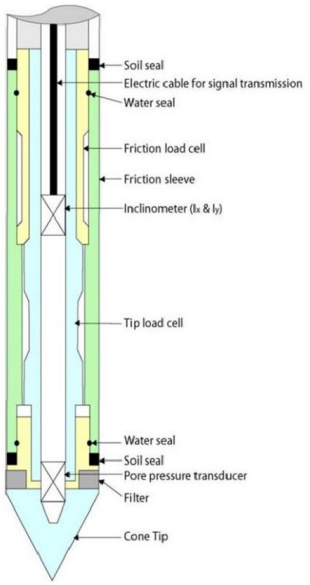


Figure 4.1 – CPTU equipment representation

4.1.2. Derived Geotechnical Parameters

When the piezocone was introduced in the CPT, becaming CPTU, it was necessary to correct the raw cone resistance, q_c, in order to take into account this pore water pressure measurement. This is explained by the cone geometry where there is the existence of an unequal area effect which is taken into account by the area factor, a. This ratio results in the division of the cross sectional area of the load cell, A_n by the projected area of the cone, A_c (Matos Fernandes, 2015).

$$a = \frac{A_n}{A_c} \tag{4.1}$$

Two different piezocones were used for the CPTU campaign which possesses the area factors represented in Table 4.1.

Table 4.1 – Area factors for all the CPTU

area factor, a	Number of CPTU
0.6	193
0.8	109

In order to determine a, a calibration vessel and a penetrometer is used. The pressure in the vessel is increased in increments and the readings of q_c and f_s are then taken. Ideally, this value should be close to 1.0 to maximize the measurements efficiency (Lunne et al., 1997). As a result, the cone area ratio can be then calculated, by plotting the cone resistance against the applied pressure and measure the slope of each line (Figure 4.2).

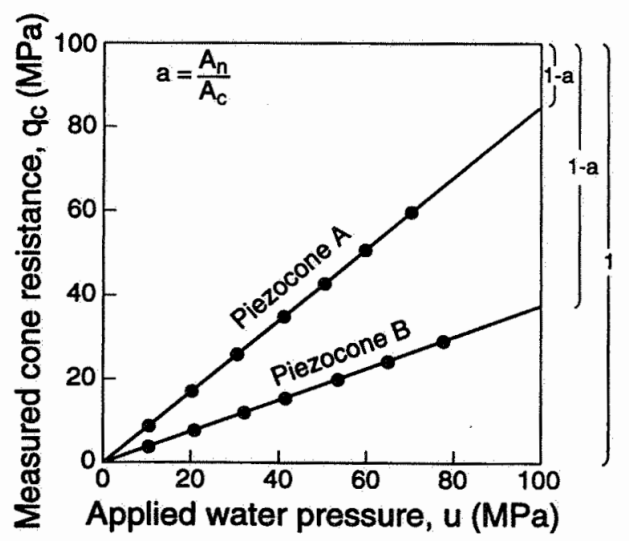


Figure 4.2 – Determination of the cone area ration in a calibration vessel (Lunne et al., 1997)

In very soft fine-grained soils, which is the focus of this work, this correction has a major contribution to the corrected total cone resistance, q_t. In fact since the values of q_c are normally very low in this type of soils, combined with the fact that the pore water pressure behind the cone, u_2, is normally high

(considering its undrained behaviour), it is mandatory to normalize the cone resistance (Matos Fernandes, 2015). The corrected total cone resistance (q_t) is given by the following equation:

$$q_t = q_c + u_2(1-a) \tag{4.2}$$

4.1.3. Data Presentation

As previously refereed, the CPTU campaign consisted in 302 tests done around the entire area of the project. Each CPTU dataset was imported to a Python environment where every test was compiled into one single dataset. It combines a total an amount of 80016 readings. Different geotechnical parameters were plotted in order to visualize the overall trend and scatter for each graph.

4.1.3.1. CPTU Readings Errors

When filtering the CPTU data, and producing the scatters for the CPTU parameters it was evident that some CPTU results had negative readings in the cone resistance, q_c. This can be explained by the fact that the soil in its superficial parts is so soft that only the weight of the CPTU equipment in enough to introduce the CPTU the gyttja layer. In order to correct this occurrence, it was imposed that only the positive readings were considered (i.e $q_c > 0$ MPa). Figure 4.3 demonstrates an example of reading errors for the CPT_A_111 result in the first 16cm of penetration.

Depth m	Cone MPa
0.000	0.0000
0.002	-0.0024
0.009	0.0000
0.018	0.0001
0.026	-0.0020
0.035	-0.0075
0.044	-0.0072
0.053	-0.0074
0.062	-0.0069
0.071	-0.0074
0.081	-0.0074
0.090	-0.0074
0.100	-0.0074
0.110	-0.0074
0.119	-0.0069
0.129	-0.0070
0.139	-0.0078
0.149	-0.0078
0.160	-0.0069

Figure 4.3 – Cone resistance readings in the first 16cm depth of specimen CPT_A_111

4.1.4. CPTU Parameters

In Figure 4.4 the cone resistance, q_c, evolution with depth is presented which came directly from the raw measurements of the tests. It reveals a general increment of q_c with depth. Overall at the seabed level the data is more concentrated between $0.0 < qc < 0.2$ (MPa) and $0.2 < qc < 0.4$ (MPa) at the bottom of this post glacial deposit.

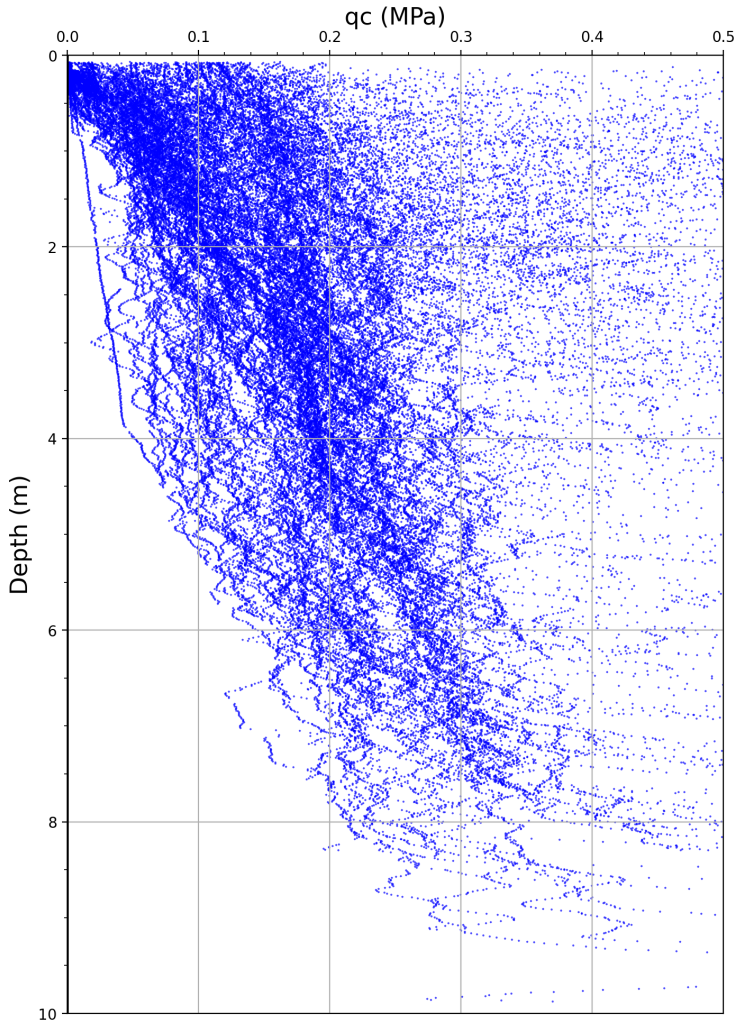


Figure 4.4 – Cone resistance, q_c, evolution with depth for the entire CPTU data

Regarding the pore pressure parameter, u_2 it also possible to observe a natural increment with depth Figure 4.5. A curious aspect that is clear to observe is the existence of 2 distinct trends of evolution where in between the two of them, exists a data gap of approximately 50 kPa. Visually it is possible to also conclude that the left trend possesses a higher concentration of points than the other one on the right. However it was not possible to reach a conclusion to understand the reason behind this 2 different trends.

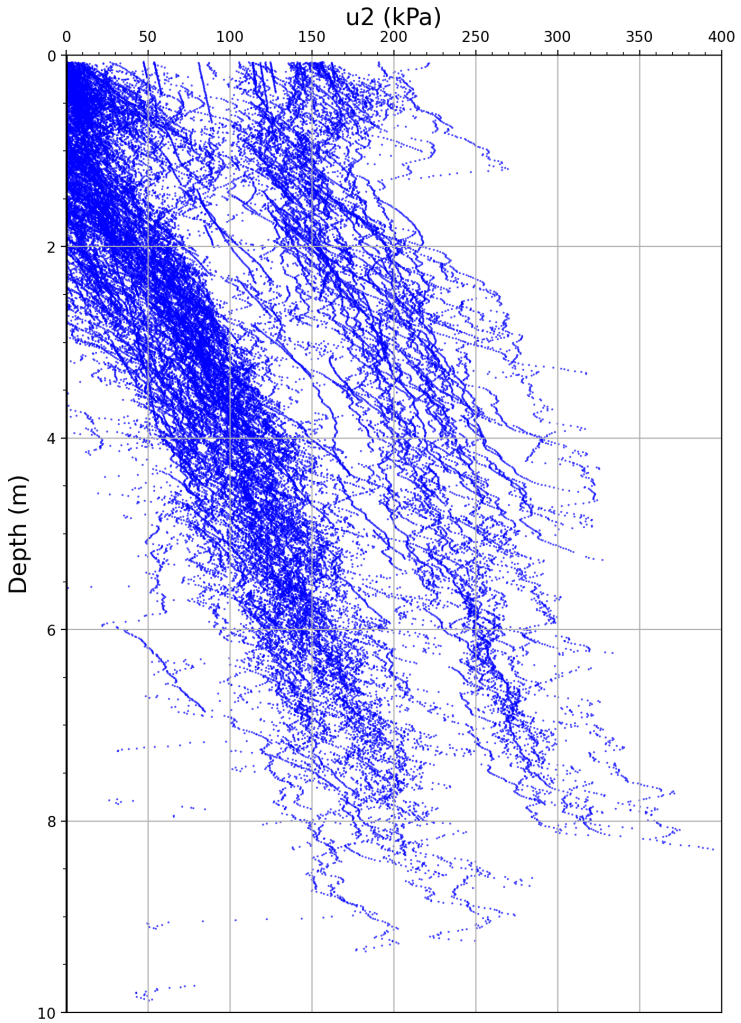


Figure 4.5 – Pore pressure, u_2, evolution with depth for the entire CPTU data

On Figure 4.6 it is possible to observe the plot for the q_t, where it is revealed, as expected, low values for the normalized cone resistance. Almost all of the data fits in the interval of $0 < q_t < 0.6$ (MPa). Generally speaking, the q_t values are higher than the q_c, revealing the expected undrained behaviour explained by the excess of pore pressure created by the cone when penetrating the soil.

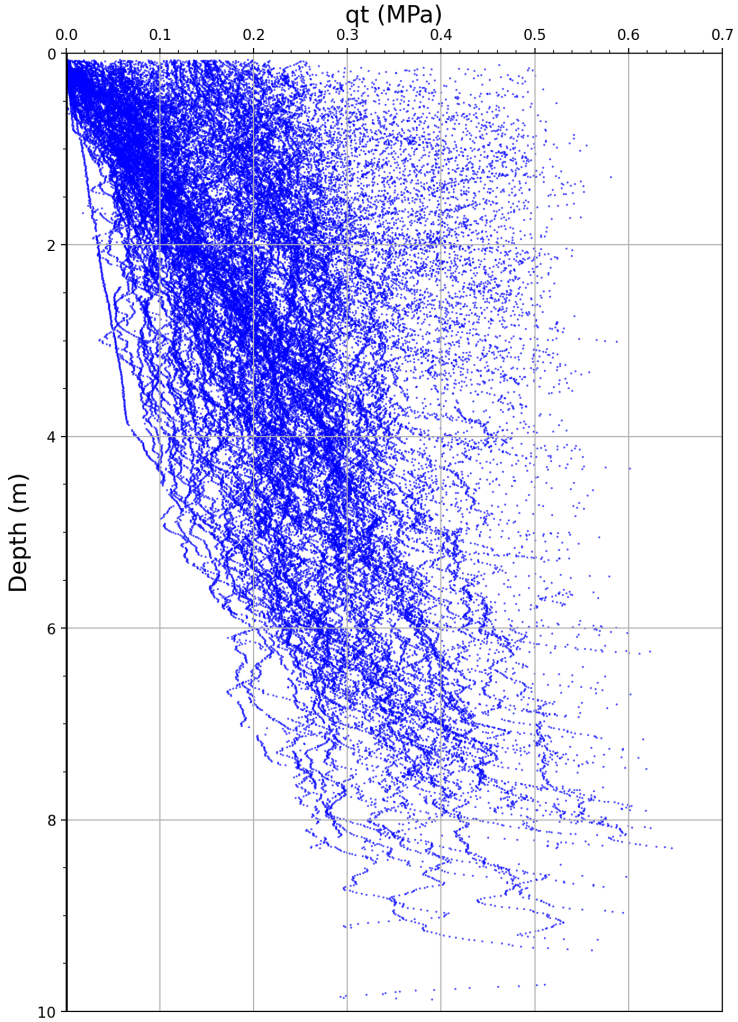


Figure 4.6 – Normalized cone resistance, q_t, evolution with depth for the entire CPTU data

In Figure 4.7 is represented the sleeve friction, f_s, where most of the points are below 10 kPa, being the higher concentration below 5 kPa. It reveals an almost uniform evolution with depth where it exists a higher density of data within the interval of about 5 kPa.

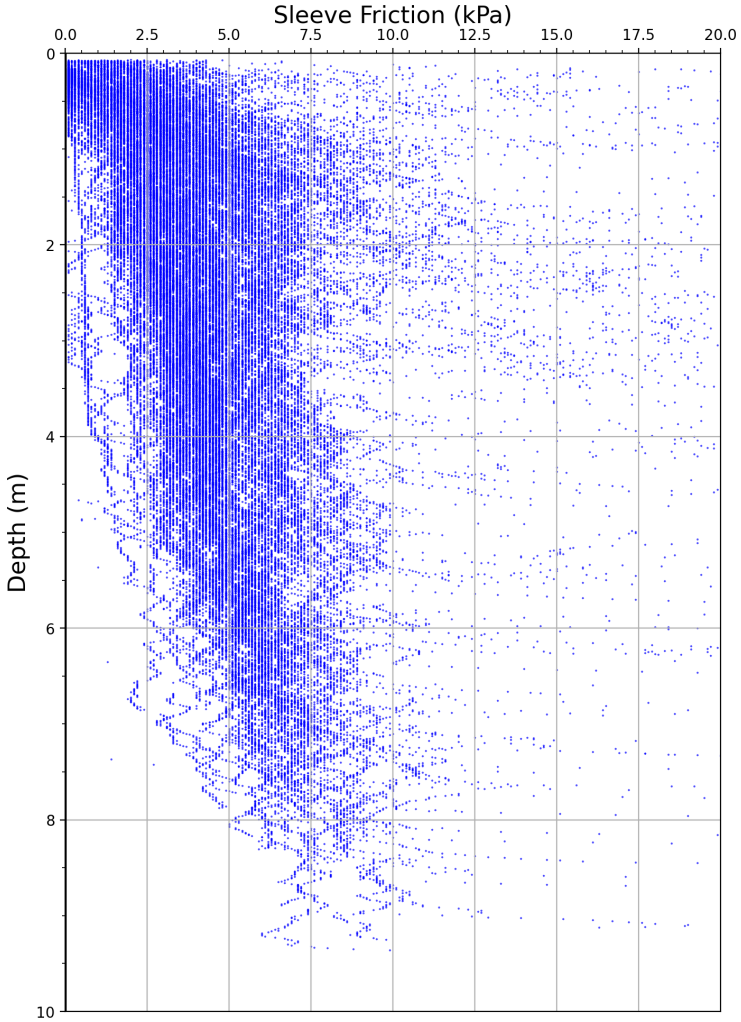


Figure 4.7 – Sleeve friction, f_s, evolution with depth for the entire CPTU data

4.1.5. Gyttja Thickness Evaluation

The CPTU were typically stopped just below or a few meters below the post-glacial deposits where it is possible to see a rapid increase of the tip resistance. The gyttja layer limits in the CPTU tests were set visually (manual reading), based on the CPTU peak resistance, q_c. Considering the fact that gyttja is a very soft soil that often presents a very low resistance to penetration, there is the possibility to estimate the layer depth based on that CPTU data. However since this test doesn't allow to collect samples it is also important to take into account the nearby borehole logs in order to add more certainty to the layering assessment. In Figure 4.8 it is revealed the typical CPTU log intercepting a low resistance soil.

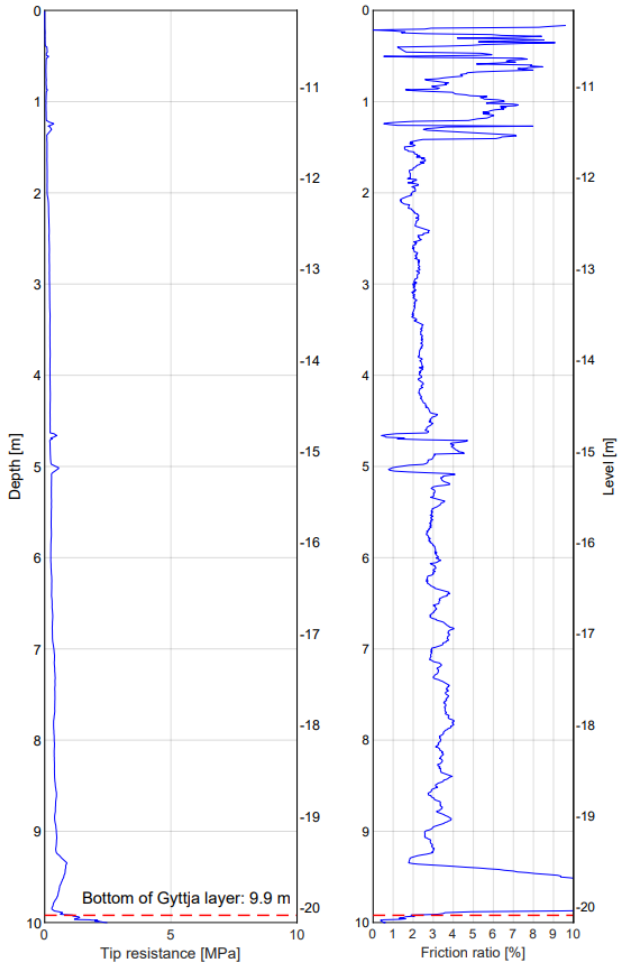


Figure 4.8 – CPTU single specimen tip resistance (q_c) and friction sleeve stress (f_s)

Based on the CPTU resistance trend, the penetrated layers are classed in two main groups based on:

- Post-glacial deposits (mainly gyttja with features of post-glacial sand and fill)
- Stiff soil deposits (mostly limestone and moraines in some parts of the area)

4.1.6. CPTU Soil Classification Charts

With CPTU it is also possible to execute soil profiling and understand the soil type. Typically q_t is high in sands and low in soft clays and the friction ratio ($R_f = f_s/q_t$) is low in sands and high in clays. Even thought the CPTU cannot be expected to provide accurate predictions of soil type based on physical characteristics, such as, grain size distribution, it can provide a guide to the mechanical characteristics (strength, stiffness and compressibility) of the soil, or the soil behavior type, SBT (Robertson & Cabal, 2014).

4.1.6.1. Non-Normalized Charts (SBT)

One of the most commonly used CPTU soil behavior type (SBT) chart (Figure 4.9) was suggested by (Robertson et al., 1986) which uses the basic CPTU parameters of cone penetration (q_t and R_f). Is is considered that this chart can provide reasonable predictions of soil behavior type for CPTU soundings up to about 20m in depth.

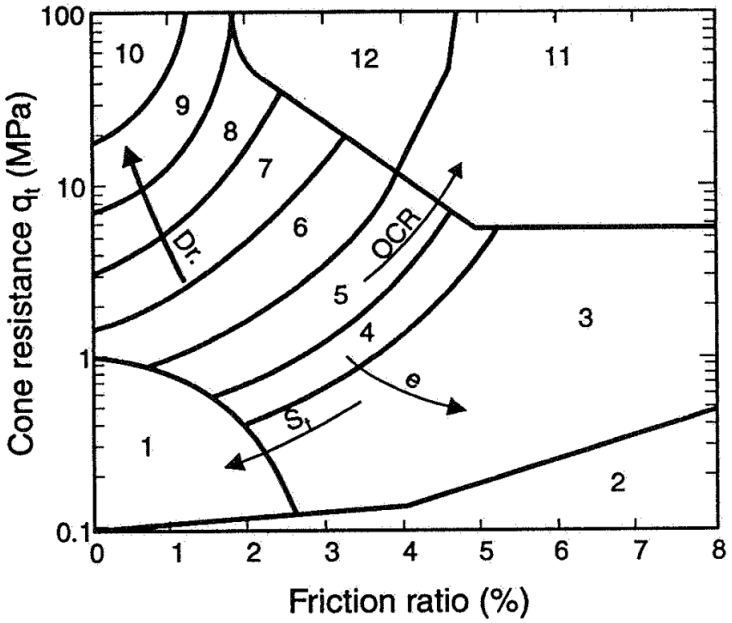


Figure 4.9 – CPT soil behaviour type classification chart (Robertson et al., 1986)

Table 4.2 – Soil behaviour type description from (Robertson et al., 1986)

Zone	Soil Behaviour Type
1	Sensitive Fine-Grained
2	Organic Soil
3	Clay
4	Clay to Silty Clay
5	Silty Clay to Clayey Silt
6	Clayey Silt to Sandy Silt
7	Sandy Silt to Silty Sand
8	Silty Sand to Sand
9	Sand
10	Sand to Gravely Sand
11	Very Stiff Fine-Grained
12	Overconsolidated or Cemented Sand to Clayey Sand

In Figure 4.10 it is represented the soil behaviour chart from the post glacial deposits in the project area. It is possible to observe a reasonable result in this chart (mostly zones 1,2 and 3). In fact, despite this soil doesn't appear to have sensitivity in practice, it shows signs of this parameter from the conducted tests. The organic classification also makes sense since this soil has a fair amount of organic matter. Since this is a very fine grained soil, the clay type behaviour is also expectable from the zone 3 area in the chart.

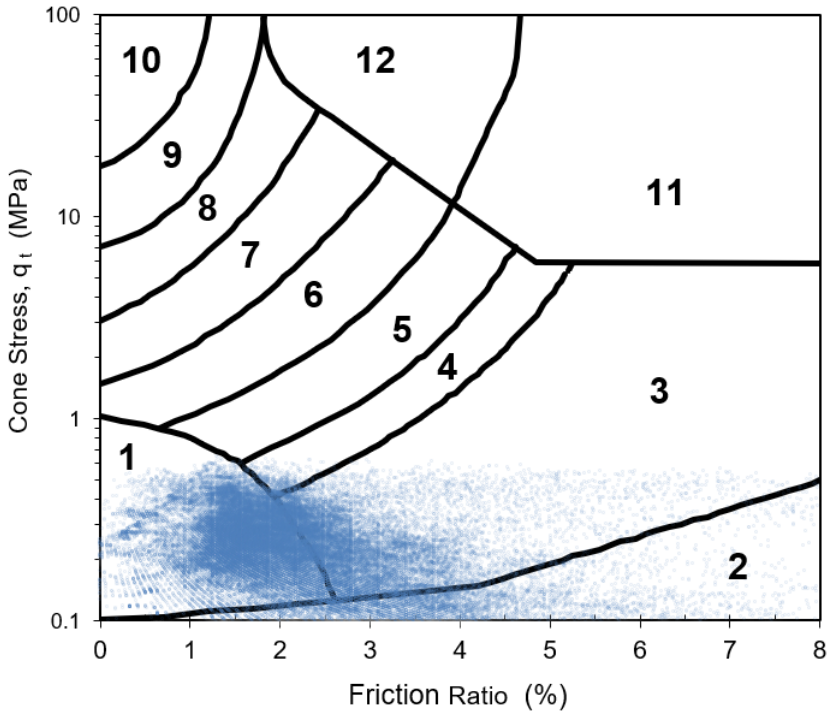


Figure 4.10 – CPTU Soil behaviour chart with CPTU data

In order to understand the soil behaviour with depth, Robertson (2010) proposed a soil classification chart based on the non-normalized soil behaviour classification represented in Figure 4.9, where is represented the soil classification along the depth. This classification for gyttja is represented in Figure 4.11 where it is possible to observe in the yellow scatter, the CPTU readings inserted in the classification chart. This graph was obtained from the CPeT-IT software, connecting the 80016 readings stored in a single python dataframe to CPeT-IT.

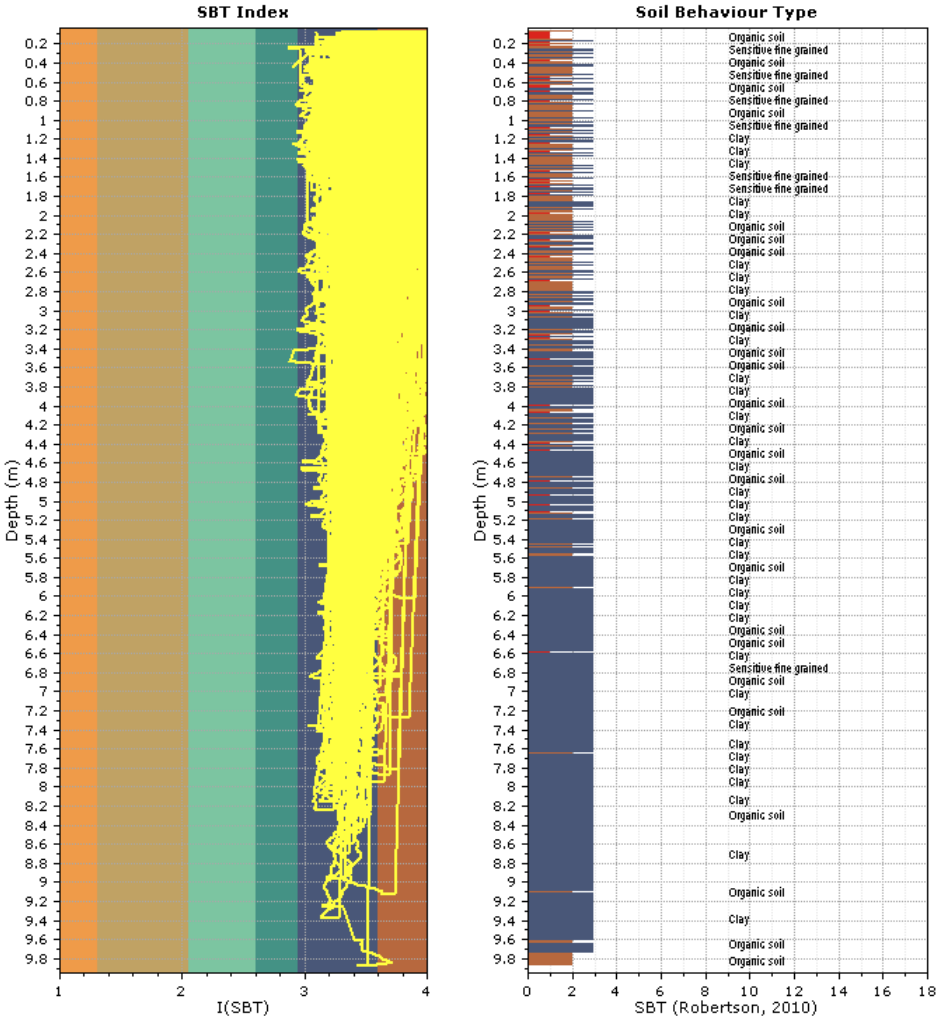


Figure 4.11 – Soil behaviour type variation with depth classification from (Robertson, 2010)

4.1.6.2. Normalized Charts (SBT$_n$)

Since both q_t and f_s increase with depth due to the increase of effective overburden stress, σ'_{v0}, the CPTU data requires normalization for overburden stress (Lunne et al., 1997). For that reason, instead of using q_t, this chart uses the normalized cone resistance, Q_t, and normalized friction ratio, F_r, that can be determined by the following equations:

$$Q_t = \frac{q_t - \sigma_{vo}}{\sigma'_{vo}} \tag{4.3}$$

$$F_r = \frac{f_s}{q_t - \sigma_{vo}} \tag{4.4}$$

Robertson (1990) proposed a CPTU soil behavior chart based on normalized CPTU data, shown in Figure 4.12. A zone has been identified in which the CPTU results will plot for most young, uncemented, insensitive and normally consolidated soils. The chart identifies general trends in ground response, such

as, increasing soil density, OCR, age and cementation for sandy soils. In cohesive soils the increasing stress history, OCR, and soil sensitivity, S_t, are the main parameters achieved. It is important to realise that this chart is global in nature and provides only a guide to soil behavior type (SBT). Overlap in some zones should be expected and zones can be modified based on local experience.

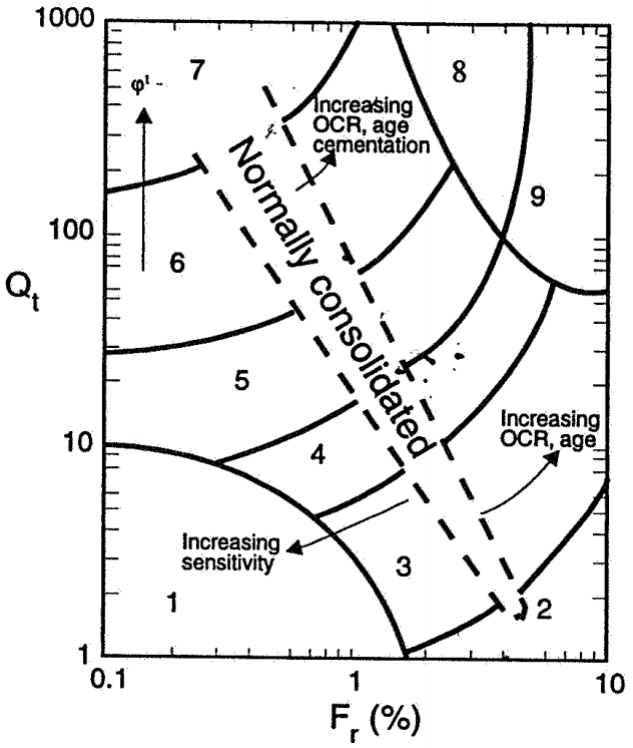


Figure 4.12 – CPTU soil behaviour type by (Robertson, 1990)

Table 4.3 – Soil behaviour type description from 1990

Zone	Soil Behaviour Type
1	Sensitive, fine grained
2	Organic soils - clay
3	Clay – silty clay to clay
4	Silt mixtures – clayey silt to silty clay
5	Sand mixtures – silty sand to sandy sil
6	Sands – clean sand to silty sand
7	Gravelly sand to dense sand
8	Very stiff sand to clayey sand
9	Very stiff fine grained

In the chart shown in Figure 4.13 reveals different results from the previous plot in Figure 4.10. Here it is possible to observe that most of the points are included in the zones 3, 4 and 5. From that it is possible to conclude that the normalization of the cone strength and friction parameters had a major impact in the obtained results. This point distribution evidences a clayey/silty behaviour. The absence of points in zone 1 could be explained by the sensitivity evaluation in 3.3.4.3.. Also the reduced number of readings from zone 2 can be considered valid, considering that this soil is not considered highly organic (3.3.4.1.).

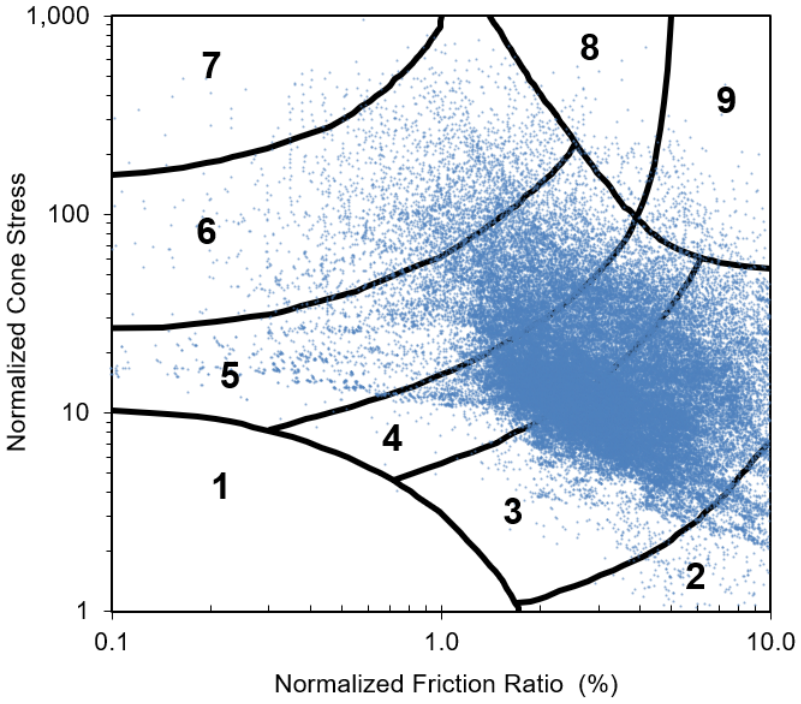


Figure 4.13 – CPTU Soil behaviour chart with CPTU data

In order to understand how the soil behaves with depth, it was represented in Figure 4.14 the using the normalized soil behaviour approach proposed by Robertson (1990). By the analysis of this evolution it is possible to conclude that in the superficial part, the soil has a higher silty behaviour than the deepest part. With the increase of depth, the data tends to be more concentrated in a more clayey behaviour. This could be explained by the existence of intermediate soil such as fill material and post glacial silt mixed with gyttja.

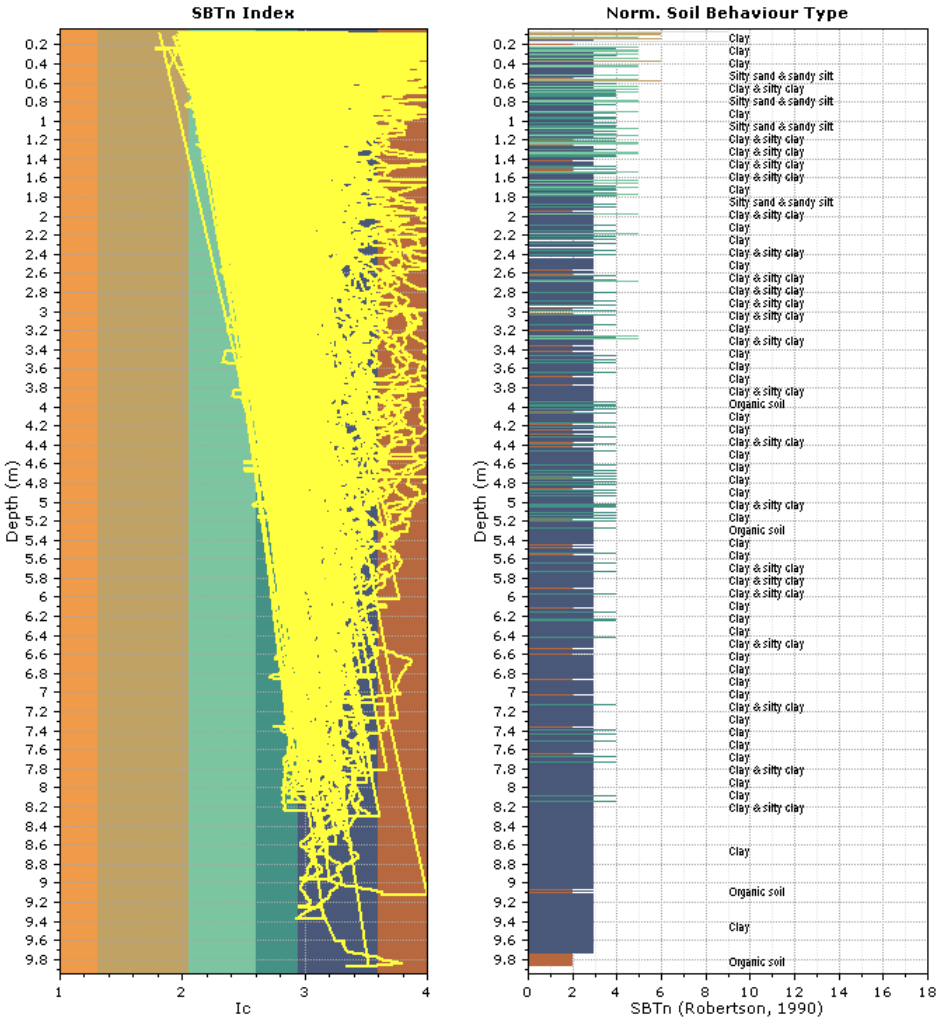


Figure 4.14 – Normalized soil behaviour type variation with depth classification from (Robertson, 1990)

4.1.6.3. Eslami-Fellenius Chart

During the application study of CPT for pile designs, (Eslami & Fellenius, 1997) developed a soil classification method. The chart is based on non-normalized sleeve friction f_s and on effective cone resistance, q_E that corrects the pore pressure acting on the shoulder.

$$q_E = q_t - u_2 \tag{4.5}$$

It incorporates five soil zones in the soil classification chart presented in Figure 4.15 which was based on a large amount of CPT data. The boundaries shown in the diagram were obtained by enveloping approximately 90% of all points of each main soil category. This soil profiling approach differs from the one used by Robertson et al. (1986) and Robertson (1990). It is believed by Eslami and Fellenius (1997) that those manners of plotting distorts the data since it implies that a variable is plotted versus its own inverse value in the charts, which violates the fundamental rule which states that dependent and independent variables must be rigorously separated.

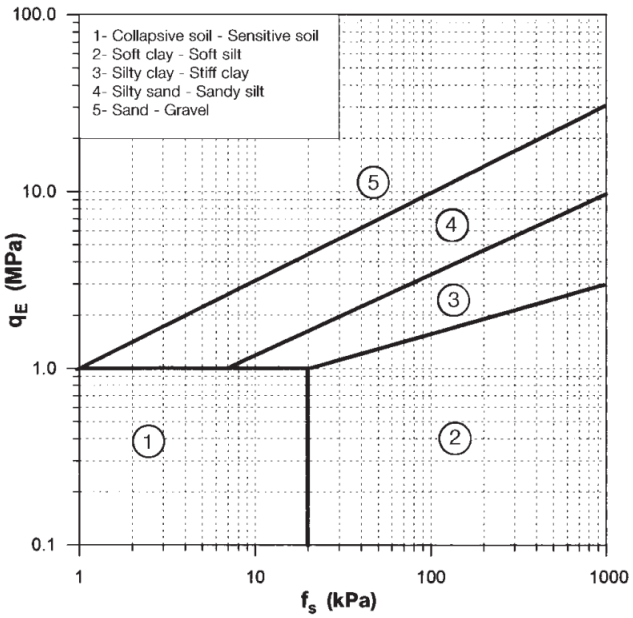


Figure 4.15 – Eslami and Fellenius soil profiling chart with soil type classification (Eslami & Fellenius, 1997)

The graph in Figure 4.16 shows a great concentration of points in zone 1 and a moderate number of data in zone 1. This means, according to this chart, that this gyttja is more close to a collapsive/sensitive type of soil.

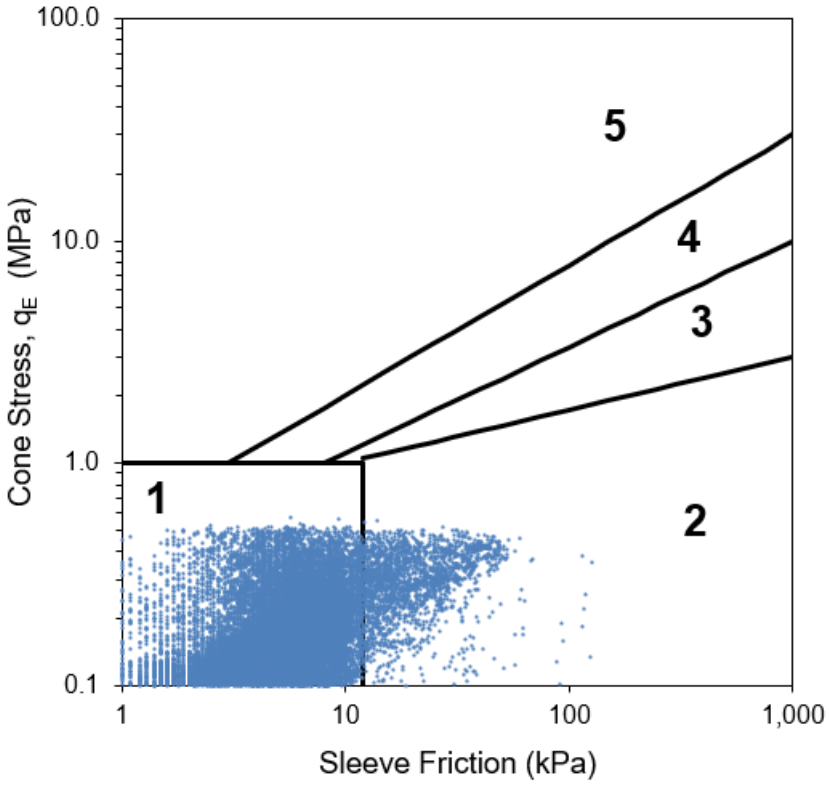


Figure 4.16 – Eslami and Fellenius soil scatter

4.2. UNDRAINED SHEAR STRENGTH

The undrained shear strength, c_u, is a geotechnical parameter used to evaluate foundation bearing capacity (shallow footings, rafts, and pilings) and also short-term stability of excavations, slopes, and embankments of clayey soils. Since clay type soils are practically impervious, it is important to refer the Tresca criterion which states that the strength is independent of the normal stress since the response to loading only increases the pore water pressure and not the effective stress. This can be demonstrated with the Mohr envelope in Figure 4.17 that demonstrates that the failure of a clay soil is independent of the friction angle, ϕ and from the total stress path at failure, TSP (TSP=TT). Within the classical understanding on the behavior of soils, the undrained shear strength can be taken as the maximum shear stress, $c_u = \tau_{max}$, for a stress path at constant volume (Mayne & Peuchen, 2018).

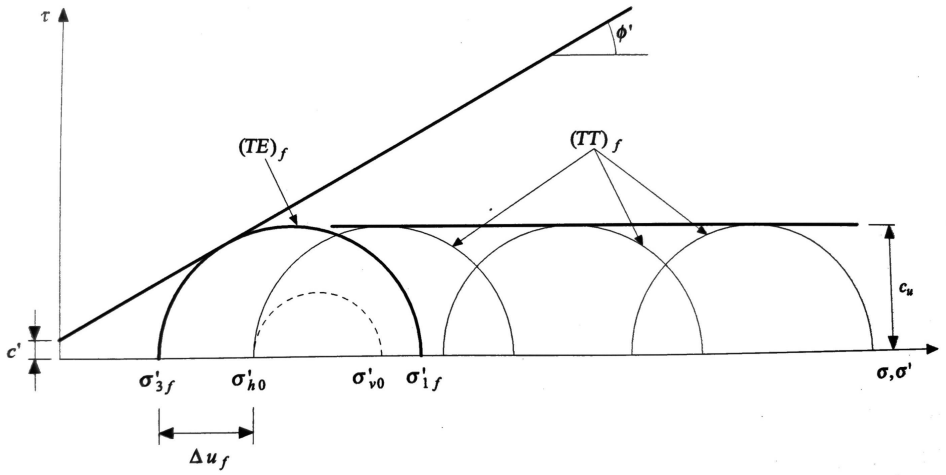


Figure 4.17 – Total stress Mohr envelope for clays (Matos Fernandes, 2016)

However, because of the complex effects of strain rate, anisotropy, direction of loading, and boundary conditions, assigning a single value of c_u to a specific clay is not possible. Instead, a family of c_u values must be considered to evaluate shear in compression and extension in different ways (Mayne & Peuchen, 2018). One of the main ways to determine the undrained shear strength in clayey soils is with anisotropically consolidated undrained triaxial compression tests(CAUC).

4.2.1. CAUC LABORATORY DATA

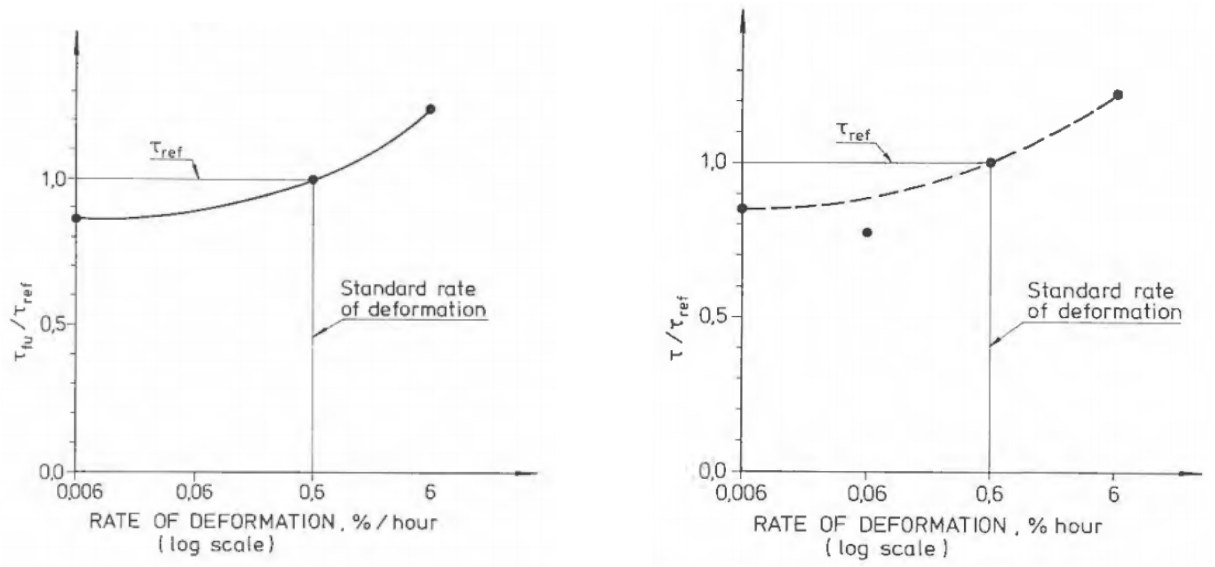
Based on 5 boreholes, 15 valid CAUC tests were conducted to determine the undrained shear strength of 15 specimens of gyttja. The dimensions of each specimen were 70mm for both diameter and height. Those tests were consolidated at 3 different stress levels:

- Sample type 1 - $\sigma_1^{'} \approx \sigma_{vo,est}^{'}$ (initial stress predicted scenario)
- Sample type 2 - $\sigma_1^{'} \approx \sigma_{vo,est}^{'} + 30kPa$ (intermediate situation during the filling construction)
- Sample type 3 - $\sigma_1^{'} \approx$ predicted maximum vertical stress at the end of construction works

Where $\sigma_1^{'}$ represents the major principal stress and $\sigma_{vo,est}^{'}$ the estimated in-situ vertical effective stress at rest. The COWI aim in performing those consolidated triaxial compression tests is to observe the

strength gain that is expected for gyttja after the completion of fill works. The tests were performed with 4 different strain rates in order to access the impact of increasing the strain rate in strength. The shear phase for each test had comprised 7 to 8 shear phases by adjusting the strain rate, which were 0.07, 0.7, 7 and 70 %/h.

From previous experience in Scandinavia, the strain rate was found to have an important effect on undrained strength. According to (Larsson, 1990) a tenfold decrease in testing rate brought a decrease in evaluated c_u of 10%, in comparison to standard triaxial tests conducted with a strain rate of 0.6%/h. In Figure 3.15, the results obtained by (Larsson, 1990) are presented which correspond to organic clays from 2 locations in Sweden (Valen and Lilla Mellosa).



(a) (b)

Figure 4.18 – Undrained shear strength as a function of rate of deformation in organic clays from: (a) Valen , (b) Lilla Mellosa (Larsson, 1990)

From that experience it can be concluded that it is conservative to adopt the lowest strain rate possible in order to evaluate c_u in gyttja. For that reason, the lowest strain rate (0.07%) was chosen to determine this parameter. In a example in Figure 4.19 it is possible to see a test performed on this project gyttja, plotting in blue the real measured test result and in black the 4 curves that represent the theoretical prediction for each strain rate.

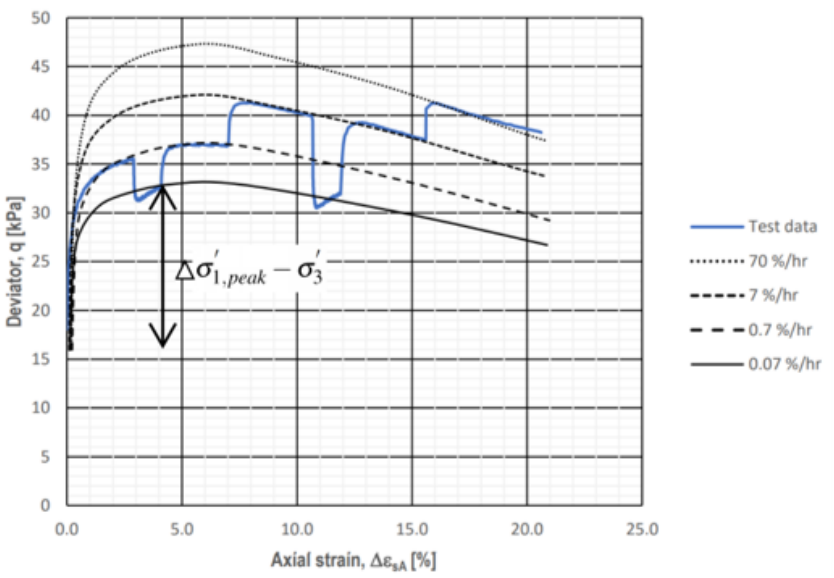


Figure 4.19 – Peak deviator stress variation with axial strain during shear phase for specimen 3_2 from BH_P_25 (COWI/AS, 2020)

The c_u parameter was interpreted from the maximum shear stress, τ_{max}, that can be seen as half of the peak deviator stress, q_{peak} during shear phase,

$$c_{u,TC} = \tau_{max} = \frac{q_{peak}}{2} \tag{4.6}$$

Being q_{peak} the difference between the peak major stress, $\sigma'_{1,peak}$, and the minor stress, σ'_3,

$$q_{peak} = \sigma'_{1,peak} - \sigma'_3 \tag{4.7}$$

From the specimen in Figure 4.19 it is concluded that the lowest peak deviator stress, q_{peak}, is 33 kPa and the c_u is equal to 16.5 kPa. In Table 4.4 is represented the CAUC results for all the specimens, where is also corresponded the major stress at the end of the consolidation stage (begin of shear phase), $\sigma'_{1,cons}$.

Table 4.4 – Laboratory CAUC results

Borehole	Specimen	Average depth	σ'_{v0} (kPa)	$\sigma'_{1,peak}$ (kPa)	σ'_3 (kPa)	q_{peak} (kPa)	$\sigma'_{1,cons}$ (kPa)	c_u (kPa)
BH_A_15	3_1	2.385	10.5	22	3	19	11	9.5
	3_3	2.155	9.5	150	46	104	207	52.0
BH_P_25	3_1	2.225	9.8	15	2	13	12	6.5
	3_2	2.655	11.7	42	9	33	44	16.5
	3_3	2.935	12.9	165	44	121	185	60.5
	8_1	6.845	30.1	42	10	32	33	16.0
	8_3	6.635	29.2	194	67	127	214	63.5
BH_P_33	7_1	5.575	24.5	40.4	7.9	32.5	28.3	16.3
	7_2	5.425	23.9	57.1	13.6	43.5	58.3	21.8
	7_5	5.465	24.0	170.4	49.4	121	205.4	60.5
BH_P_34	3_1	2.585	11.4	12.2	3.9	8.3	12.1	4.2
	3_2	2.705	11.9	38.9	10.4	28.5	41	14.3
	3_3	2.455	10.8	164.6	47.6	117	186.3	58.5
BH_P_84	7_1	5.695	25.1	30.9	3.9	27	29.3	13.5
	7_3	5.545	24.4	133	38	95	195	47.5

From the data in Table 4.4 the evaluation of the undrained shear strength was plotted against the vertical effective stress after the consolidation, $\sigma'_{1,cons}$ Figure 4.20. The linear regression that fits the data of this evolution resulted in the following strength evolution:

$$c_{u,TC} = 0.26\sigma'_v + 5.4(kPa) \tag{4.8}$$

Also it resulted in a coefficient of determination, R^2=0.97, which reveals a great quality in the results obtained from the tests. This parameter represents the percentage variation in y (in this case, c_u) which is explained by all the x (in this case, $\sigma'_{1,cons}$) variables together.

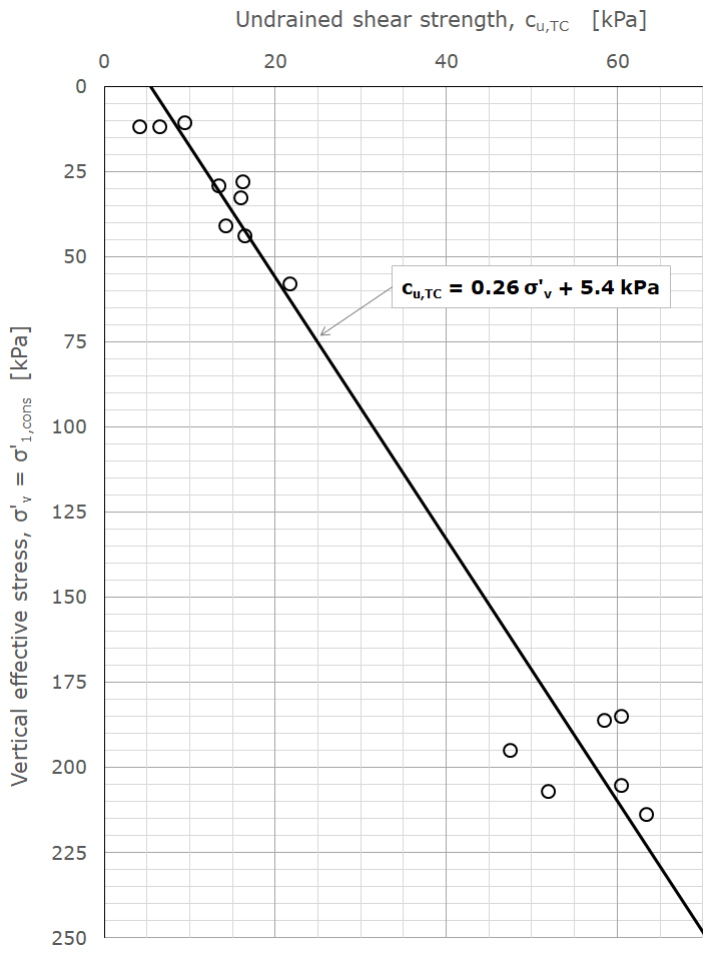


Figure 4.20 – Evaluation of the undrained shear strength, cu_{TC} of the triaxial tests, with the representation of the linear regression

The location of each borehole where the specimens for the triaxial tests were taken are represented in Figure 4.21. Here it is possible to visualize that the borehole locations can be very distant from each other in the entire site. Yet, from the previous results it is possible to conclude that since the R^2 is close to 1, there is not a relevant spacial variability in this gyttja. In other words it can be stated that this soil can be practically homogeneous throughout the entire site.

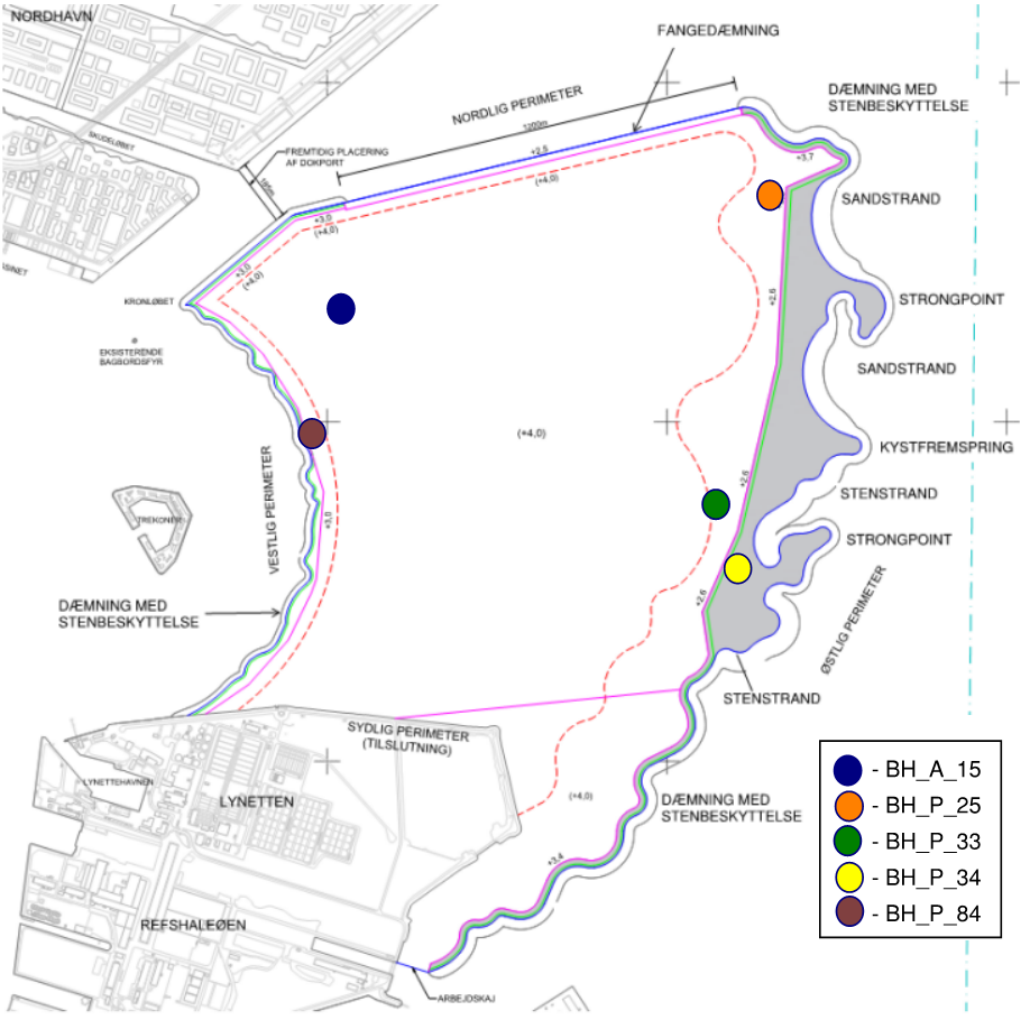


Figure 4.21 – Boreholes location in site where CAUC specimens where taken

The drained strength parameters were interpreted from the peak deviator stress within 10% additional axial strain in the shear phase from the stress-strain curve. The peak stresses in s'–t coordinates are presented in Figure 4.22. The best-fit line is described by the following equation:

$$t' = 0.510s' + 2.99(kPa) \tag{4.9}$$

The effective cohesion, c' and friction angle, ϕ' were derived from that expression and the results are demonstrated in Table 4.5.

Table 4.5 – Effective cohesion and friction angle obtained

c' (kPa)	$\phi'(^\circ)$
2.2	30.7

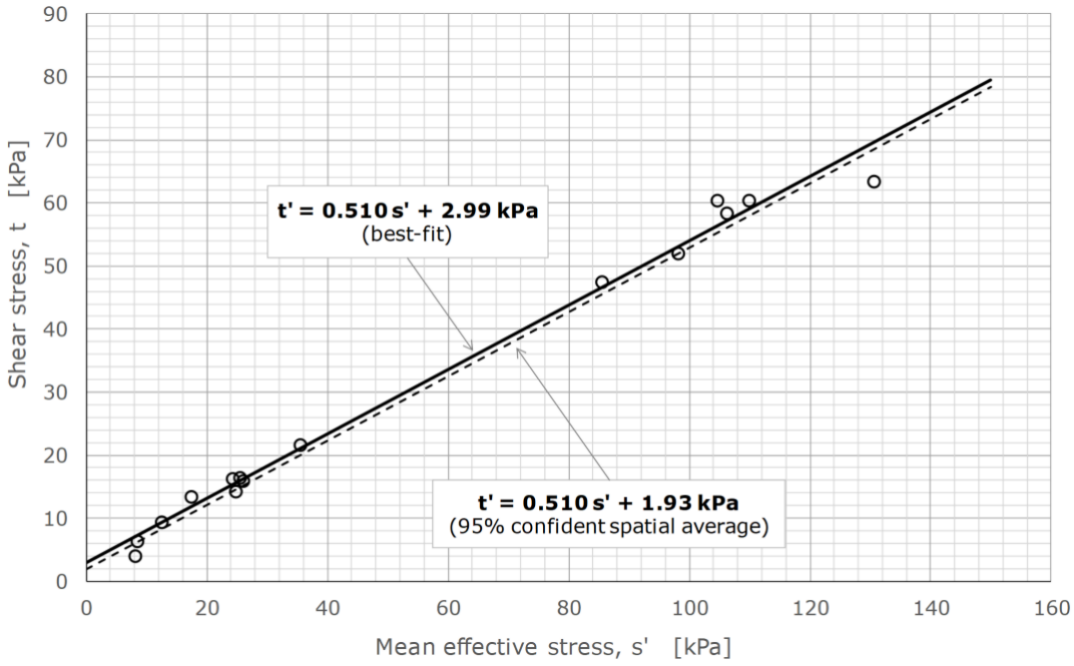
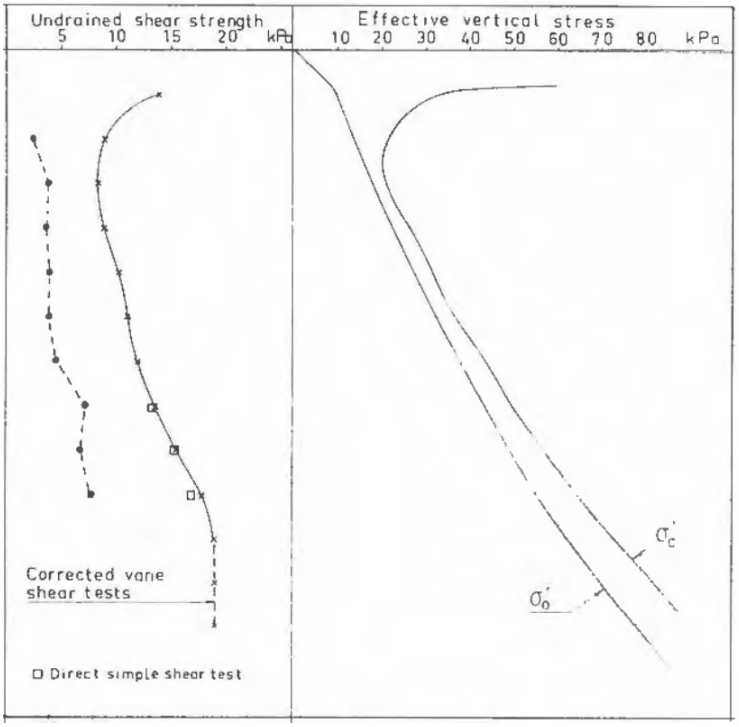


Figure 4.22 – Effective peak stresses

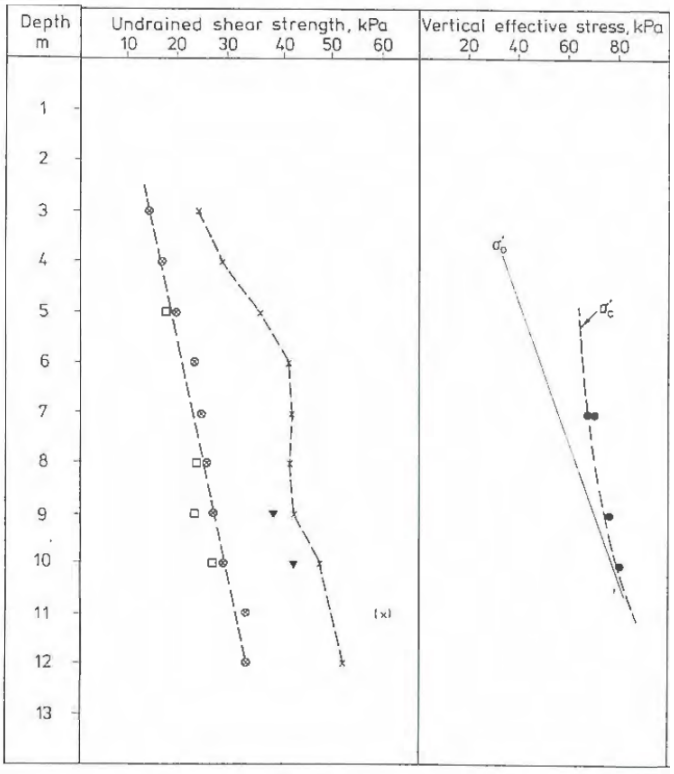
4.2.2. SIMILAR SOILS EXPERIENCE

The soil profile in Lilla Mellosa is typical for a large number of similar profiles where the upper post-glacial soil layers are organic (gyttja) or slightly organic and the soil is coloured black or dark grey by a certain content of sulphides (Larsson, 1990). The undrained shear strength was evaluated via vane shear test, VST and the results are shown in Figure 4.23 (a). From its analysis it is possible to observe that the range of c_u is from 2 to 18 kPa. A linear regression in the data would result in a relation of around c_u/σ'_{vo}=0.2.

Another Swedish soil in Gideabacka typically possessed about 10 metres of mainly black organic silt or clayey organic silt. In a layer between 8 and 10 metres depth the clay content is slightly higher than 20%, which changes the classification to a silty organic clay Figure 3.10. The soil there has the typical green/grey colour of gyttja-bearing soil. Here the c_u ranges from 14 to 50 kPa and possesses an strength evolution rate of c_u/σ'_{vo}=0.27 (Figure 4.23(b)).



(a)



(b)

Figure 4.23 – Undrained shear strength evaluation from Swedish soils: (a) Lilla Mellosa , (b) Gideabacka (Larsson, 1990)

4.2.3. Effect of Anisotropy

One interesting aspect is the study of the induced anisotropy of gyttja. In fact clayey soils can exhibit different values for the undrained shear strength under compression, $c_u(v)$ and for the same parameter under extension, $c_u(h)$. This means that this type of soils normally reveal to have strength anisotropy that can be quantified using the k_s parameter:

$$k_s = \frac{c_u(h)}{c_u(v)} \tag{4.10}$$

This parameter depends on the direction of the major stress, meaning that anisotropy is induced by the incremental stress that is applied to a certain soil sample. In order to understand the anisotropy phenomenon, we can imagine two similar soil samples where one was submitted to a triaxial compression test and the other to a triaxial extension. Both the tests had the same conditions where the initial stress was the same for both of the samples. The result of this experiment revealed that the stress path for both of the samples was different. From the analysis of Figure 4.24 it is possible to reach that the extension total stress path ($TSP_{ext} = TTT_{ext}$) is longer that the compression one. Admitting that the soil is isotropic in relation to the excess pore pressure rate, a longer stress path in extension will lead to higher excess pore pressure, Δu_f, which will lead the effective stress path to failure at a lower value.

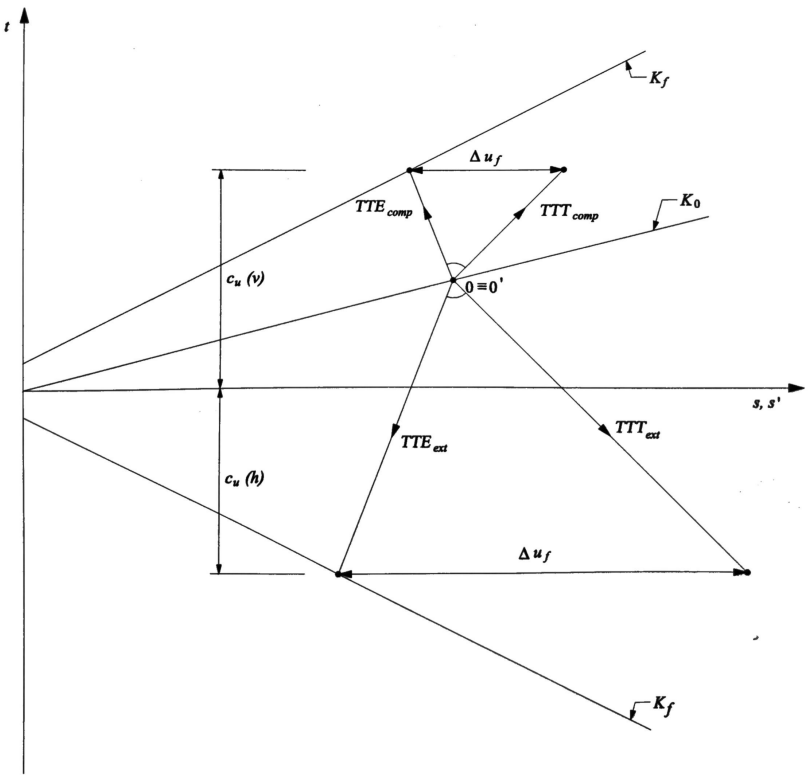


Figure 4.24 – Simplified total and effective stress path obtained from triaxial compression and extension tests over similar samples (Matos Fernandes, 2016)

This failure interception value represents the $c_u(h)$ for the soil. This parameter can be determined using the following expression:

$$c_u(h) = \frac{c'cos\phi'}{1-sin\phi'+2A_f sen\phi'} + \sigma'_{vo}\frac{sin\phi'(1-A_f+K_oA_f)}{1-sin\phi'+2A_f sin\phi'} \tag{4.11}$$

Considering the value obtained for ϕ' in Table 4.5, it was possible to determine the earth pressure coefficient at rest, K_o, for normally consolidated soils:

$$K_o = 1 - sen\phi' \tag{4.12}$$

Resulting the following value:

$$K_o = 0.49 \tag{4.13}$$

The A_f parameter proposed by Skempton (1954), indicates the relation at the moment of failure between the excess pore pressure, Δu_f, and the major total stress $\Delta\sigma_{1f}$, since $\Delta\sigma_3 = 0$:

$$A_f = \frac{\Delta u_f}{\Delta\sigma_{1f}} \tag{4.14}$$

This parameter was determined by interpretation of the lab tests where it was registered for each specimen the excess pore pressure at the moment of failure. Knowing already the initial axial stress of the test, σ'_{1o} and the peak deviator stress, q_{peak}, we can determine the value of A_f for each of the specimens. Figure 4.25 demonstrates the evolution of the excess pore pressure, Δu and the stress ratio, σ'_A/σ'_R versus the variation of the axial strain during shear phase, $\Delta\varepsilon_{sA}$.

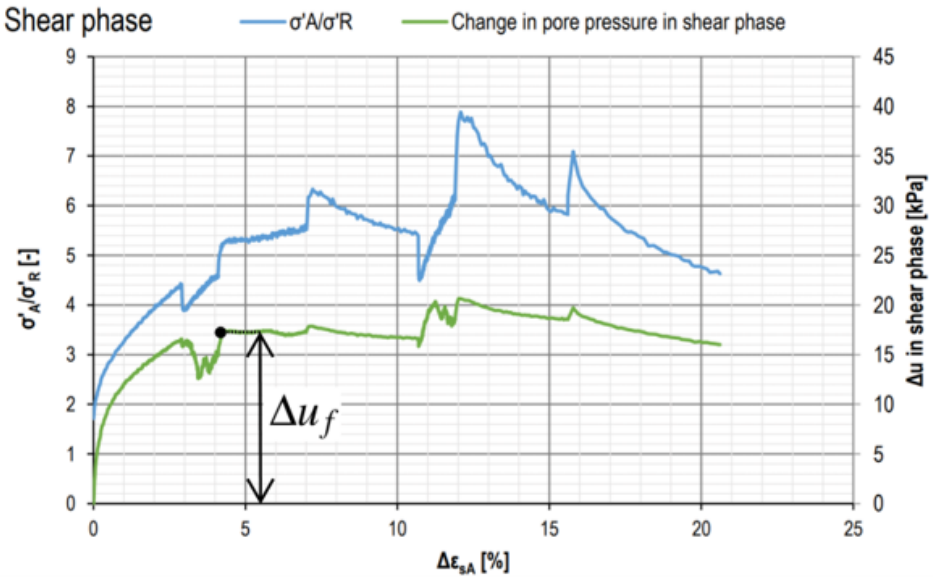


Figure 4.25 – Evolution of excess pore pressure and strength ratio with axial strain, during shear phase (specimen 3_2 from BH_P_25) (COWI/AS, 2020)

The anisotropy evaluation is determined in the shear phase of the CAUC tests (i.e, after the consolidation phase). For that reason, only the tests performed at in situ consolidation stresses (Sample

type 1) were used. Following Equation 4.11 it is possible to determine the undrained shear strength under extension, $c_u(h)$. Also the value of K_o that was used in Equation 4.11 was evaluated for each sample after the consolidation phase, dividing $\sigma'_{1,cons}/\sigma'_{1,cons}$ instead of the value obtained in Equation 4.13. The obtained results are revealed in Table 4.6 where the value for the anisotropy coefficient, k_s was finally calculated. The specimen 3_1 from BH_P_34 was removed from this evaluation since the strength after consolidation was approximately the same at the initial conditions. This resulted in a value extremely high for the A_f parameter.

Table 4.6 – Laboratory determination of anisotropy

Borehole	Specimen	$\Delta\sigma f$ (kPa)	Δu_f (kPa)	A_f	K_o	$\sigma'_{1,cons}$ (kPa)	$c_u(v)$ (kPa)	$c_u(h)$ (kPa)	k_s
BH_P_25	3_1	14	5	0.36	0.83	12	6.5	9.0	1.38
	8_1	22	17	0.77	0.82	33	16	12.8	0.80
BH_P_33	7_1	26.2	14	0.53	0.78	28.3	16.25	14.1	0.87
BH_P_84	7_1	17.3	19	1.10	0.83	29.3	13.5	8.7	0.64

From the analysis of the k_s results, it is possible to determine the average values for the A_f and for the k_s (Table 4.7). Is is possible to observe that the obtained value of A_f, is included in the typical range of normally to slightly consolidated clays Table 4.8.

Table 4.7 – Average values for A_f and k_s

$\bar{A_f}$	$\bar{k_s}$
0.69	0.92

Table 4.8 – Typical values for A_f from triaxial tests. Adapted from Matos Fernandes (2016)

Soil type	A_f
Highly consolidated clays	-0.5 to 0.0
Averagely consolidated clays	0.0 to 0.3
Slightly consolidated clays	0.3 to 0.7
Normally consolidated clays	0.7 to 1.3
Quick clays	>1.3

Experiments conducted on normally and slightly consolidated soils allowed the creation of an empirical graph (Figure 4.26) for the evaluation of k_s depending on the variation of A_f and ϕ'. From its analysis it is possible to state that there is not a great difference in the results from the direct determination of $c_u(h)$ from the Equation 4.11 and from this empirical graph considering an angle of shearing resistance of 30.7°.

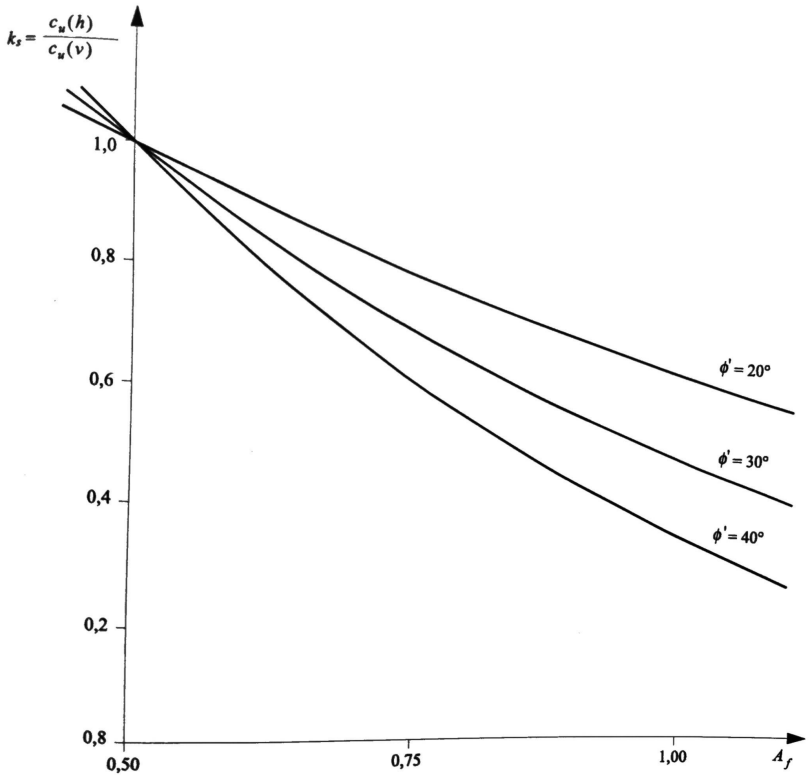


Figure 4.26 – Evolution of k_s depending on A_f and ϕ' (Matos Fernandes, 2016)

About the strength anisotropy from gyttja in Lynetteholm it is possible to conclude that there is not signs of induced anisotropy in this material since the values of k_s is near the unit.

4.2.4. Estimation of the N_{kt}

Since possible effects of sample disturbance and strain rate will inevitably influence the results of all in-situ tests, their interpretation will necessarily require some empirical content to take into account these factors (Lunne et al., 1997). The calibration of the CPTU with either selective laboratory strength testing performed on high-quality samples and/or selective field vane shear tests, VST, is the best approach. However, in order to do that it is required a considerable amount of time and financial expense due to more sophisticated testing program, costs of drilling, sampling, transport, and testing (Mayne & Peuchen, 2018). There are several expressions available for interpreting the in-situ undrained shear strength in clays from CPTU results, however, the most common and reliable is given by Equation 4.15. The use of corrected tip resistance, q_t is especially important in the case of soft clays, where the measured pore pressure, u_2, can be nearly as large as the measured tip resistance, q_c, therefore the difference between q_c and q_t can be significant .

$$c_u = \frac{q_t - \sigma_{vo}}{N_{kt}} = \frac{q_{net}}{N_{kt}} \tag{4.15}$$

where σ_{vo} represents the total overburden stress, q_{net} is the net cone resistance and N_{kt} is the empirical cone factor. The appropriate choice of the N_{kt} could be made on the basis of theoretical, experimental,

and/or statistics relationships. Moreover, the effects of sample disturbance when collecting the in-situ samples in laboratory results are essentially inevitable and unavoidable in most instances.

The N_{kt} values normally vary over a wide range, between 4 and 29. In Figure 4.27 is represented an historical range for this cone factor proposed from different authors. Certain studies have found that the cone factor is a function of certain soil parameters (e.g. plasticity index, overconsolidation ratio, pore pressure parameter), but later works did not confirm the presence of such relationships. Therefore it seems rather complicated to define a single soil property that influences the cone factors, probably because there are more other factors affecting the N_{kt} values (Rémai, 2013).

N_{kt} value range	Reference test	Comments	Reference
8-16	triaxial compression, triaxial extension and direct shear	For clays ($3\% < I_p < 50\%$) N_{kt} increases with I_p	Aas et al. (1986)
11-18		Found no correlation between N_{kt} and I_p	La Rochelle et al. (1988)
8-29	Triaxial compression	N_{kt} varies with OCR	Rad and Lunne (1988)
10-20	Triaxial compression		Powell and Quarterman (1988)
6-15	Triaxial compression	N_{kt} decreases with B_q	Karlsrud (1996)
7-20	Triaxial compression	Busan clay, Korea $25\% < I_p < 40\%$	Hong et al. (2010)
4-16	Vane shear	High plasticity, soft clay, $42\% < I_p < 400\%$	Almeida et al. (2010)

Figure 4.27 – N_{kt} historical range recommendations (Rémai, 2013)

For the determination of the cone factor, N_{kt}, the following procedure was carried:

- Identifying the locations where existed both CPTU and Boreholes with CAUC tests. The distance between this two tests ranged from 0 to 2 meters.
- From all cases in such circumstances the samples that were consolidated around initial in situ stress (samples type 1) were selected. Five samples type 1 were available (samples type 1).
- Within the CAUC sample length (0.7m), it was determined the average net cone resistance, $q_{net,avg}$ for each location.
- It was determined the undrained shear strength of each specimen that fitted the Equation 4.8 for the average depth of the specimen, $c_{u,TC,avg}$.
- Based on Equation 4.15 the cone factor was determined based on empirical practice where, for each specimen the cone factor was evaluated:

$$N_{kt} = \frac{q_{net,avg}}{c_{u,TC,avg}} \tag{4.16}$$

The cross section in Figure 4.28 reveals the example of a nearby CPTU and Borehole. It shows the specimen location and the adjacent CPTU measurement of the average net cone resistance, $q_{net,avg}$.

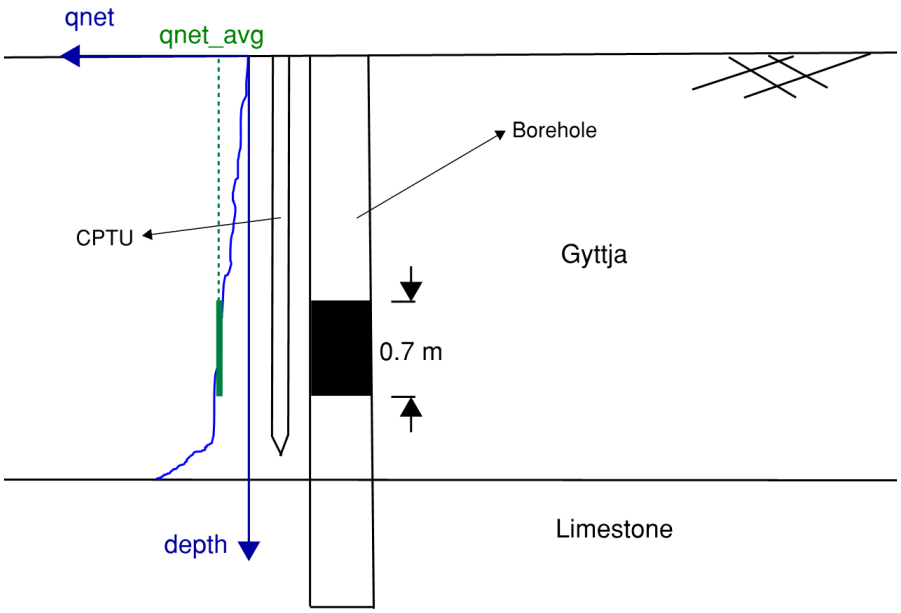


Figure 4.28 – Cross section showing an example location where both CPTU and Boreholes were executed

In Figure 4.29 is represented a flowchart, indicating the procedure used for the determination of N_{kt}.

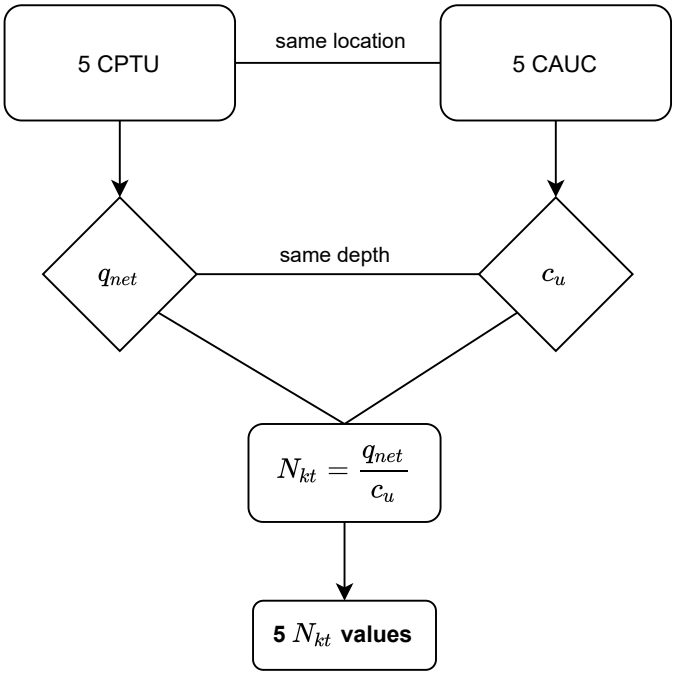


Figure 4.29 – Flowchart indicating the N_{kt} procedure

For each CAUC specimen the results obtained for all the parameters for $c_{u,TC,avg}$, $q_{net,avg}$ and N_{kt} are presented in (Table 4.9). It is possible to observe that there is a considerable range for the cone factor ($17.2 < N_{kt} < 24.5$). The average value obtained for this parameter is 19.2.

Table 4.9 – Representation of the values of $c_{u,TC,avg}$, $q_{net,avg}$ and N_{kt} for each specimen, corresponding to the indicated adjacent CPTU

Borehole	Specimen	Top depth (m)	Bottom depth (m)	$c_{u,TC,avg}$ (kPa)	CPTU	$q_{net,avg}$ (MPa)	N_{kt}
BH_P_25	3_1	2.19	2.26	7.7	CPT_A_235	0.133	17.2
	8_1	6.81	6.88	12.5		0.208	16.6
BH_P_33	7_1	5.54	5.61	11.2	CPT_A_193	0.237	21.2
BH_P_34	3_1	2.55	2.62	8.1	CPT_A_179	0.135	16.7
BH_P_84	7_1	5.66	5.73	11.3	CPT_P_84	0.277	24.5

4.3. CHAPTER SUMMARY

Regarding the evaluation of CPTU strength parameters, it is possible to observe that gyttja evidences a behaviour that is typical for a soft soil considering the results from the q_c (low resistance) and u_2 (positive pore pressure). Regarding f_s, it is interesting to observe that there is a wide range in the observed values that can lead to a behaviour close to a sensitive soil (lower f_s) or a more organic soil (higher f_s). The results obtained regarding the soil behaviour is highly dependent on the methodology followed by the different authors, i.e which parameters should be used in order to execute that evaluation.

The undrained shear strength for gyttja evaluated in CAUC tests is in line with previous experience in similar soils from different locations in Sweden. Also there is an indication that gyttja in Lynetteholm appears to have low spatial variability, evidenced by the fact that the CAUC tests were conducted in 5 different locations in the site and the results converge to a defined value of c_u.

The results obtained for the strength anisotropy of gyttja is also aligned with previous experience with this soil, in which it seems that there is not a great difference between c_u under compression, $c_u(v)$, and extension, $c_u(h)$.

For the determination of N_{kt}, it is interesting to observe that the dependency of this parameter in not unanimous among different proposals (Figure 4.27). It seems that this parameter is highly dependent not only on the type and way tests were conducted. For that reason it is not possible to ensure that the procedure used herein is more valid than other proposals previously elaborated. Also, the number of triaxial tests from where N_{kt} values were obtained is not huge that could explain a clear and defined trend.

5
PROBABILISTIC APPROACHES

5.1. INTRODUCTION

Considering the determination (in the previous chapter) of N_{kt}, it is gathered the conditions to evaluate c_u from CPTU. In order to do so, is was elaborated 3 different approaches, considering different statistical strategies. All 3 approaches are focused on the c_u linear evolution with depth. Approach 1 is conducted considering the average value from the 5 determined N_{kt} and considers every CPTU in the same analysis. The second approach also considers the average N_{kt}, but evaluates the each CPTU separately and independent from the other results. The final approach (Approach 3) used the same data analysis as Approach 1, however, is was studied the influence of modifying N_{kt} in c_u evaluation. Figure 5.1 demonstrates a diagram resuming the 3 CPTU approaches.

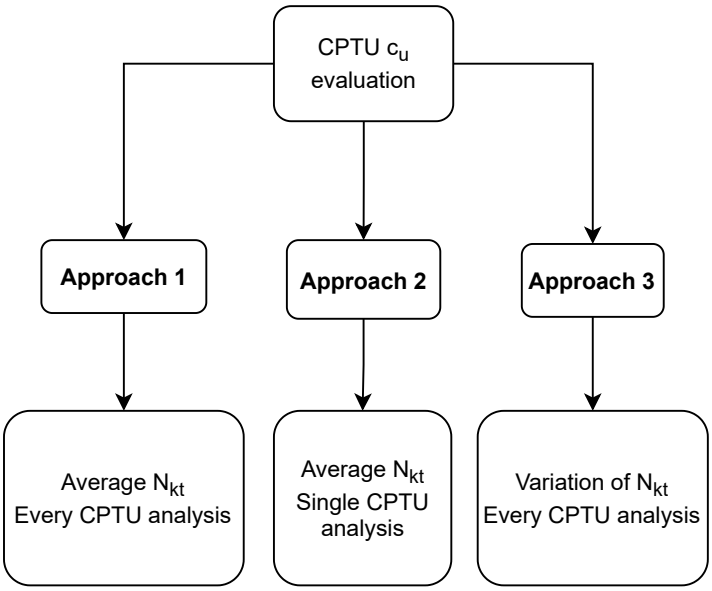


Figure 5.1 – Resume of the approaches for c_u evaluation from CPTU

5.2. LINEAR REGRESSION THEORETICAL EXPLANATION

The following section briefly explains the theoretical background behind the linear evolution with depth concerning c_u. It indicates the procedure for the execution of a linear regression in order to characterize data.

5.2.1. UNDRAINED SHEAR STRENGTH ESTIMATION WITH DEPTH

Let Y be a soil variable, such as a strength parameter, whose variation with depth z can be reasonably well modelled as a linear function. Y is then a so-called dependent variable, whereas z is independent. Lets assume that n observations of pairs (z_i,y_i), are available from a soil investigation campaign. The variation of Y with depth can be now expressed by the following notation:

$$Y = a_0 + a_1 z + \varepsilon \tag{5.1}$$

where the term $a_0 + a_1 z$ represents the linear mean variation with depth and the term ε represents the natural variability of Y about the mean, and where z denotes the depth below the soil surface. The coefficients a_0 and a_1 represent the surface intercept and the depth gradient, respectively, of the mean of Y. The variability term ε has zero mean and its standard deviation is denoted σ. The standard deviation σ is assumed to be constant, i.e. it is assumed to be independent of the depth z. Figure 5.2 shows the linear model evaluation depending on the parameters a_0 and a_1.

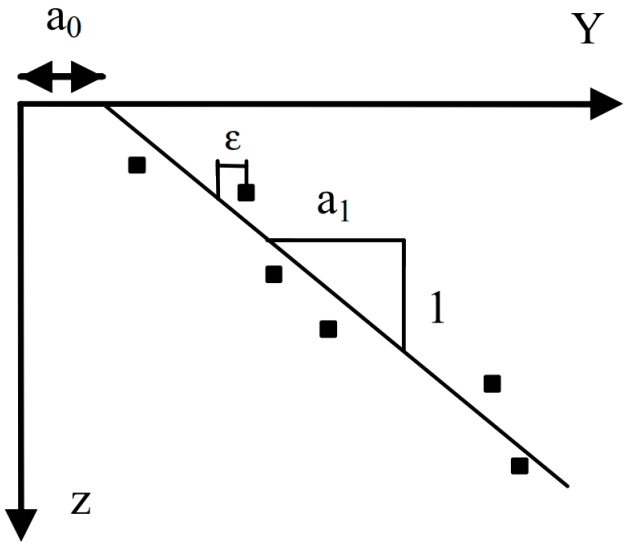


Figure 5.2 – Undrained shear strength linear evaluation with depth (Veritas, 2012)

The coefficients a_0 and a_1 can be expressed in the linear expression from the observed n data pairs (z,y). The parameters $\bar{y}$ and $\bar{z}$ represent the average value for the strength parameter, Y, and variation with depth parameter, z. Those parameters can be expressed by the following equations:

$$\hat{a}_0 = \bar{y} - \hat{a}_1 \bar{z} \tag{5.2}$$

$$\hat{a}_1 = \frac{\sum_{i=1}^{n} (z_i - \bar{z})(y_i - \bar{y})}{\sum_{i=1}^{n} (z_i - \bar{z})^2} \tag{5.3}$$

$$\bar{y} = \frac{1}{n}\sum_{i=1}^{n} y_i \tag{5.4}$$

$$\bar{z} = \frac{1}{n}\sum_{i=1}^{n} z_i \tag{5.5}$$

The estimators $\hat{a}_0$ and $\hat{a}_1$ are provided with uncertainty due to the variability of data. Those uncertainties can be represented by their respective standard deviation, named as standard error, *se*, obtained by:

$$se(\hat{a}_0) = s\sqrt{\frac{1}{n} + \frac{\bar{z}^2}{\sum_{i=1}^{n}(z_i - \bar{z})^2}} \tag{5.6}$$

$$se(\hat{a}_1) = \frac{s}{\sqrt{\sum_{i=1}^{n}(z_i - \bar{z})^2}} \tag{5.7}$$

5.3. Undrained Strength Approaches

5.3.1. Approach 1 - Every CPTU in The Same Evaluation

Based on the obtained values for the N_{kt} it is possible, based on Equation 4.15 to determine the c_u for the CPTU data. This evaluation was done based on a single value of N_{kt} for the entire dataset. For a first approach it was chosen the average value from Table 4.9, which resulted in: $N_{kt,avg} = 19.2$.

By the analysis of Figure 5.3 it is possible to observe the maximum value for the c_u of about 30 kPa. The overall interval trend on the first superficial meters close to the seabed seems to be included in the interval of $0 < c_u < 13$ kPa where it is possible to observe a higher density in the plot. This indicates the existence of an overconsolidated superficial crust which could be explained by erosive processes or mass movements that remove part of the sedimentary material.

Based on the data from the scatter it is possible to determine the linear evolution of c_u with depth (below the overconsolidated crust) for the entire dataset. It has resulted in the following linear development:

$$c_{u,CPTU} = 0.28\sigma_v^{'} + 5.5kPa \tag{5.8}$$

The result obtained was close to the one obtained from the CAUC data (Equation 4.8), meaning that there is a match in the obtained data. For this regression it resulted in a $R^2 = 0.191$ which is considerably lower than the one based on the triaxial tests. However the amount of data is considerably higher and the layering for the CPTU had contemplated other types of material than pure gyttja (e.g. filling material and post glacial sand), which may explain the high scatter, conversely to what happened to the triaxial tests.

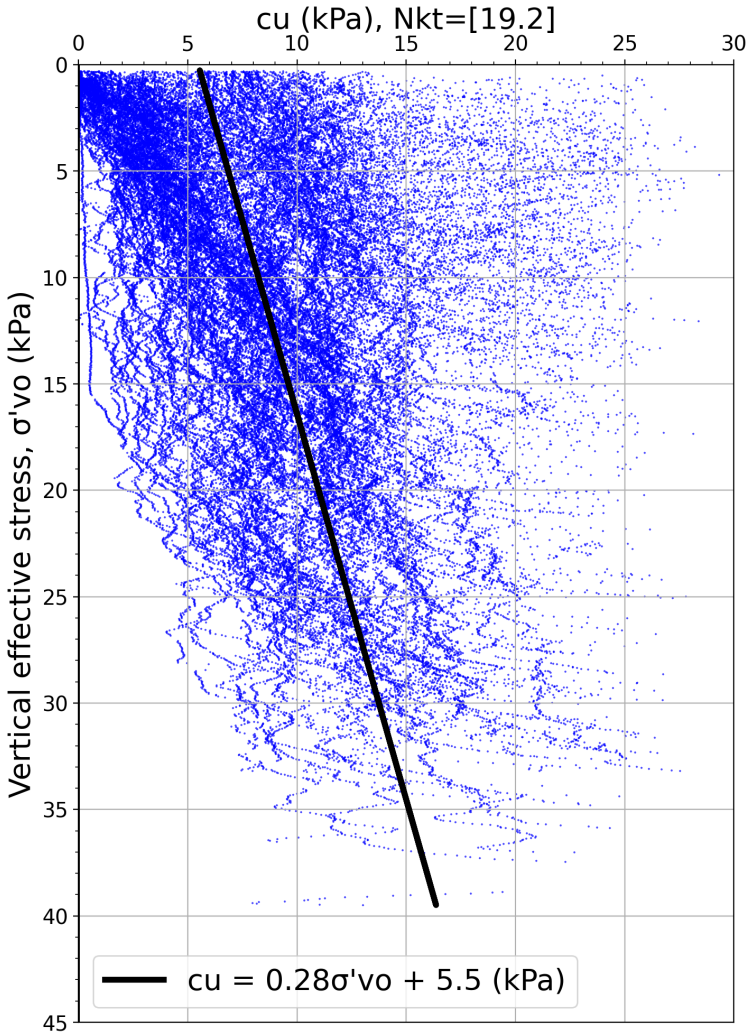


Figure 5.3 – Undrained shear strength, c_u, evaluation using the average value for the cone factor, $Nkt,avg = 19.2$. The line in black represents the linear regression of the scatter

In order to understand how the data is distributed in the scatter, it was determined the frequency of data and the respective probability density function. It was admitted that c_u followed a normal distribution. From the analysis of the plot in Figure 5.4 it is possible to realise that the normal distribution fits approximately well the obtained data. This graph was obtained for the undrained shear strength along the depth. The average value and standard deviation for c_u are, respectively:

- $c_{u,avg} = 8.7kPa$
- $c_{u,st.dev.} = 5.2kPa$

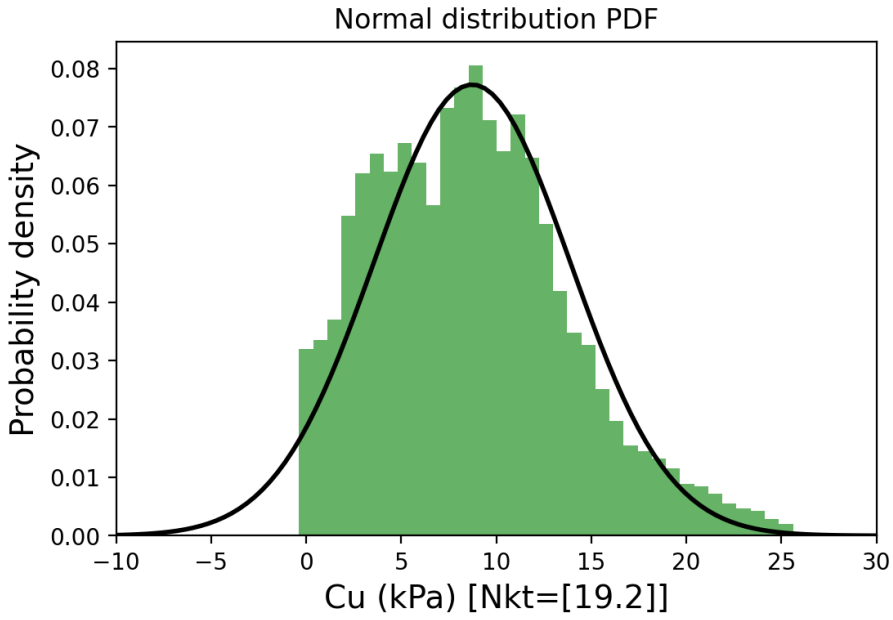


Figure 5.4 – Histogram and Normal distribution Probability Density Function, considering the distribution of c_u without depth dependency

The standard errors associated with both the intercept $se(\hat{a}_0)$ and slope $se(\hat{a}_1)$ associated with the Equation 5.8 resulted in:

$$se(\hat{a}_0) = se(c_{u,0m}) = 0.029; \qquad se(\hat{a}_1) = se(c_u/\sigma'_{vo}) = 0.002 \tag{5.9}$$

From this analysis, it is possible to conclude that this variability is extremely low from a geotechnical point of view, meaning that this uncertainty has almost no significance. With that said it is not possible to conduct a probabilistic analysis in order to access the variability of the c_u parameter. The outcome of producing a probabilistic analysis considering the results obtained would practically match in producing a deterministic analysis using the Equation 5.8 parameters.

5.3.2. Approach 2 - Separated CPTU Analysis

In this second approach, every single CPTU result was analysed independently (i.e. without considering the scatter effect of analysing all the CPTU readings at the same time). This consideration was conducted using the same layering criteria as the approach 1. Also the average value of $N_{kt} = 19.2$ was also used in this approach.

Basically, for each CPTU result the c_u evolution via linear regression was determined (also using the least squares method) in order to interpret the results obtained. For the first analysis plotted in Figure 5.5, every CPTU was considered, without any interval filtering regarding the obtained results. Visually analysing the plot, it is possible to observe a huge variation in the obtained results.

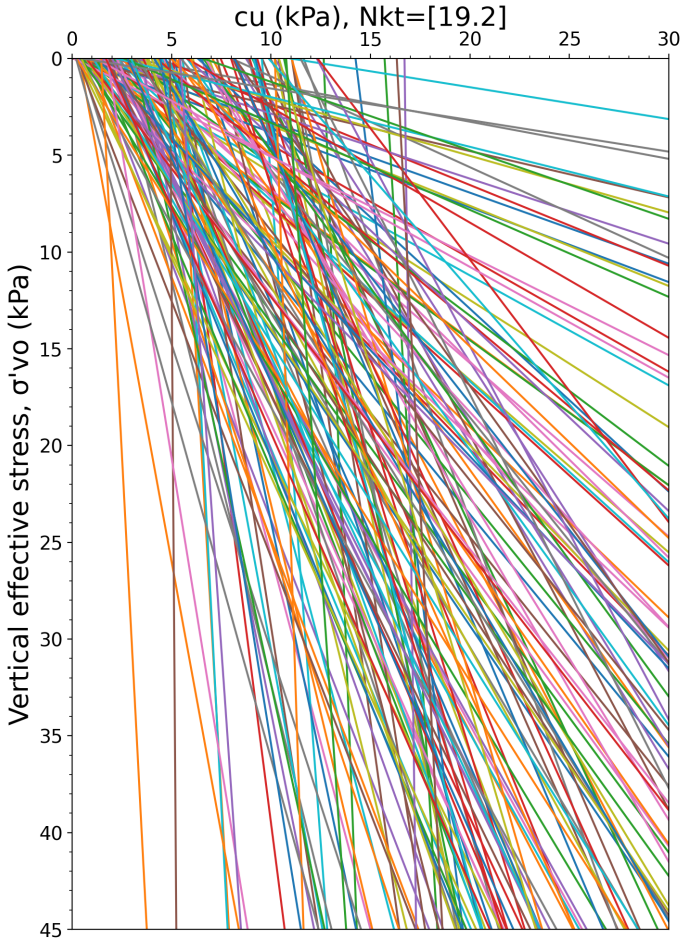


Figure 5.5 – Linear regression for c_u evaluation in every CPTU log

In order to understand the interval with more detail the range of variation of the linear strength evolution, the frequency of results was determined for each one of the linear regression coefficients: rate of change (c_u/σ'_{vo}) and undrained strength at the top of the layer ($c_u(0m)$). From the analysis of Figure 5.6 it is possible to take the following conclusions:

- There is a great concentration of data (more than 5 occurrences) from 0 until 1
- It reveals existent values that seem to be nonsense from a typical c_u evolution in a soft soil (all the values higher that the unit)
- From $c_u/\sigma'_{vo} > 1.8$, the data looks considerably disperse, considering the frequency and the existent gaps between the observations.
- Overall the data distribution in incoherent for soft cohesive soils and even less coherent for this Lynetteholm gyttja in particular (that is a very soft soil).

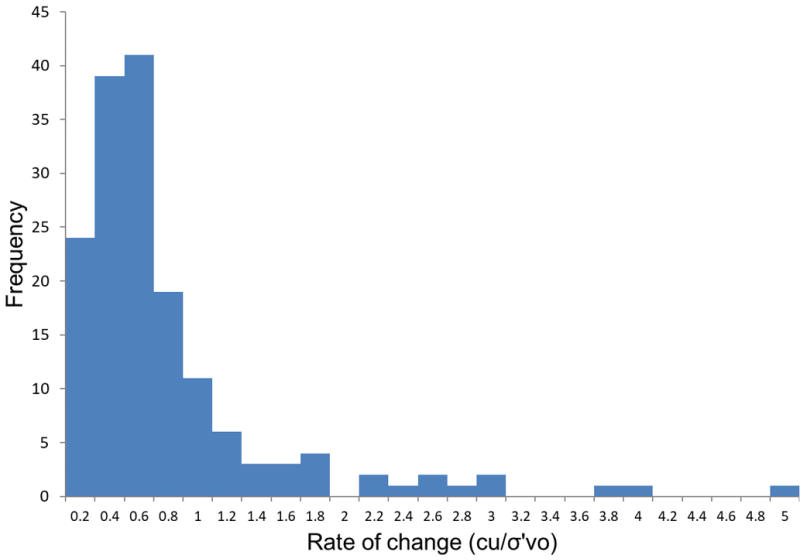


Figure 5.6 – Histogram for the rate of change of every linear regression

The frequency of the obtained results were also determined for $c_{u(0m)}$ (Figure 5.7). Herein it is possible to observe a frequency decrease with strength increase. It is also possible to visualize a data gap between 13 and 14 kPa. In this case, from a geotechnical point of view, considering this soil behaviour, the data distribution seem to be realistic.

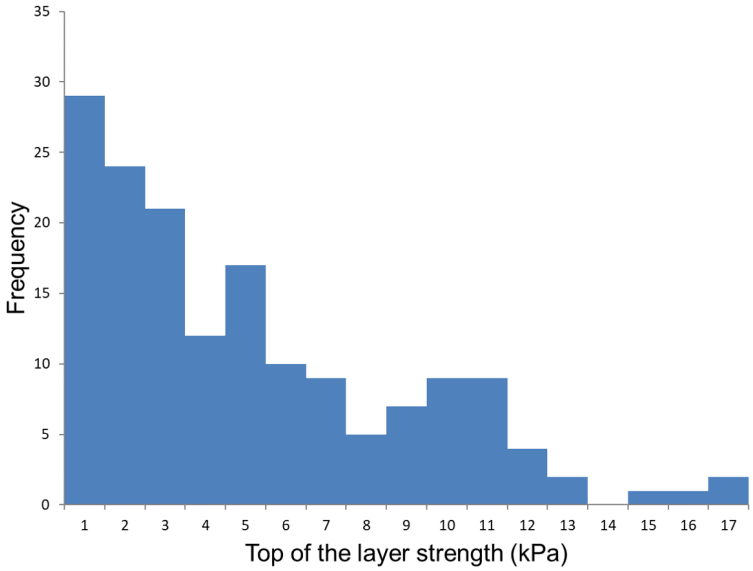


Figure 5.7 – Histogram for the undrained strength at the top of the gyttja layer considering every linear regression

On a second analysis in this approach, unwanted data was removed (that seemed to be out of a reasonably interval for this soil). In order to conduct that approach, the coefficient that was used to filter the data was c_u/σ'_{vo} since it was the one which manifested the most important significance and had the greatest variability compared to its importance.

The data was filtered based on the following assumptions:

- Data visualization (locate in the histogram where the data is more concentrated)
- Distribution appearance - where was tried to understand if the data looked like fitting a typical distribution for a geotechnical parameter (e.g. fitted in a normal distribution)
- Geotechnical reasonableness - a typical soft soil does not reveal a higher c_u/σ'_{vo} of 1 (previous experience with normally consolidated soils reveals that the interval for this coefficient is around $0.2 < c_u/\sigma'_{vo} < 0.4$ (Matos Fernandes, 2016).

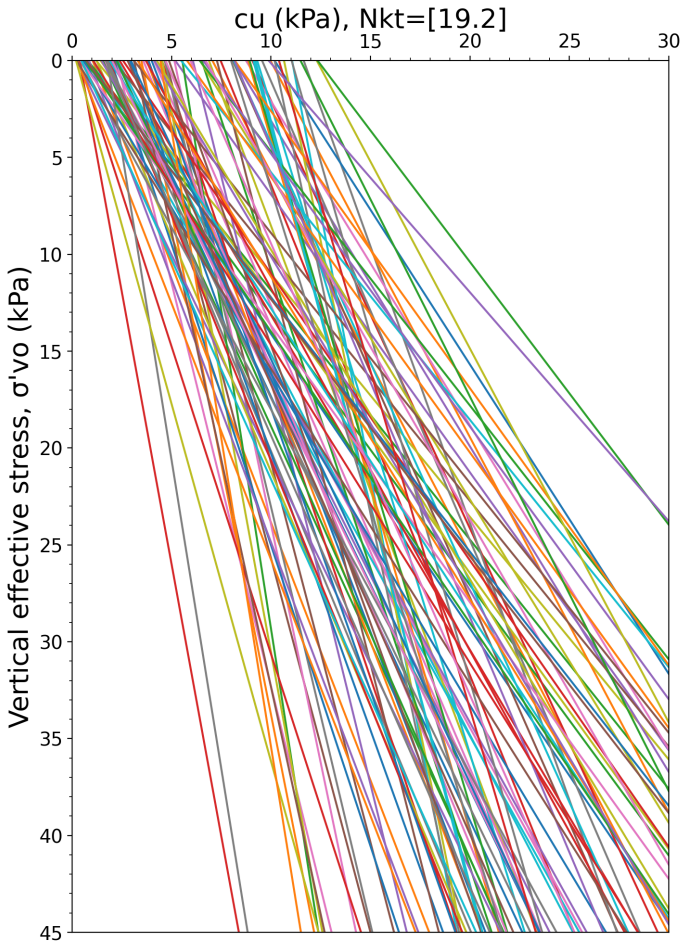


Figure 5.8 – Linear regression for c_u evaluation in every CPTU result filtered ($0.15 < c_u/\sigma'_{vo} < 0.85$)

Based on the enumerated assumption the data was filtered to be inserted to the interval of: $0.15 < c_u/\sigma'_{vo} < 0.85$. From the analysis of Figure 5.9 it is possible to observe that data does not follow by far a typical data distribution for a geotechnical parameter (i.e. normal, lognormal, etc.).

The values obtained demonstrate a frequency peak of 14 and 16 observations between the range of $0.35 \leq c_u/\sigma'_{vo} \leq 0.45$. Also for the interval of $0.15 \leq c_u/\sigma'_{vo} \leq 0.35$ and $0.45 \leq c_u/\sigma'_{vo} \leq 0.75$, it is possible to observe a reasonably amount of values (from 5 to 9 observations). The filtered results for the top of the layer strength demonstrates decreasing trend of results which disables the option of agglomerate data from single analysis

With that said, it is possible to state the following conclusions from this Approach 2:

- The values can be seen as undefined from a geotechnical point of view - it exists a wide range of frequent values that negatively affects the statistical and geotechnical definition of c_u in the post glacial soil layer.
- The most frequent observations from Figure 5.9 reveal a considerably high rate of strength change: $0.35 \leq c_u/\sigma'_{vo} \leq 0.45$. This interval is considered to be relatively different from the values previously obtained from the triaxial tests (Equation 4.8) and from the CPTU (Equation 5.8) in Approach 1. Also this approach is not on the safe side since the interval inserts the undrained strength in a higher range than the other tests.
- It is considered that the simplistic way of layering (explained in 4.1.5.) is not compatible to this Approach 2. The bottom of gyttja layer is cropped visually (based on q_c), and the accuracy of this method is not enough to have it cropped consistently in order to avoid layering discrepancies such as local peaks of strength.
- Overall the approach did not met valid requirements to conduct a further probabilistic analysis

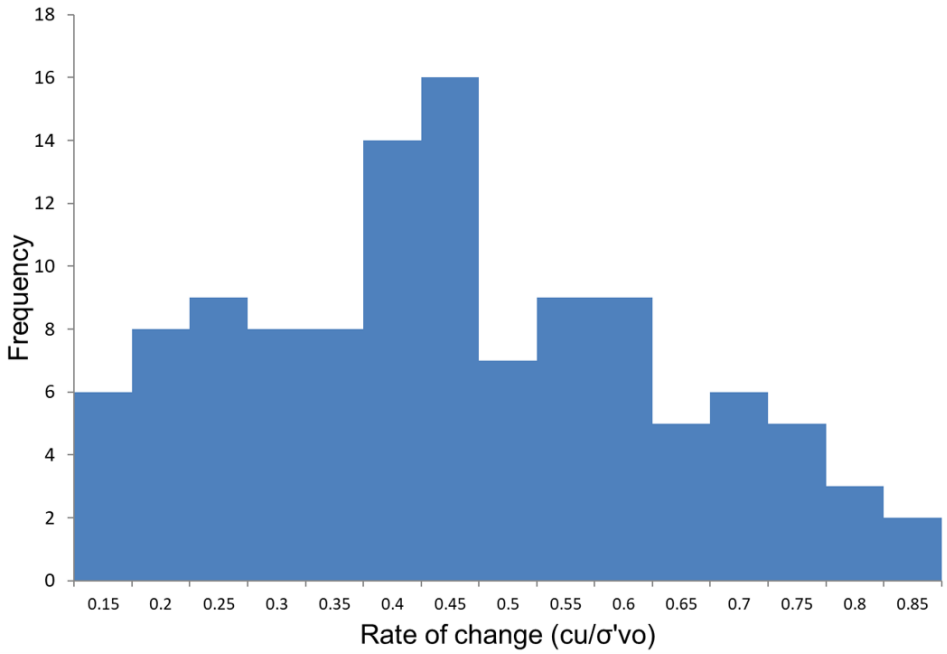


Figure 5.9 – Histogram for the rate of change considering the range: $0.15 \leq c_u/\sigma'_{vo} \leq 0.85$

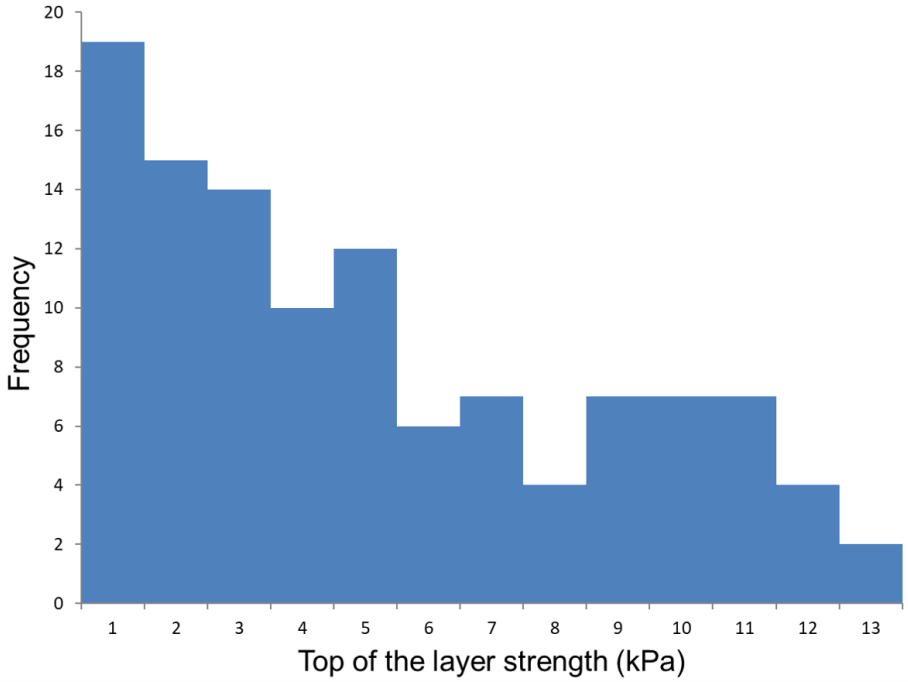


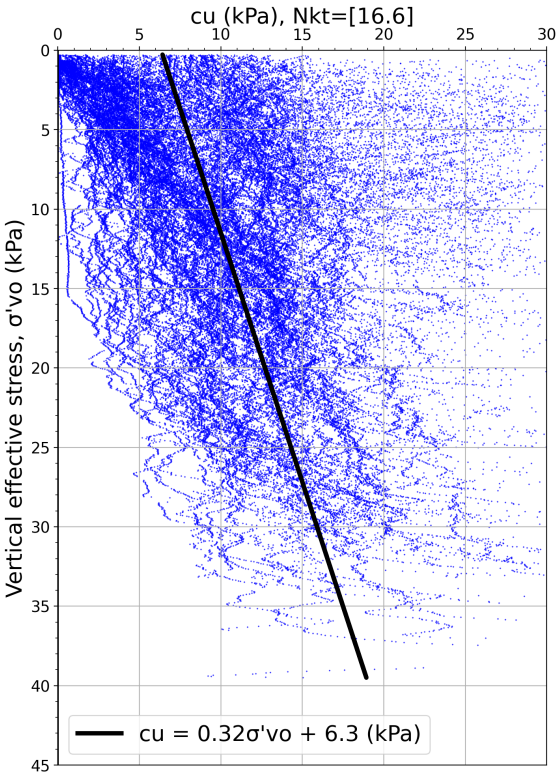
Figure 5.10 – Histogram for the undrained strength at the top of the gyttja layer considering the range: $1 \leq c_u(0m) \leq 13$

5.3.3. Approach 3 - Impact of Nkt variation

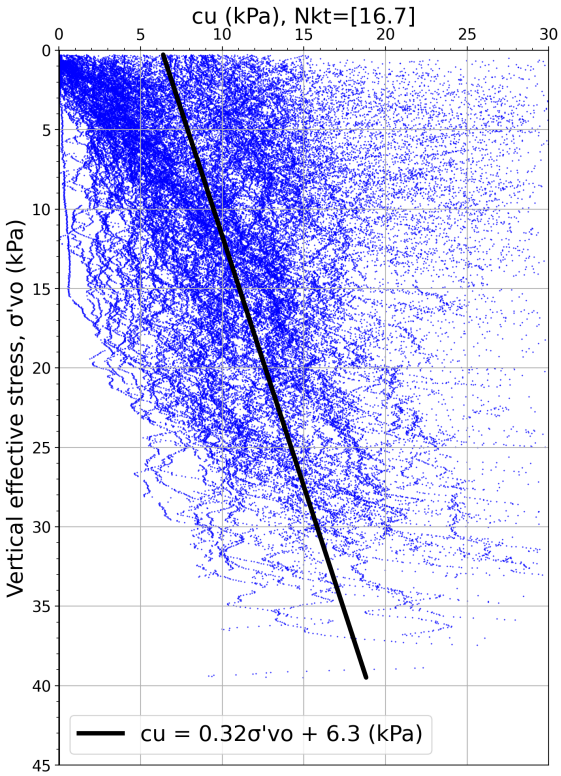
Considering the results from the previous analysis, where it was concluded that both approaches were not a good option to understand the variability effect of c_u, i.e:

- Approach 1 did not possess enough variability to conduct a probabilistic approach that could be used for a probabilistic design case.
- Approach 2 had a incredibly high amount of variability but the interval is considered to be out of geotechnical boundaries for gyttja.

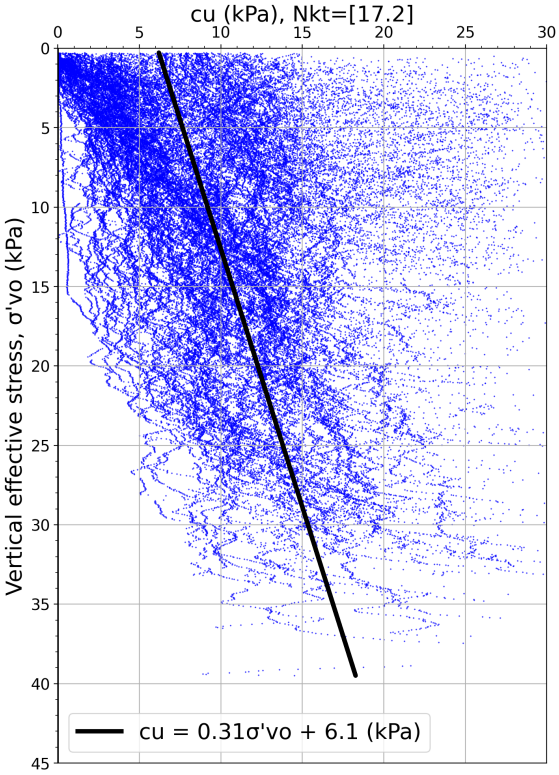
For those reasons it was decided to produce a different approach considering the variability of a parameter that relates the CPTU parameters and the triaxial parameters: N_{kt}. For every N_{kt} value obtained for each sample presented in Table 4.9, the c_u evolution was determined for all the CPTU data using each N_{kt} value. Since it exists in total 5 samples it was determined 5 linear regressions. The plots for each situation are demonstrated in Figure 5.9.


cu (kPa), Nkt=[16.6]
Vertical effective stress, σ'vo (kPa)
cu = 0.32σ'vo + 6.3 (kPa)

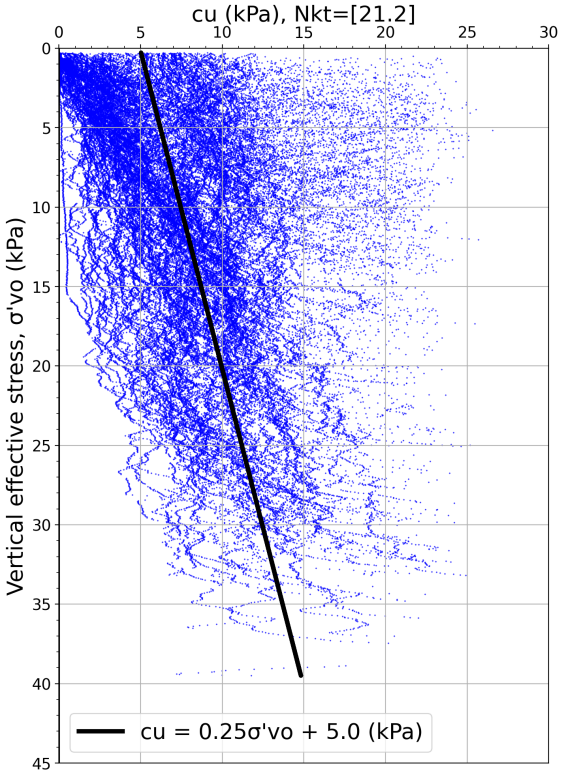
(a)


cu (kPa), Nkt=[16.7]
Vertical effective stress, σ'vo (kPa)
cu = 0.32σ'vo + 6.3 (kPa)

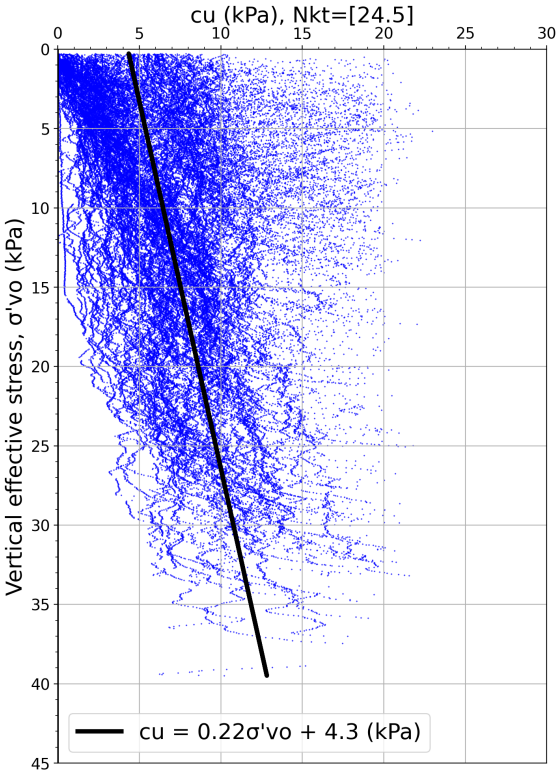
(b)


cu (kPa), Nkt=[17.2]
Vertical effective stress, σ'vo (kPa)
cu = 0.31σ'vo + 6.1 (kPa)

(c)


cu (kPa), Nkt=[21.2]
Vertical effective stress, σ'vo (kPa)
cu = 0.25σ'vo + 5.0 (kPa)

(d)



(e)

Figure 5.9 – Undrained shear strength evaluation from using different values for N_{kt}: (a) N_{kt}=16.6, (b) N_{kt}=16.7, (c) N_{kt}=17.2, (d) N_{kt}=21.2, (e) N_{kt}=24.5. For each scatter, the line in black represents the linear regression of data

As expected, the higher this parameter is, the lower the value for the c_u, as the Equation 4.15 demonstrates. It is interesting, however, to observe the effect of this parameter in the c_u evolution. When N_{kt} presents lower values, the scatter is more dispersed, the strength rate of change, c_u/σ'_{vo}, is flatter (higher strength) and c_u is distributed along a greater range (e.g in Figure 5.9 (a) the strength interval is around: $0 < c_u < 30$ (kPa))

Table 5.1 – Linear regression results depending on the N_{kt} variation

N_{kt}	c_u/σ'_{vo}	$c_{u,(0m)}$ (kPa)	Figure 5.9 case
16.6	0.319	6.3	(a)
16.7	0.317	6.3	(b)
17.2	0.308	6.1	(c)
21.2	0.250	5.0	(d)
24.5	0.216	4.3	(e)

Based on the probabilistic approach that was chosen in the previous chapter, the strength parameters were introduced based on probability distributions. Since the strength evaluation is based on the undrained shear strength, c_u, it was determined the probabilistic density function, PDF, for both the rate of change

coefficient and the c_u at the top of the layer.

Laboratory results on natural soils have shown that most soil properties can be considered as variables that follow a normal distribution function. For that reason it was assumed that both parameters fit in a normal distribution. However, since the number of observations are limited to 5, it was decided to truncate the normal distributions in order to represent the values for both coefficients included in the interval for the observations. The objective is to have an interval that can be evidenced from a geotechnical point of view.

It can be noticed in Figure 5.10, that the rate of change PDF is cropped from minimum value until the maximum value is observed in Table 5.1.

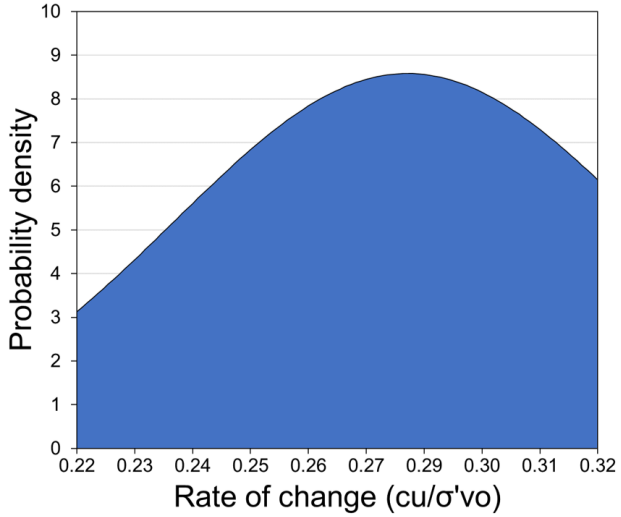


Figure 5.10 – Truncated probability density function for c_u/σ'_{vo}

Figure 5.11 demonstrates the cumulative density function for c_u/σ'_{vo}, according to the PDF in Figure 5.10.

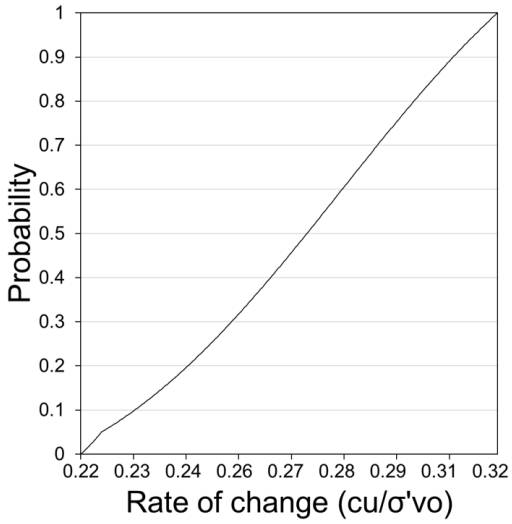


Figure 5.11 – Cumulative density function for c_u/σ'_{vo}

Regarding the undrained strength at the top of the layer parameter, it was also admitted a truncated normal distribution (Figure 5.12) and the respective cumulative density function (Figure 5.13).

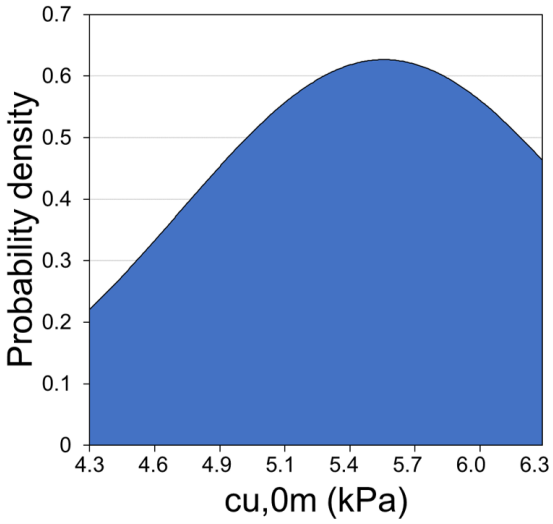


Figure 5.12 – Truncated probability density function for the undrained shear strength at the top of layer

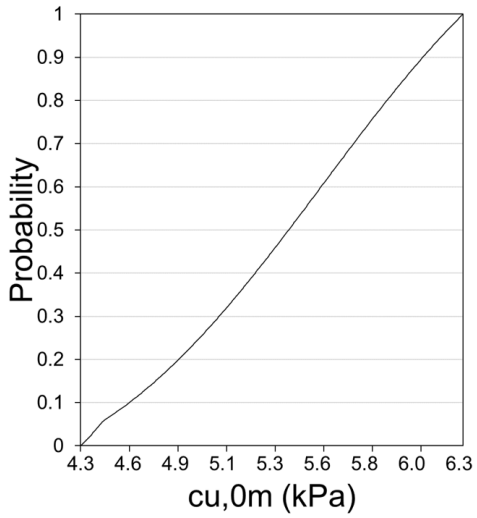


Figure 5.13 – Cumulative density function for the undrained strength at the top of the layer

This approach was the one chosen to conduct a further slope stability probabilistic analysis. Even though it mixes data from different plots considering different assumptions of the N_{kt}, it has met a considerable degree of variability. Also it served to prove the effect on c_u/σ'_{vo} and $c_{u,0m}$ by changing the value of N_{kt}. We can state that the calibration of N_{kt} has a considerable impact of the undrained shear strength evaluation.

In order to simplify the c_u evaluation in Approach 3, it was plotted 3 relations relating the 3 parameters obtained in Table 5.1. As it can be observed in Figure 5.14, Figure 5.15 and Figure 5.16, the data has a linear evolution for every scatter. For that reason it was determined for each plot, the linear regression that relates those coefficients.

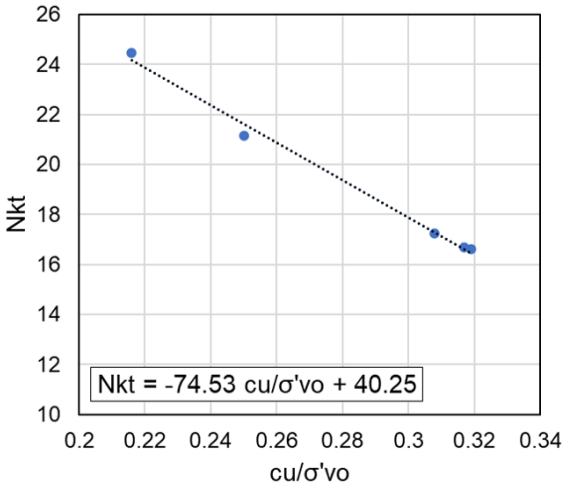


Figure 5.14 – Relation between N_{kt} and c_u/σ'_{vo}, indicating the linear regression (dotted line)

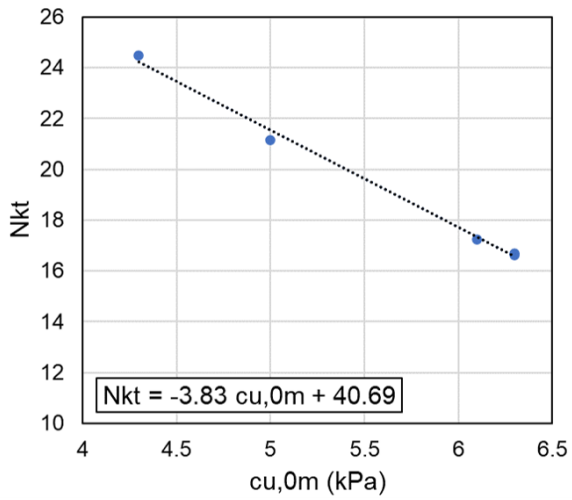


Figure 5.15 – Relation between N_{kt} and $c_{u,0m}$, indicating the linear regression (dotted line)

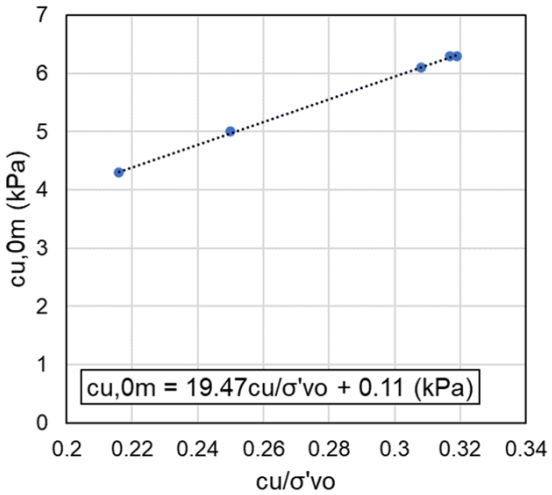


Figure 5.16 – Relation between $c_{u,0m}$ and c_u/σ'_{vo}, indicating the linear regression (dotted line)

In Table 5.2 is demonstrated the relation between the coefficients grouped in pairs. Those simple expressions can be used to rapidly evaluate the linear regression that best fits the data from the 80016 readings. It can be stated that those expressions explain the c_u evaluation with depth by modifying the N_{kt} parameter. In simplified terms this expressions resulted in producing linear regressions based from a compilation of linear regressions (from the scatters in Figure 5.9). The reason behind the linear trend in those graphs can be explained by the proportionality relation between N_{kt} and c_u (Equation 4.15). This is also supported by an obtained value of R^2 near to 1 (great prediction).

Table 5.2 – Indication of the linear regressions of

Linear regression	R^2	Figure
$N_{kt} = -74.53\frac{c_u}{\sigma'_{vo}} + 40.25$	0.993	Figure 5.14
$N_{kt} = -3.83c_{u,0m} + 40.69$	0.995	Figure 5.15
$c_{u,0m} = 19.47\frac{c_u}{\sigma'_{vo}} + 0.11$	1.000	Figure 5.16

5.4. CHAPTER SUMMARY

With Approach 1, is was possible to conclude that the c_u evolution from CPTU, considering 80016 readings, matches the CAUC evolution (considering 15 readings). One of the conclusions extracted from this chapter in Approach 1 is the validation of a previous thought that indicates that there is not a great motive to consider the spatial variability of gyttja in the project area. When combining the c_u results obtained in CAUC tests (Equation 4.8), the spread CAUC location (Figure 4.21) and the results obtained in CPTU (Equation 5.8), there is the possibility to conclude that this is a soil that don't possess spatial variability, i.e the strength of gyttja in not dependent from the place it is located. However, this statement can be criticised based on the existent amount (only 5 values) of CAUC tests and consequently N_{kt} values that could be seen as not very reliable. Also from the results obtained in Approach 2, considering the independent CPTU results, the spatial variability conclusion seem to be the exact opposite as previous stated. Yet, the explanation for this phenomenon is considered to be the straightforward thickness evaluation of gyttja (explained in 4.1.5.) that was used. This thickness evaluation based on manually cropping the soil based on q_c ignore aspects, such as local peaks (evidenced in Figure 4.8) that are relevant when analysing single readings with depth. Also the q_c reading scale used to do it, is not very accurate for gyttja since the interval for this soil is included in $0 < q_c < 0.5$ (MPa) and the scale in Figure 4.8 only have an accuracy of about 1 MPa. This is considered to be the reason behind the great result dispersion in Approach 2. Here the results for the c_u evolution seem to be not valid from a geotechnical perspective since the interval is far from expected for a clayey soil. Approach 3 served mostly to prove the effect of N_{kt} variability in c_u results. The higher this parameter is, the less resistant and concentrated are the overall c_u points. Statistically speaking, this approach could be considered to be not very valid since it creates a PDF based on 5 linear regressions. Not only the number of N_{kt} values are few, but is also difficult to predict that those 5 values follow a normal distribution. However the point here was to prove the importance of N_{kt} and not to create a purely statistical approach. Also this approach was important to resume the c_u evolution from 80016 readings in 3 linear expressions that represent the direct effect of N_{kt} in c_u evolution.

6
SLOPE STABILITY

6.1. INTRODUCTION

The following chapter will disclosure an application of Approach 3 for slope stability design. A probabilistic analysis for both short and medium term analysis is performed. In addition, a slope stability deterministic analysis considering the short, medium and long term analysis is presented.

6.2. FACTOR OF SAFETY METHOD

This evaluation will be carried out by using a software, SLOPE/W that computes the method of slices developed on the basis of limit equilibrium. The method of slices used in this work will be the Morgenstern-Price method, which is considered be a good and validated method in engineering practice. From a synthetic point of view, Morgenstern-Price method, satisfies both moment and force equilibrium, considers both shear and normal interslice forces and allows for a variety of user-selected interslice force functions. (GEO-SLOPE, 2012). Except for the last idea, Morgenstern-Price method is similar to the Spencer method.

6.3. PROBABILISTIC METHODS APPLIED TO SLOPE STABILITY

6.3.1. MONTE CARLO METHOD

The Monte Carlo method, MCM, is a simple and versatile probabilistic method, that is commonly used in geotechnical engineering practice.

It may be considered exact in obtaining the probabilistic distribution function of the dependent variable, since it solves randomly the engineering formulation for the dependent variable (performance indicator) N times, generating a sample of results, and when N is a number large enough, the statistics of the resulting sample do not change any more, achieving its stability, indicating that the results are final and considered exact.

Software that use limit equilibrium methods, LEM, such as SLOPE/W have incorporated the MCM in the stability computing. This method applied in a slope stability software involves the following steps:

- Choice of the deterministic solution procedure (Morgenstern-Price) that is going to be used for the determination of the safety factor.

- Probabilistic modelling of the input parameters (strength rate of change and top layer strength) that represent their variability based on the selected distribution model (Normal distribution).
- Based on the chosen number of Monte Carlo samples, N, and the distribution function for each strength parameter, N sets of random values for those parameters are generated.
- The LEM is going to be executed where, for each slice, its going to be computed the deterministic procedure N times for each slice.
- In each slice there is going to be determined the probability of failure, p_f, that depends from the number of solutions that have a factor of safety, FS, less that 1.0. For example, in an analysis with 2000 MC trials, 1860 trials produced a factor of safety greater than 1.0 and 372 trials produced a factor of safety of less than 1.0. The probability of failure in this case would be 20%.

For a normal probability distribution function (the admitted PDF for the variables), the sampling function has a relatively straight segment in the middle. This means that the parameters around the mean will be sampled more frequently than the values at the ends of the sampling function (Khan & Malik, 2016).

6.3.2. Number of Monte Carlo Samples

The number of Monte Carlo trials in an analysis depends on the variability of input parameters and the expected probability of failure. The number of required Monte Carlo trials in general, is proportional to the material parameter variability. A higher variability of a certain soil parameter, will require a higher number of samples in order to have a solid convergence. It has been suggested by (GEO-SLOPE, 2012) that the number of required Monte Carlo trials is dependent on the desired level of confidence in the solution, as well as the number of variables being considered. An important aspect herein is to know when the number MC simulations is large enough and the results can be considered already stabilised. In order to understand the number of MC simulations exists a statistical formulation that estimates the number of MC simulations, assuming the possible occurrence of an error α, which is expressed by:

$$N = \left(\frac{Z^2_{\alpha/2}}{4\alpha^2} \right)^2 \tag{6.1}$$

Where N is the desirable number of MC simulations, $Z_\alpha/2$ is the number of standard deviations around the mean to reach an error $\alpha/2$ at each distribution tail and n is the number of input variables. This statistical formulation usually results in an enormous number of MC simulations (Assis, 2020). Therefore, commonly the criterion to verify the stabilisation of the number of MC samples is observational, considering a number of samples that reaches a good level of stabilization. In this work it is going to be conducted 2 different analysis with 1000 and 2000 samples in order to understand the effect on results when increasing the amount of Monte Carlo samples.

6.3.3. Reliability Assessment

A very important concept when speaking about the safety approaches in geotechnical design is the term reliability. Often the concept of reliability is conceived in an absolute way – the structure either is or is

not reliable. In accordance with this approach the positive statement is understood in the sense that "a failure of a certain structure will never occur". This interpretation is not accurate from a real point of view. Although it may be unpleasant and for many people perhaps unacceptable, the hypothetical area of absolute reliability for most structures simply does not exist in reality. Even if a certain structure is considered reliable, there is always a small probability of collapse. The failures are accepted as a part of the real world and the probability or frequency of their occurrence should be considered. In fact, in the design it is necessary to admit a certain small probability that a failure may occur within the intended life of the structure. Otherwise designing of civil engineering structures would not be possible at all (Diamantidis & Holickỳ, 2010).

The regulation documents such as the Eurocodes are based in the statement that ”a structure shall be designed and executed in such a way that it will, during its intended life with appropriate degrees of reliability and in an economic way sustain all actions and influences likely to occur during execution and use, and remain fit for the use for which it is required”. The basic reliability measures include the probability of failure and reliability index (EN 1990, 2002).

6.3.4. Probability of failure

The probability of failure is the probability of obtaining a factor of safety less than 1.0. The probability of failure can be understood in two different ways:

- If a certain slope is going to be constructed many times, what percentage of such slopes would fail.
- The level of confidence that can be placed in a design of a specific slope.

The first interpretation may be relevant to slopes where the same slope is constructed several times, while the second interpretation is more relevant where slopes are only to be constructed once and it either fails or it does not. The project is about continuous slopes that are going to be constructed along a considerable distance from the entire perimeter.

There is no direct relationship between the deterministic factor of safety and probability of failure. A slope with a higher factor of safety may not be more stable than a slope with a lower factor of safety (Khan & Malik, 2016).

6.3.5. Reliability Index

Apart from the probability of failure, p_f, the reliability index, β, is frequently used in reliability consideration as an equivalent alternative to p_f. This index β can be related to the failure probability by the expression:

$$p_f = \Phi(-\beta) \approx 10^{-\beta} \tag{6.2}$$

In Equation 6.2, Φ, represents the cumulative distribution function of the standardised normal distribution. Based on this approach, reliability acceptance criteria can be defined. In terms of acceptable values for design it is possible to use the admissible failure probability, p_d, and the

acceptable reliability indices β_d. These quantities are recommended as reasonable minimum requirements, meaning that p_d and β_d are formal conventional quantities only and may not correspond to actual frequency of failures.

In design analysis of a structure it is generally required that:

$$p_f \leq p_d \tag{6.3}$$

or equivalently in terms of reliability index:

$$\beta \geq \beta_d \tag{6.4}$$

In order to understand the exact relation between p_f and β there was made the compilation of this relation in Table 6.1

Table 6.1 – Relation between p_f and β (adapted from (EN 1990, 2002))

p_f	$p_f(\%)$	β
10^{-1}	10	1.28
10^{-2}	1	2.32
10^{-3}	0.1	3.09
10^{-4}	0.01	3.72
10^{-5}	0.001	4.27
10^{-6}	0.0001	4.75
10^{-7}	0.00001	5.20

6.3.5.1. Reliability Classes

The design failure probability is usually indicated in relation to the expected social and economical consequences in order to reflect the risk acceptance criteria. In Figure 6.1 is revealed the classification of target reliability levels provided in (EN 1990, 2002). Reliability indexes, β are given for two reference periods (1 year and 50 years), without any explicit link to the design working life T_d. The values from Figure 6.1 are based on calibration and optimization and reflect results from several studies. It should be underlined that the β_a and β_d values specified for each reliability class (for 1 year and 50 years) correspond approximately to the same reliability level. Practical application of these values depends on the time period T_a considered in the verification, which may be connected with available statistical information concerning time variant actions (wind, earthquake, etc.)

Typical example structures of reliability class 1 (RC1) are greenhouses and agricultural structures with limited risk to human life. Structures of reliability class 2 (RC2) are residential and office buildings. Stadiums, public buildings and bridges are structures included in reliability class 3 (RC3) (Diamantidis & Holickỳ, 2010).

Reliability classes	Consequences of failure	Reliability index β	
		β_a for T= 1 year	β_d for T= 50 years
RC3 – high	High	5.2	4.3
RC2 – normal	Medium	4.7	3.8
RC1 – low	Low	4.2	3.3

Figure 6.1 – Reliability classes from the Eurocode approach (EN 1990, 2002)

The output of a slope stability analysis can be defined as a probability density function of the factor of safety and a cumulative density function of the probability of failure. For that reason it is important to have an idea of the admissible values for the probability of safety based on different parameters. Santamarina et al. (1992) developed criteria for using these output distributions for assessing the consequences of slope failure (Figure 6.2), based on a logic analysis of responses to a survey of geotechnical engineers. These criteria associate acceptable levels of probability of failure with various design conditions.

Conditions	Criteria for Probability of Failure	Equivalent Event
Temporary structures with low repair cost	10^{-1}	1 in 10
Existing large cut on interstate highway	10^{-2}	1 in 100
Acceptable in most cases except if lives may be lost	10^{-3}	1 in 1,000
Acceptable for all slopes	10^{-4}	1 in 10,000
Unnecessarily low	10^{-5}	1 in 100,000

Figure 6.2 – Probability of failure criteria for slope stability purposes (Santamarina et al., 1992)

These criteria depend on these different aspects:

- Cost of lowering probability of failure with respect to post failure repairs
- Loss of human life
- Economic loss
- Type and importance of service
- Existing or new construction
- Temporary or permanent duration

6.4. Types of Stability Analysis

In order to conduct the stability analysis on gyttja, according to Figure 3.17, the two different analysis were considered depending on the timing of the execution of phase 2 expressed on Table 3.3. In fact the

excavation of the soft soil will be a temporary construction since the gyttja slope will be later stabilized by the sand fill that will be deposited in between, preventing a slope failure after this point. However it was not previously decided if the execution of phase 2 will be conducted that fast, preventing the dissipation of the excess pore pressure after its construction, and consequently preventing the drop of shear strength until the application of that stabilisation force. For that reason it was considered a short term analysis (right after the excavation) and an analysis considering part of the dissipation of the excess pore pressure, but considering the undrained behaviour (medium term analysis). Additionally, a simple long term analysis was also performed to serve as reference, based on the effective stress parameters obtained from the CAUC tests.

6.4.1. Short Term Analysis

In this case, the analysis is performed right after the excavation of gyttja (short term), without dissipation of the excess pore pressure. In Figure 6.3 it is possible to observe that, in this case, the evolution of shear strength starts at the beginning of the layer. After the excavation, for a certain point in the slope surface (A), the shear strength is the same for every point for the same depth. The top of the layer represents the datum for the start of the strength evolution rate. This is explained by the fact that the dissipation of the excess pore pressure hasn't occurred yet.

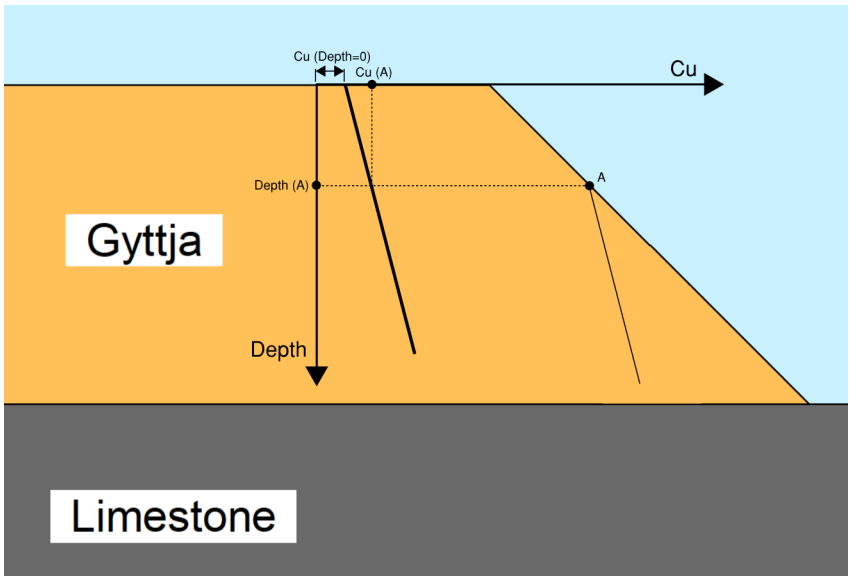


Figure 6.3 – Shear strength as a function of depth below the seabed surface (short term analysis)

6.4.2. Medium Term Analysis

The execution of an excavation will lead to a reduction of the average stress (i.e, $(\Delta\sigma_1 + \Delta\sigma_3)/2 < 0$), caused by the removal of a soil mass. In normal consolidated soils, such as this gyttja in particular, possess considerable high values of the A parameter (similar value to A_f determined in Table 4.7). Following the Equation 6.5 proposed by Skempton (1954), it is possible to perceive that the reduction of the average strength will develop a negative excess pore pressure ($\Delta u < 0$).

$$\Delta u = \frac{(\Delta\sigma_1 + \Delta\sigma_3)}{2} + \frac{(2A-1)(\Delta\sigma_1 - \Delta\sigma_3)}{2} \tag{6.5}$$

After the excavation process, pore pressure will increase and the effective strength will decrease due to the consolidation process. Consequently, the shear strength and the safety factor will also decrease. The minimum value for the factor of safety will be reached at the end of the consolidation process, where the equilibrium is reached, i.e the dissipation of the excess pore pressure had occurred totally (Matos Fernandes, 2015). Figure 6.4 demonstrates the evolution of pore pressure and safety factor with time. This includes the moment from the begging of the excavation until the moment where equilibrium is reached.

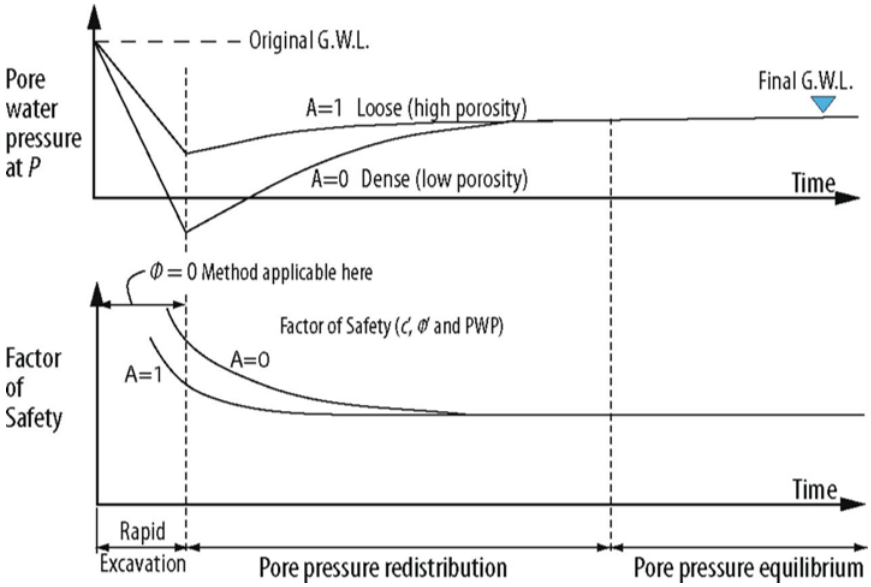


Figure 6.4 – Variation of pore water pressure and safety factor with time (Bishop & Bjerrum, 1960)

As described before, phase 1 will be a temporary construction. This means that the time necessary for the entire dissipation of the excess pore pressure will be much higher than the execution of phase 2. For that reason it was considered an analysis (medium term) that admitted the dissipation of an important parcel of the excess pore pressure.

This means that every point of the slope surface of the layer possess the same shear strength at the top of the layer. Now, every point along the slope surface has its own strength evolution referential. The reason for considering an undrained behaviour is due to the fact that the predicted construction pace will be higher than the time necessary to finish the consolidation process. We can conclude that from this both 2 analysis that the medium term analysis represents the most critical scenario for practice to evaluate the slope stability. Previous experience with gyttja has proved that normally, for temporary excavations, the time spent until further stabilization is lower than the time necessary for the consolidation process.

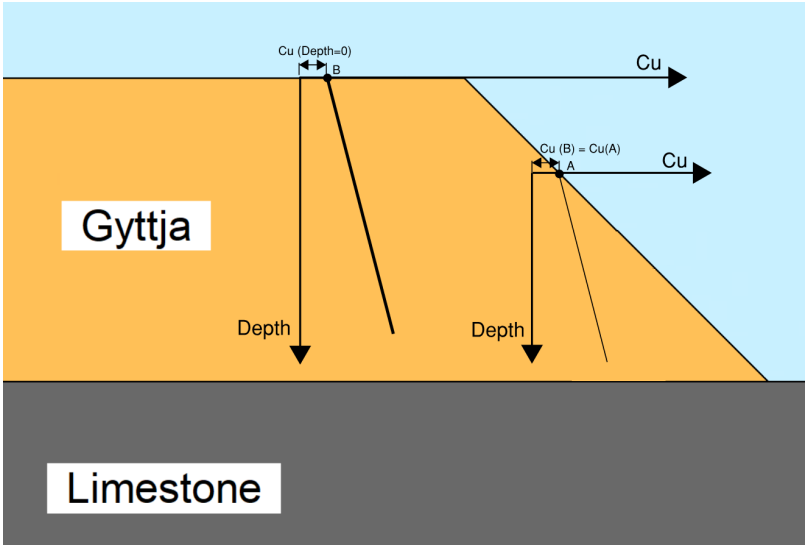


Figure 6.5 – Shear strength as a function of depth (medium term analysis)

6.4.3. Long Term Analysis

For reference, a long term analysis was also performed considering that the consolidation process has already totally occurred. From a practical point of view, this analysis in not very relevant since the excavation of gyttja is a temporary construction where the slopes will be later stabilized by the sand fill layer. This analysis would be interesting if this excavation was a definitive construction, which is not the case. For this reason, a very simplistic analysis was performed without a great deal of detail and without considering any probabilistic approach for the effective stress parameters. Those parameters were just interpreted from the CAUC tests at the peak deviator stress as summarized in Table 4.5. This aim of this evaluation was to have a comparison to the medium term analysis in terms of the safety factors.

6.5. Stability Analysis Results

For the representation of results the most critical scenario for the slope stability analysis (Figure 6.6) is the one that corresponds to the case were the thickness of gyttja reaches the 9m and the slope have an angle of 45 degrees (1:1). Regarding the strength evolution, the selection is based on the most critical one that corresponds to the medium term analysis.

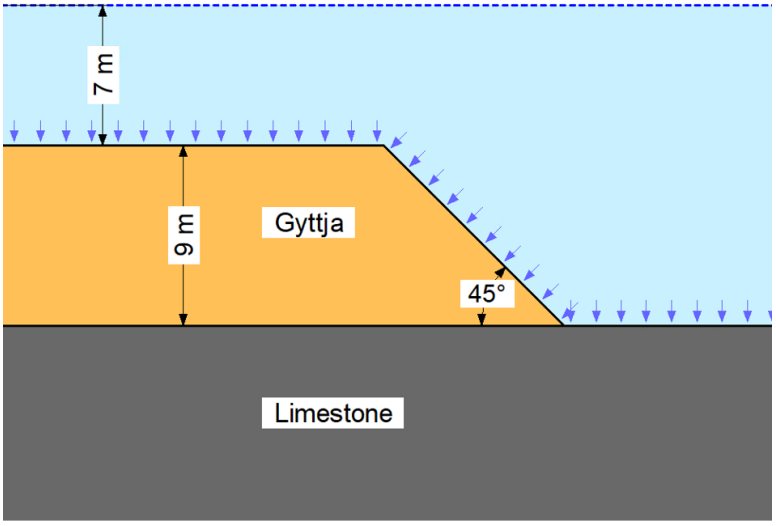


Figure 6.6 – Slope geometry of the represented results case

6.5.1. Factor of Safety Interpretation

In Figure 6.7, is represented the output of the distribution of the factor of safety for the critical slice obtained is represented, where it is possible to observe the frequency versus the variation of this value. The curve in blue represents the fitted normal distribution to the values obtained.

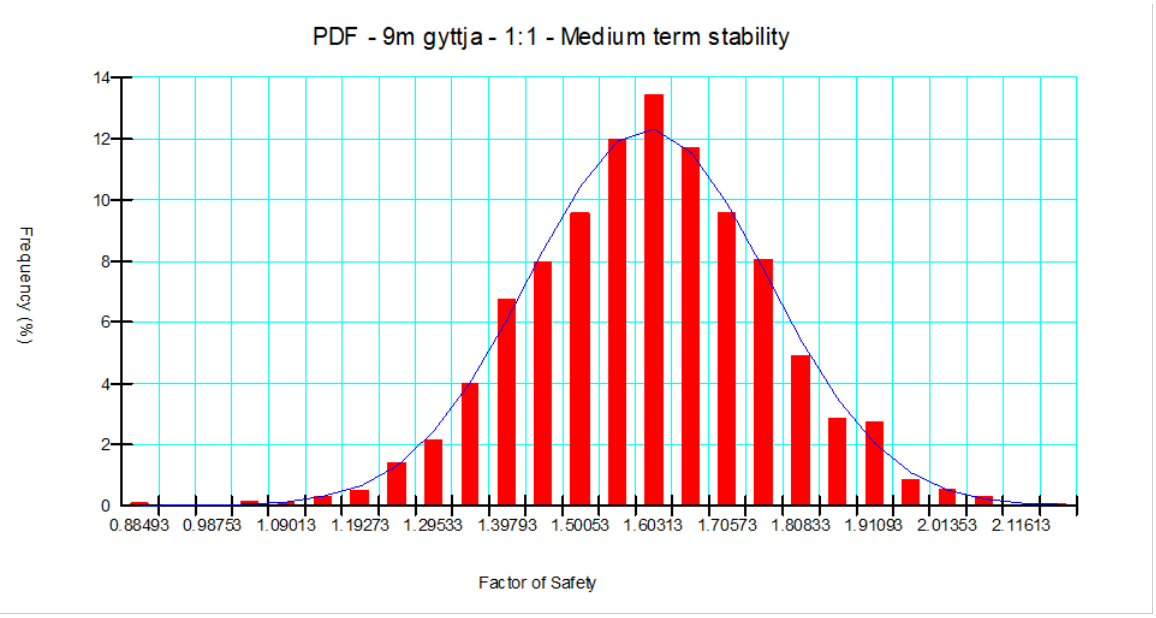


Figure 6.7 – Factor of Safety histogram distribution and the fitted normal distribution to the values obtained

The factor of safety, FS, was also determined for a deterministic analysis considering the average value obtained from the fitted normal distribution from the strength parameters obtained in Approach 3:

$$c_u = 0.28\sigma' vo + 5.6(kPa) \tag{6.6}$$

It is possible to observe in Figure 6.8 that the critical slip surface has a great geometrical dimension.

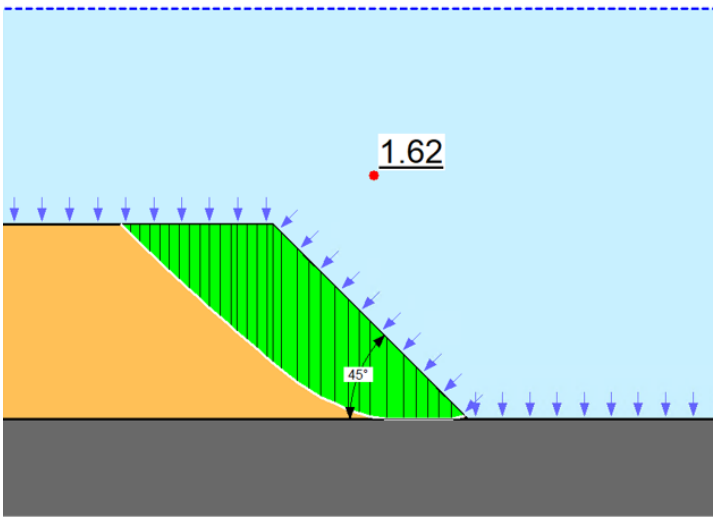


Figure 6.8 – Factor of safety for the critical slice in the considered scenario (deterministic analysis)

In order to understand the probability associated to the variation of the factor of safety, this graph reveals, for a certain point, the cumulative probability of the factor of safety to be equal or less that the respective value. For example when observing Figure 6.9, the probability for the factor of safety to be equal or less than 1.4 is around 10%. The objective for this type of plot is also to access the probability of failure that is formulated by the probability for the FS being less or equal than 1. Here, it is possible to observe that the probability associated to this occurrence is 0 or very close to 0.

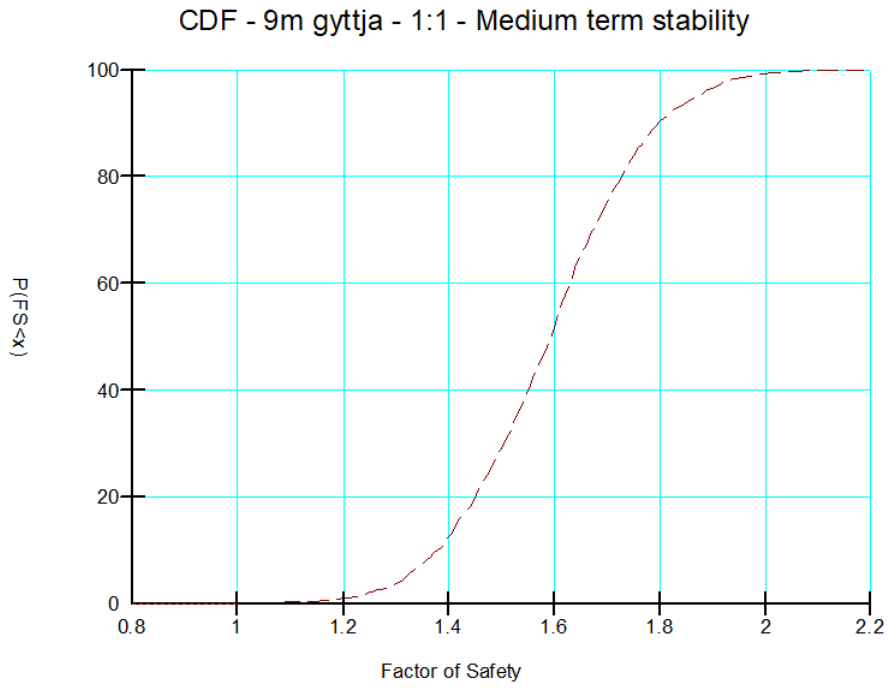


Figure 6.9 – Cumulative density function for the factor of safety

6.5.2. Monte Carlo Convergence

6.5.2.1. Probability of Failure

In order to understand the convergence for the probability of failure obtained with the increase of the number of samples, it was plotted the graph in Figure 6.10 that reveals for the critical slice, the evolution of the probability of failure with the increment of the number of samples. In this case is possible to understand that the convergence trend is constant and equal to zero until the run number reaches 1100. From that point until the end of the run, it exists more 2 trends that seem to have no convergence relation between them. This type of evolution graph can be explained by the fact that the values of the probability of failure are considerable low and most likely the accuracy of the computation in not sufficient to detail the value for the probability of failure that far.

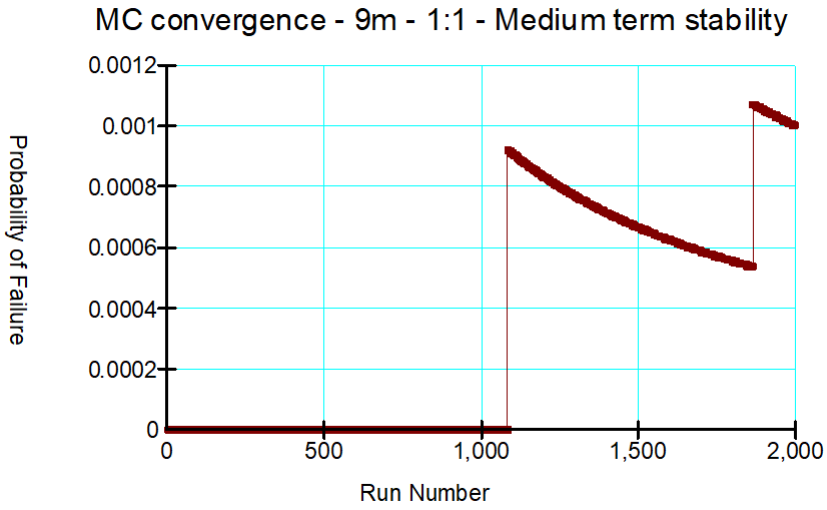


Figure 6.10 – Probability of failure - MC convergence graph

6.5.2.2. Mean Factor of Safety

Considering the analysis of Figure 6.11, it is possible to observe the convergence of the mean factor of safety, FS_{avg} with the run analysis increasement. At a certain point (when the run number reaches 1000), the parameter FS_{avg} starts to converge. As it is possible to observe, the value of FS_{avg} is similar to the value of FS obtained in Figure 6.8.

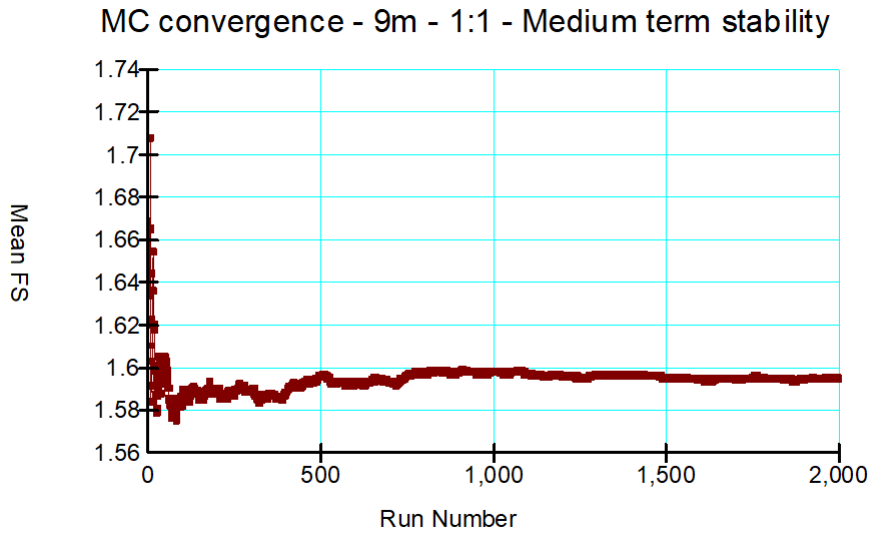


Figure 6.11 – Mean factor of safety - MC convergence graph

6.5.2.3. Standard Deviation of the Mean Factor of Safety

Similar to the plot before described, it is demonstrated in Figure 6.12 the Monte Carlo convergence graph for the standard deviation of the mean factor of safety, σ_{FSavg}. Here the convergence value is around 500 samples.

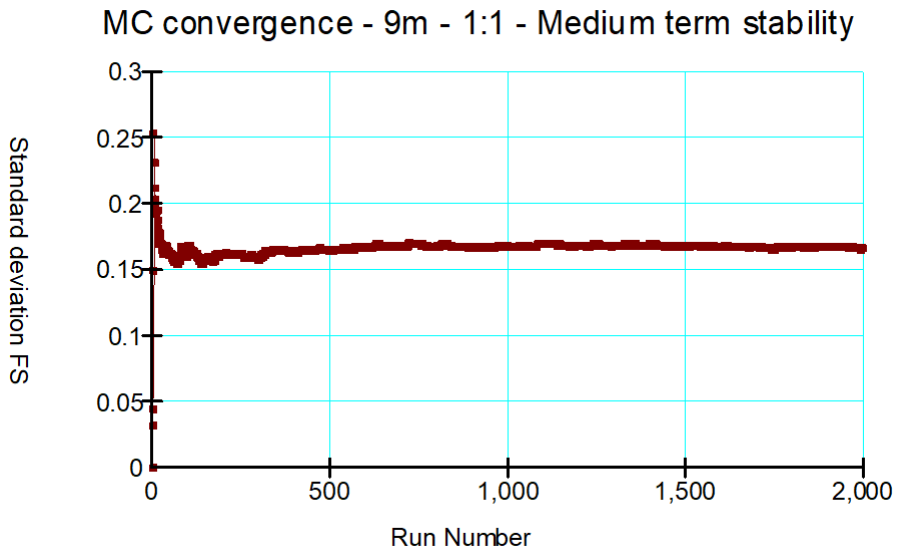


Figure 6.12 – Standard deviation of the mean factor of safety - MC convergence graph

6.5.3. Comparison of Factors of Safety

After running all the analyses in SLOPE/W, the results were compiled for the medium term analysis (most critical) in Table 6.2 and the short term analysis in Table 6.3.

The results were calculated for both 2000 and 1000 Monte Carlo samples in order to understand the effect of the number of samples in the results obtained. The results show that there is not a significant difference when doubling the number of samples. It can be noticed that probability of failure for any situation is considerably low. The slope calculations didn't possess enough certainty to detail values with $p_f < 0.1\%$. Every value below that point is considered 0 by the software output computing. As expected the factor of safety value for the deterministic analysis, FS, matches the value obtained for the probabilistic analysis, FS_{avg}. However the difference between those analysis can be explained by the fact that the normal distributions for c_u/σ'_{vo} (Figure 5.10) and $c_{u,0m}$ (Figure 5.12) are truncated. With that said the average value for a truncated normal distribution is different from a non truncated one, explaining the difference in results. The values for the reliability index, β are also indicated in those tables

Table 6.2 – Medium term stability results from SLOPE/W (characteristic values)

Gyttja depth	Slope	FS_{det}	2000 MC samples				1000 MC samples			
			FS_{avg}	σ_{FSavg}	p_f	β	FS_{avg}	σ_{FSavg}	p_f	β
9m	1:3	2.76	2.72	0.29	0	5.95	2.71	0.28	0.0%	6.06
	1:2	2.20	2.17	0.23	0.0%	5.09	2.16	0.22	0.0%	5.20
	2:3	1.92	1.89	0.20	0.0%	4.51	1.89	0.19	0.0%	4.58
	1:1	1.62	1.60	0.17	0.1%	3.59	1.59	0.16	0.2%	3.65
6m	1:3	3.64	3.59	0.42	0.0%	6.21	3.57	0.40	0.0%	6.36
	1:2	2.83	2.79	0.33	0.0%	5.48	2.79	0.32	0.0%	5.58
	2:3	2.46	2.43	0.28	0.0%	5.02	2.42	0.28	0.0%	5.13
	1:1	2.10	2.09	0.24	0.1%	4.43	2.04	0.23	0.0%	4.49
3m	1:3	6.25	6.18	0.81	0.0%	6.37	5.81	0.74	0.0%	6.49
	1:2	4.68	4.64	0.62	0.0%	5.87	4.64	0.61	0.0%	5.99
	2:3	4.07	4.03	0.54	0.0%	5.61	4.04	0.53	0.0%	5.73
	1:1	3.41	3.38	0.45	0.0%	5.30	3.38	0.44	0.0%	5.41

Table 6.3 – Short term stability results from SLOPE/W (characteristic values)

Gyttja depth	Slope	FS_{det}	2000 MC samples				1000 MC samples			
			FS_{avg}	σ_{FSavg}	p_f	β	FS_{avg}	σ_{FSavg}	p_f	β
9m	1:3	3.63	3.56	0.33	0	7.85	3.55	0.32	0.0%	7.96
	1:2	2.88	2.83	0.26	0.0%	7.01	2.82	0.26	0.0%	7.12
	2:3	2.47	2.43	0.23	0.0%	6.34	2.42	0.22	0.0%	6.44
	1:1	2.03	2.00	0.19	0.0%	5.34	1.99	0.18	0.0%	5.40
6m	1:3	4.39	4.31	0.43	0.0%	7.69	4.32	0.42	0.0%	7.82
	1:2	3.50	3.44	0.35	0.0%	7.05	3.44	0.34	0.0%	7.18
	2:3	3.01	2.97	0.30	0.0%	6.51	2.96	0.30	0.0%	6.63
	1:1	2.50	2.46	0.25	0.0%	5.76	2.44	0.25	0.0%	5.84
3m	1:3	6.66	6.58	0.78	0.0%	7.16	6.60	0.77	0.0%	7.32
	1:2	5.34	5.29	0.63	0.0%	6.80	5.25	0.61	0.0%	6.97
	2:3	4.61	4.56	0.55	0.0%	6.49	4.55	0.54	0.0%	6.61
	1:1	3.80	3.76	0.46	0.0%	6.05	3.76	0.45	0.0%	6.17

It was considered that this structure in particular has a medium level of consequences regarding failure, meaning that is inserted in the reliability class 2 (RC2). The design working life of the structure is not known in prior since the timing execution of phase 2 is unknown. Despite this timing uncertainty, considering that this perimeter excavation is a temporary work, it was considered the less critical situation for reliability, $\beta_d = 3.8$. Considering the criteria regarding the reliability index, it was reached the slope design solutions demonstrated in Table 6.4. For every situation (except for the most critical one), the design solution for the slope proportion was 1:1.

Table 6.4 – Gyttja design slope solutions for both long and short term

Gyttja depth	Medium term design slope	Short term design slope
9m	2:3	1:1
6m	1:1	1:1
3m	1:1	1:1

From an academic point of view it was also evaluated the slope stability considering a drained behaviour using the effective strength parameters indicated in Table 4.5. In this case, since the analysis considers the effective stress, the material model used was the Mohr-Coulomb. As it is possible to observe in Table 6.5, the results obtained for FS are lower in the overall, indicating that this long term analysis is more critical than the medium term one obtained in Table 6.2.

Table 6.5 – Factor of safety obtained from drained strength parameters (Long term analysis)

Gyttja depth	Slope	FS
9m	1:3	2.76
	1:2	2.04
	2:3	1.67
	1:1	1.29
6m	1:3	3.27
	1:2	2.34
	2:3	1.94
	1:1	1.52
3m	1:3	4.11
	1:2	3.16
	2:3	2.66
	1:1	2.13

6.6. EUROCODE 7 - SAFETY FACTORS

Besides producing the slope design approach using the characteristic strength values, it was made the same evaluation using the partial safety factors from the Eurocode 7, EC7. Concerning this design problem in particular, the only property that is going to be affected is going to be the undrained shear strength, c_u. Since this work is developed in Denmark, it was considered the approach from the Danish Annex where it appoints a partial factor for the undrained shear strength, γ_{c_u}, of 1.8 .

6.6.1. OVER DESIGN FACTOR

Considering the partial factors from EC7, an over design factor, ODF, is calculated instead of the factor of safety, FS. Figure 6.13 demonstrates the PDF for the ODF. As it is possible to observe the average value for the ODF is less than the unit. From that it is possible to understand that this scenario in particular (9m gyttja, slope 1:1) violates safety.

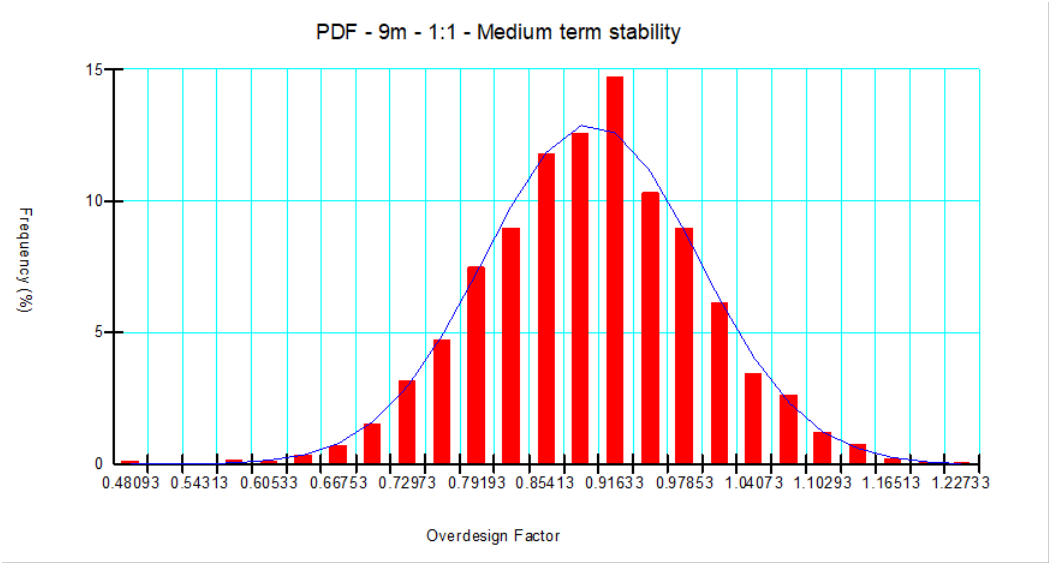


Figure 6.13 – Over Design Factor histogram distribution and the fitted normal distribution to the values obtained

In Figure 6.14, is represented the CDF, considering the PDF in Figure 6.13. The dotted line represented in the graph, represents the probability for the over design factor being less than 1, P(ODF<1). In this case the probability of this occurrence is considerable (87.1%).

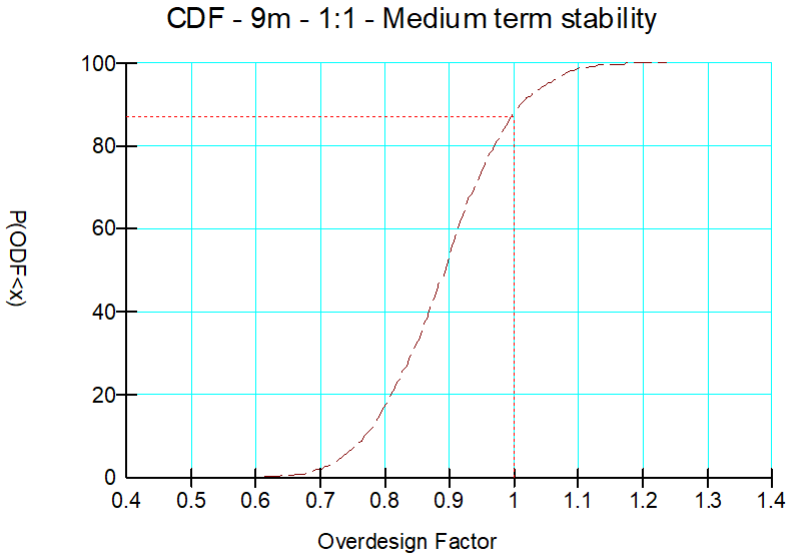


Figure 6.14 – Cumulative density function for the over design factor

6.6.2. Monte Carlo Convergence

6.6.2.1. Probability of Over Design Failure

In Figure 6.15 it can be observed the MC convergence for the probability of over design failure, $p_{f,OD}$. In this case it is possible to observe a convergence on the results when the run number reaches 1000 samples.

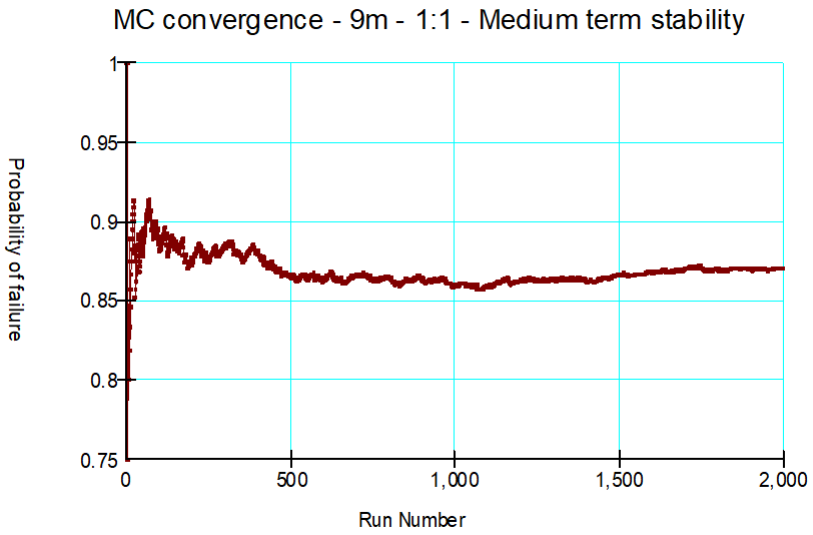


Figure 6.15 – Probability of over design failure - MC convergence graph

6.6.2.2. Mean Over Design Factor

Regarding the mean over design factor, ODF_{avg}, it was also determined the convergence evolution for this parameter. In this case a convergence of when reaching 1000 samples is also evidenced.

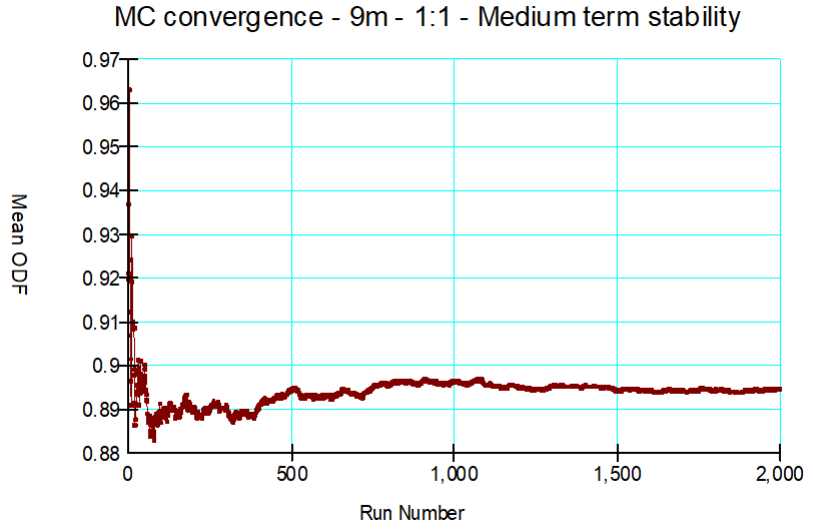


Figure 6.16 – Mean over design factor - MC convergence graph

6.6.2.3. Standard Deviation of the Mean Over Design Factor

Finally, the standard deviation of the mean over design factor is also demonstrated in Figure 6.17. Here a considerable level of convergence is obtained when reaching 500 samples.

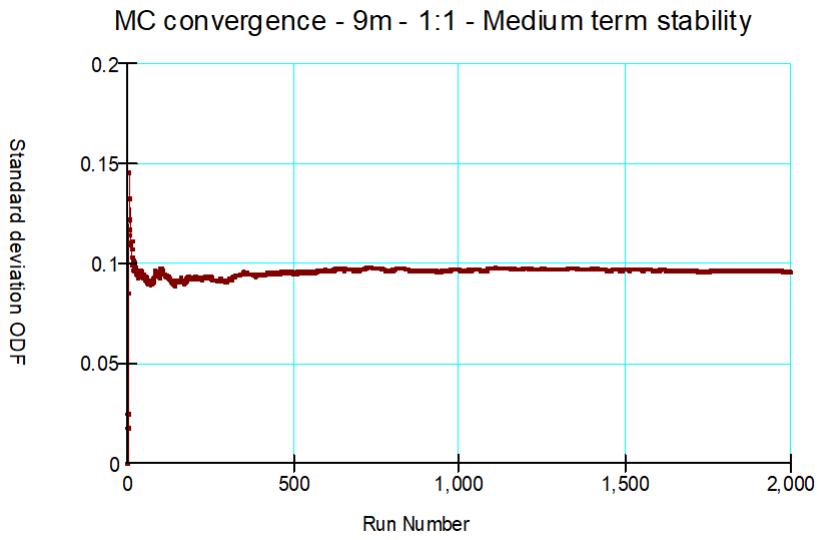


Figure 6.17 – Standard deviation of the mean over design factor - MC convergence graph

Table 6.6 – Medium term stability results from SLOPE/W (EC7 partial factor values)

Gyttja depth	Slope	ODF_{det}	2000 MC samples				1000 MC samples			
			ODF_{avg}	σ_{ODFavg}	$p_{f,OD}$	β_{OD}	ODF_{avg}	σ_{ODFavg}	$p_{f,OD}$	β_{OD}
9m	1:3	1.53	1.51	0.16	0.3%	3.17	1.51	0.16	0.2%	3.23
	1:2	1.22	1.20	0.13	5.6%	1.60	1.20	0.12	4.8%	1.63
	2:3	1.07	1.05	0.11	32.2%	0.45	1.05	0.11	31.7%	0.48
	1:1	0.91	0.89	0.10	87.1%	-1.10	0.89	0.09	87.1%	-1.12
6m	1:3	2.02	2.00	0.23	0.1%	4.30	1.98	0.22	0.0%	4.38
	1:2	1.57	1.55	0.18	0.3%	3.04	1.55	0.18	0.2%	3.02
	2:3	1.36	1.35	0.16	1.3%	2.21	1.35	0.15	1.3%	2.26
	1:1	1.16	1.12	0.12	15.3%	1.00	1.11	0.12	16.5%	0.94
3m	1:3	3.47	3.44	0.45	0.0%	5.39	3.24	0.41	0.0%	5.43
	1:2	2.60	2.58	0.34	0.1%	4.58	2.58	0.34	0.0%	4.67
	2:3	2.26	2.24	0.30	0.1%	4.14	2.24	0.29	0.1%	4.22
	1:1	1.89	1.88	0.25	0.2%	3.52	1.88	0.25	0.2%	3.59

Table 6.7 – Short term stability results from SLOPE/W (EC7 partial factor values)

Gyttja depth	Slope	ODF_{det}	2000 MC samples				1000 MC samples			
			ODF_{avg}	σ_{ODFavg}	$p_{f,OD}$	β_{OD}	ODF_{avg}	σ_{ODFavg}	$p_{f,OD}$	β_{OD}
9m	1:3	2.02	1.98	0.18	0.0%	5.40	1.97	0.18	0.0%	5.47
	1:2	1.60	1.57	0.15	0.1%	3.94	1.57	0.14	0.0%	4.00
	2:3	1.38	1.35	0.13	0.3%	2.79	1.35	0.12	0.2%	2.82
	1:1	1.13	1.11	0.10	14.6%	1.04	1.10	0.10	16.7%	1.02
6m	1:3	2.44	2.40	0.24	0.0%	5.83	2.40	0.24	0.0%	5.93
	1:2	1.94	1.91	0.19	0.0%	4.74	1.91	0.19	0.0%	4.84
	2:3	1.68	1.65	0.17	0.1%	3.87	1.65	0.16	0.1%	3.93
	1:1	1.39	1.37	0.14	0.6%	2.61	1.35	0.14	0.5%	2.59
3m	1:3	3.70	3.66	0.43	0.0%	6.14	3.67	0.42	0.0%	6.28
	1:2	2.96	2.94	0.35	0.0%	5.53	2.92	0.34	0.0%	5.66
	2:3	2.56	2.53	0.30	0.0%	5.03	2.53	0.30	0.0%	5.13
	1:1	2.12	2.09	0.25	0.1%	4.30	2.09	0.25	0.0%	4.39

In Table 6.6 and Table 6.7 is demonstrated the medium and short term obtained results using the EC7 approach. Apart from the parameters previously mentioned, there is also represented the over design reliability index, β_{OD}. From the designer perspective there is not any difference in the obtained results, considering the most optimized over design factor, ODF, of 1. However there is the possibility to link both characteristic and EC7 analysis in order to understand, for instance the p_f and β that matches an ODF higher than 1. With that said the results obtained in Table 6.4 match this Eurocode approach.

6.6.3. Run Analysis Duration

In order to understand the impact in executing a probabilistic analysis in SLOPE/W, it was registered the duration of each solver scenario (Table 6.8). This information is merely indicative, since it is dependent on the computer performance of each user. However it is possible to understand the time impact in producing a probabilistic analysis in comparison to a deterministic analysis. Also it is possible to the see the duration difference in increasing by 1000 the number of MC samples. As expected the difference between a probabilistic and deterministic analysis is considerable. It is also interesting to observe the time saved between producing an analysis with 1000 less samples. Moreover, that reduction in MC samples does not produce a great impact in the obtained values neither the design solution.

Table 6.8 – Run analysis duration for each one of the

Analysis	Solver duration
Probabilistic (2000 MC samples)	2h30min
Probabilistic (1000 MC samples)	1h50min
Deterministic	40s

6.7. CHAPTER SUMMARY

This slope stability analysis served to prove that a simple deterministic analysis that follows the Eurocode safety procedure, lead (in this case) to a considerable safe design solution. In this case by only considering the criteria of ODF>1, it is guarantied highly satisfactory values for the reliability index, i.e values of β>3.8. In this case the lowest value of this parameter ($\beta = 4.43$) which is valid for design is obtained for the 6m of gyttja (medium term analysis, 1:1 slope). Even though this analysis was carried using Approach 3 (that could be seen as unreliable), it is interesting to observe that the final design results are in line with the safety criteria from the Eurocode 7. It is important, however, to highlight that this probabilistic approach followed a certain path, not only on the adoption of Approach 3 but also concerning the LEM (Morgenstern-Price) and the probabilistic method (Monte Carlo Method). By choosing other different assumptions the results could have been slightly different than the ones obtained. However it is considered that both the LEM and probabilistic method adopted, have a good degree of reliability and practical validation.

Considering the results obtained, demonstrated in the 4 tables of results (Table 6.2, 6.3, 6.6 and 6.7) and knowing in prior the safety criteria which is going to be adopted, it is clear that a great amount of LEM analysis could be avoided. This could be easily explained, since it is obvious that when the most critical scenarios guaranty safety, the less critical ones will also have that guaranty. With that said the number of considered scenarios (12 medium term + 12 short term) could have been narrowed to (3 medium term + 1 short term). Using that strategy, the analysis duration for the probabilistic analysis would have dropped considerably.

7
CONCLUSION

7.1. CONCLUSIONS

In the introduction part it was suggested some questions that were aimed to conduct the dissertation around those topics. The conclusion explanation would be formed around the initial questions previously appointed in the introduction part. Also it is going to be referred additional concluded information that was also obtained during the execution of this work.

- How much quality does the filtered CPTU data have?

  It was possible to conclude that the CPTU results did not possess a great quality from a classical analysis perspective (when analysing each CPTU separately). Based on Approach 2 it was possible to visualize a great dispersion in results and a range of results that are not very realistic from a geotechnical point of view, considering the type of soil analysed (very soft soil - gyttja). It is believed that this conclusion could be explained by the type of visual gyttja thickness evaluation method based on cone resistance, q_c. Since this simplistic layering approach ignores small resistance peaks that could possible be intermediate material mixed with gyttja (i.e. fill (L1A) or other post glacial deposits (L1B) explained in 3.3.2.1.). With that said it is possible to say that the large number of CPTU reduce the uncertainty associated to the gyttja thickness evaluation process, when analyzed all together.

- What is the spacial variability of the CPTU data?

  Spatial variability from gyttja seem to be practically nonexistent. However this statement was mainly taken from the triaxial tests results for c_u evaluation. Here it was possible to observe that different samples very spatially distanced produced an incredibly coherent results of c_u. From the CPTU evaluation this conclusion can not be formed with comparable degree of conviction that was stated previously. In fact, the scatters obtained from the CPTU evaluation seem to be disperse from a visual perspective. It is, however interesting to observe that the c_u evaluation from CPTU in Approach 1 is in line with the ones obtained in the triaxial tests. Nevertheless, the plotting scale in those graphics is considerably detailed, which can create the illusion that the data is more dispersed than a conventional CPTU result (scale comparison between Figure 4.8 and Figure 5.3) data density seem to create a defined trend for c_u evaluation. Also, it is interesting to observe a match in results when performing a linear regression in 5 CAUC results and 80016 CPTU readings. However as a result obtained in Approach 1, from all those 80016 readings, only 19.1% of them fitted in the results of the c_u evaluation.

- Is is worth to produce a CPTU probabilistic analysis for slope stability design?

  In order to answer this question it is important to form an unbiased opinion the way the results were obtained in prior. Before producing a probabilistic analysis it is not know in prior the results of that analysis. So it is not possible to know if the obtained results would have an impact on the design. In the practical case of this work, it is possible to observe a match in results obtained from both the deterministic and probabilistic analysis. However, from a deterministic analysis there is no added information rather than the factor of safety while the probabilistic analysis give a failure probability that can be used for further risk assessments. It is important to state that this conclusion is based from the application of Approach 3 which evaluates the impact of the cone factor, N_{kt}, rather than the variation of results from the data scatter (Approach 1). This methodology was important to understand the representation of data from a huge amount of readings and the possibility to obtain similar results to the evaluation from the triaxial tests. Also, it was important to understand the logic behind the formulation of regulation documents such as the Eurocodes, i.e. how the probability of failure is mitigated by affecting the soil strength (in this work focused in c_u) with the partial factors from Eurocode 7.

- What is the most appropriate probabilistic method to use for CPTU in order to evaluate c_u?

  The first thought when producing this work was to evaluate the statistical variation in Approach 1. That was considered to be the most appropriate probabilistic method to use for dealing with a great amount of CPTU. However the results of this approach concerning variability was lower that expected. It was not possible to produce a probabilistic analysis of data that possess no variability. After that, a statistical approach considering the single CPTU (Approach 2) was performed. This analysis was not appropriate due to a great difference in the obtained results, compared to the previous one. The Approach 3 differs from the previous 2 approaches, since it is not a statistical analysis of data admitting a value for the N_{kt} parameter, but a statistical impact in data from the variation of this parameter. From a statistical point of view this approach can be criticised since it produces an analysis considering different data scatters. This approach served to understand the importance of the N_{kt} and to find an alternative to conduct a probabilistic analysis, even thought it can be highly criticised the usage of this method.

- What is the impact of the determination of the N_{kt} in the c_u evaluation?

  The cone factor, N_{kt}, has a major influence in the c_u results. Approach 3 served mainly to conclude this statement above, where it was seen the variation of c_u evolution with N_{kt} variation. Intuitively it seems obvious that data with huge density results has less uncertainty. It is however still hard to quantify the effect or added value of this additional data, i.e, considering a large number of CPTU after a certain point of results convergence. A very important conclusion obtained is the idea that uncertainties associated to the determination of N_{kt} seem to be more relevant than the uncertainties associated in considering a large number of CPTU in the same analysis (Approach 1).

From the production of this work, another subjects were also investigated such as study of strength anisotropy in gyttja. It was concluded that this soil in particular did not revealed signs of induced strength anisotropy. This reinforces the previous experience from similar soils. Another interesting aspect that was concluding during the development of this dissertation was the notion of error propagation and

uncertainty from the very beginning when treating and interpretating the geotechnical tests until the slope design proposal. Also from the practical point of view it was also very enriching to understand and pass through the whole process of interpreting a huge amount of CPTU results, analysing them from a statistical point of view and investigating different perspectives for analysing data. The link to the slope stability modelling was also important, in order to observe a realistic and practical application for the analysed data.

7.2. Future Developments

It is still intriguing to realise the uncertainty in knowing how this N_{kt} parameter depends and where this dependency cames from. However it seems logic that the more amount of data from this parameter, the less uncertainty will appear regarding this cone factor. In this case it will be interesting to compare the differences using this work and a future one considering a large amount of triaxial data. It could be reached the conclusion that the amount of triaxial test is more relevant than the CPTU tests. This could have an impact in the effectiveness of a geotechnical campaign, on increasing the amount of relevant test (in this case CAUC) and reducing tests that are not that relevant and converge using a less number of tests (CPTU).

Also could be also interesting to compare the results using a different method to determine N_{kt} rather than the CAUC-CPTU method found in subsection 4.2.4.. Some alternative examples are by using vane shear test (VST) or using empirical expressions only from CPTU tests.

Another future development for this dissertation is studying the impact of using a more detailed layering method. The spatial spreading and the fact that the number of CPTU and boreholes with the objective to determine geotechnical parameters are limited, means that the estimated parameters always contain uncertainties. This layering method can be made using soil samples from the boreholes and use that information for the adjacent CPTU. That would require the same amount of boreholes and CPTU in order to do it with less uncertainty.

For every probabilistic distribution was considered that they follow normal distributions. However this was admitted based on geotechnical engineering practice and not on real distribution moulded by data. It can be interesting the fitting of data using different distributions.

BIBLIOGRAPHY

Assis, A. P. (2020). Risk management for geotechnical structures: consolidating theory into practice. *Soils and Rocks*.

Babak Hamidi, S. V. (2015). Dynamic compaction and dynamic surcharging at dubai's palm jumeira sewage treatment plants. In *Ground improvement case histories.*

Bishop, A. W., & Bjerrum, L. (1960). The relevance of the triaxial test to the solution of stability problems. *Norwegian Geotechnical Institute Publ*.

Bo, M. W., & Choa, V. (2004). *Reclamation and ground improvement*. Thomson Learning Asia.

Boskalis. (n.d.). *Backhoe dredgers.* Retrieved from https://boskalis.com/about-us/fleet-and-equipment/dredgers/backhoe-dredgers.html

By og Havn. (2020). *Lynetteholm.*

COWI/AS. (2020). *Geoteknisk vurderingsrapport.*

De Mio, G., Giacheti, H., Viana da Fonseca, A., & Ferreira, C. (2010). Cptu interpretation for stratigraphic logging: differences between sedimentary and residual soils. In *Proceedings of the second international symposium of cone penetration testing, cpt* (Vol. 10).

Diamantidis, D., & Holickỳ, M. (2010). Reliability differentiation in the eurocodes. *Advances and Trends in Structural Engineering, Mechanics and Computation*, 264.

Duong, I. (2017). Are the benefits of land reclamation worth the environmental impact they cause? *South China Morning Post*.

EN 1990. (2002). Eurocode — basis of structural design. *Eurocode 0.*

Environment, M., & Authority, P. (2008). Detailed investigations and feasibility studies on land reclamation at two indicated search areas, malta. *Technical Report 2 Volume 1: Main Text*.

Eslami, A., & Fellenius, B. H. (1997). Pile capacity by direct cpt and cptu methods applied to 102 case histories. *Canadian Geotechnical Journal*, *34*(6), 886–904.

Fertner, C. (2012). *Urbanisation, urban growth and planning in the copenhagen metropolitan region with reference studies from europe and the usa.* Forest & Landscape.

GEO-SLOPE. (2012). Stability modeling with slope/w. *GEOSLOPE International Limited*.

Griffiths, D. V., & Fenton, G. A. (2007). *Probabilistic methods in geotechnical engineering* (Vol. 491). Springer Science & Business Media.

Hansen, H., & Foged, N. (2002). Kalkens bjergmekaniske egenskaber. In J. Frederiksen (Ed.), *Ingeniørgeologiske forhold i københavn* (pp. 31–34). Danish Geotechnical Society.

Houmark-Nielsen, M., Krüger, J., & Kjær, K. H. (2005). De seneste 150.000 år i danmark. *Geoviden*, 1–19.

Jiangsu ShunYou Shipping Engineering Co., Ltd. (n.d.). *Chain bucket dredger.* Retrieved from http://en.shunyouship.com/show.asp?id=9

Karlsson, R., & Hansbo, S. (1989). Soil classification and identification. *Swedish Council for Building Research*.

Khan, F., & Malik, A. (2016). Probability and sensitivity analysis of the slope stability of naulong dam. *Pakistan Journal of Engineering and Applied Sciences*.

Kojimagumi. (n.d.). *Gosho|grab dredger.* Retrieved from http://www.kk-kojimagumi.co.jp/english/ship/ship_dredging/ship_grab-dredger/entry-254.html

Lambe, T. W., & Whitman, R. V. (1991). *Soil mechanics* (Vol. 10). John Wiley & Sons.

Larsen, G., Frederiksen, J., Villumsen, A., Fredericia, J., Gravesen, P., Foged, N., ... Baumann, J. (1995). Vejledning i ingeniørgeologisk prøvebeskrivelse. *Dansk Geoteknisk Forening Bulletin 1*.

Larsson, R. (1990). Behaviour of organic clay and gyttja. *Rapport-Statens geotekniska institut*, *38*.

Lunne, T., Robertson, P. K., & Powell, J. J. (1997). *Cone penetration testing in geotechnical practice*.

Matos Fernandes, M. (2015). Mecânica dos solos. introdução à engenharia geotécnica. *Volume II, Universidade do Porto, FEUP*.

Matos Fernandes, M. (2016). Mecânica dos solos. *Volume I, Universidade do Porto, FEUP*.

Mayne, P., & Peuchen, J. (2018). Evaluation of cptu nkt cone factor for undrained strength of clays. *Cone Penetration Testing*, 423–429.

Miner, L. (2018). Copenhagen: New island settlement to house 35,000 people and shore up sea defence. *Reuters*.

NASA Earth Observatory. (n.d.). *Land reclamation at rotterdam.* Retrieved from https://earthobservatory.nasa.gov/images/47122/land-reclamation-at-rotterdam

Port of Rotterdam. (n.d.). *Maasvlakte 2.* Retrieved from https://www.portofrotterdam.com/en/news-and-press-releases/maasvlakte-2

Rémai, Z. (2013). Correlation of undrained shear strength and cpt resistance. *Periodica Polytechnica Civil Engineering*, *57*(1), 39–44.

Richardt, N., Belhage, L., & Funder, S. (1999). Øresund i 20.000 år, scener fra et bevæget liv. *Varv*, 67–96.

Robertson, P. K. (1990). Soil classification using the cone penetration test. *Canadian Geotechnical Journal*, *27*(1), 151–158.

Robertson, P. K. (2010). Soil behaviour type from the cpt: an update. In *2nd international symposium on cone penetration testing* (Vol. 2, pp. 575–583).

Robertson, P. K., & Cabal, K. (2014). Guide to cone penetration testing for geotechnical engineering. *Gregg Drilling & Testing*.

Robertson, P. K., Campanella, R., Gillespie, D., & Greig, J. (1986). Use of piezometer cone data. In *Use of in situ tests in geotechnical engineering* (pp. 1263–1280).

Santamarina, J., Altschaeffl, A., & Chameau, J. (1992). Reliability of slopes: incorporating qualitative information (abridgment). *Transportation Research Record*(1343).

Seatools. (n.d.). *Dipmate essential – backhoe dredging monitoring system.* Retrieved from https://www.seatools.com/related-system/dipmate-essential/

Skempton, A. (1954). The pore-pressure coefficients a and b. *Geotechnique*, *4*(4), 143–147.

Stauber, J., Chariton, A., & Apte, S. (2016). Global change. In *Marine ecotoxicology* (pp. 273–313). Elsevier.

Structurae. (n.d.). *Mühlenberger loch land reclamation.* Retrieved from https://structurae.net/en/structures/muhlenberger-loch-land-reclamation

Tripathi, N., Singh, R. S., & Hills, C. D. (2016). *Reclamation of mine-impacted land for ecosystem recovery*. Wiley Online Library.

Veritas, D. N. (2012). Dnv-rp-c207: Statistical representation of soil data. *Det Norske Veritas, Høvik, Norway*.

Vlasblom, I. W. (2004). *The bucket dredger.* Retrieved from https://dredging.org/documents/ceda/downloads/vlasblom6-the-bucket-or-ladder-dredger.pdf

Wikipedia. (n.d.). *Gytje.* Retrieved from https://da.wikipedia.org/wiki/Gytje

Zhang, H., Wang, J., Sikora, F., & Moore, K. (2014). Loss on ignition method. *Soil Test Methods from the Southeastern United States; Sikora, FJ, Moore, KP, Huluka, G., Kissel, DE, Miller, R., Mylavarapu, R., Oldham, JL, Eds*, 155–158.